Design Calculation or Analysis Cover Sheet

BSC

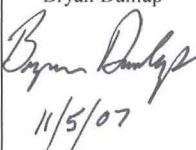*Complete only applicable items.*

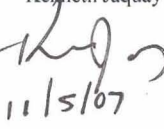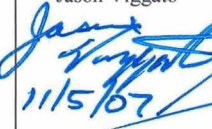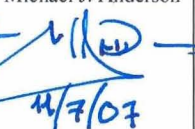1. QA: QA

3. System Monitored Geologic Repository	4. Document Identifier 000-00C-MGR0-04500-000-00A

5. Title

Waste Package Capability Analysis For Nonlithophysal Rock Impacts

6. Group

Thermal Structural Analysis

7. Document Status Designation

☐ Preliminary   ☒ Committed   ☐ Confirmed   ☐ Cancelled/Superseded

8. Notes/Comments

None.

Attachments	Total Number of Pages
Attachment I. Figures Obtained from LS-DYNA	6
Attachment II. Plots of Capability Variability Including Rock Compressive Strength Variability	4
Attachment III. Directory Listing (data DVD) of Electronic Files	12
Attachment IV. Data DVD Attachment, Electronic Files	N/A

RECORD OF REVISIONS

9. No.	10. Reason For Revision	11. Total # of Pgs.	12. Last Pg. #	13. Originator (Print/Sign/Date)	14. Checker (Print/Sign/Date)	15. EGS (Print/Sign/Date)	16. Approved/Accepted (Print/Sign/Date)
00A	Initial Issue	84	84	Bryan Dunlap 11/5/07	Kenneth Jaquay 11/5/07	Jason Viggato 11/5/07	Michael J. Anderson 11/7/07

DISCLAIMER

The calculations contained in this document were developed by Bechtel SAIC Company, LLC (BSC) and are intended solely for the use of BSC in its work for the Yucca Mountain Project.

CONTENTS

FIGURES

Page

TABLES

Page

ACRONYMS

ACC	Project Accession Number for a Reference
ASM	American Society for Metals
ASME	American Society of Mechanical Engineers
ASTM	American Society for Testing and Materials
BSC	Bechtel SAIC Company, LLC.
BWR	Boiling Water Reactor
CS	Carbon Steel
DHLW	Defense High Level Waste
DOE	U.S. Department of Energy
EP	Emplacement Pallet
ETF	Expended Toughness Fraction
EWA	Element Wall-Averaged
FE	Finite Element
FER	Finite Element Representation
J	Joules (Energy, Newton·meter)
LA	License Application
LSTC	Livermore Software Technology Corporation
MT	Metric Ton (1,000 kilograms)
MPa	Mega Pascal (force per unit area)
OCB	Outer Corrosion Barrier
PRA	Probabilistic Risk Assessment
RT	Room Temperature
SI	Stress Intensity
SNF	Spent Nuclear Fuel
SS	Stainless Steel
TAD	Transportation, Aging, and Disposal
TIC	Technical Information Center Record Number
VM	von Mises
WP	Waste Package

1. PURPOSE

The purpose of this calculation:

- The application of a methodology that supports a Probabilistic Risk Assessment (PRA) of the pre-closure structural response of emplaced waste packages (WPs) to nonlithophysal rock impacts (large intact rock) (Reference 2.2.16, Section 11.2.3.1.4). Considering:

  - The use of nominal (typical) material property sets obtained from metals vendors (affects WP Capability).

  - The use of multi-axial tensile instability adjustments to the material property sets to predict more realistic material structural performance (affects WP Capability).

  - Analyze the designs of the:

    - Transportation, Aging and Disposal (TAD) canister bearing WP (TAD bearing WP).

    - 5DHLW/DOE Co-disposal Short WP (Co-disposal Short WP).

  - All WPs analyzed while resting on an emplacement pallet (EP).

- A range of rock impact scenarios will be analyzed at two different locations on the WP to determine the maximum outer corrosion barrier (OCB) stresses and strain energy values.

  - The selected locations are based on results of deterministic calculations (Reference 2.2.53) and produce the maximum OCB response (affects Capability).

  - The mass and kinetic energy of impacting rock fall will cover the range of expected PRA Demand.

    - Considerations for rock kinetic energy (affects Demand).

    - Considerations for rock impact location (affects Demand).

- The scope of the calculation is limited to reporting the structural response of the WPs OCB in the form of expended toughness fractions (ETFs) based on strain energy densities, material toughness index values (I_T), and element wall-averaged (EWA) von Mises (VM) effective stresses and strains. The ETFs versus rock mass and impact velocity, along with material toughness variability, will be used in producing the Capability portion of the PRA. The WP will be considered failed if these analyses predict OCB void formation and imminent ductile rupture under primary loading.

- This calculation will support the Subsurface Engineering Organization activities for future iterations of the *HLW/DOE SNF Co-disposal Waste Package Design Report*, 000-00C-DS00-00600-000-00, and in the *TAD Waste Package Design Report*, 000-00C-DSC0-00100-000-00.

- This calculation is intended for use in support of Preclosure Safety Analysis Group's PRA activities for the license application (LA) (Reference 2.2.58).

2. REFERENCES

2.1 PROCEDURES/DIRECTIVES

2.1.1. EG-PRO-3DP-G04B-00037, Rev. 10. *Calculations and Analyses*. Las Vegas, Nevada: Bechtel SAIC Company. ACC: ENG.20071018.0001.

2.1.2. IT-PRO-0011, Rev. 7, ICN 0. *Software Management*. Las Vegas, NV: Bechtel SAIC Company. ACC: DOC.20070905.0007.

2.1.3. ORD (Office of Repository Development) 2007. *Repository Project Management Automation Plan*. 000-PLN-MGR0-00200-000, Rev. 00E. Las Vegas, Nevada: U.S. Department of Energy, Office of Repository Development. ACC: ENG.20070326.0019.

2.2 DESIGN INPUTS

2.2.1. Dieter, G.E. 1976. *Mechanical Metallurgy.* 2nd Edition. Materials Science and Engineering Series. New York, New York: McGraw-Hill Book Company. TIC: 247879. ISBN: 0-07-016891-1.

2.2.2. ASM (American Society for Metals) 1980. *Properties and Selection: Stainless Steels, Tool Materials and Special-Purpose Metals*. Volume 3 of *Metals Handbook.* 9th Edition. Benjamin, D., ed. Metals Park, Ohio: American Society for Metals. TIC: 209801. ISBN: 0-87170-009-3.

2.2.3. ASME (American Society of Mechanical Engineers) 2001. *2001 ASME Boiler and Pressure Vessel Code (includes 2002 addenda)*. New York, New York: American Society of Mechanical Engineers. TIC: 251425.

2.2.4. ASTM (American Society for Testing and Materials) G 1-90 (Reapproved 1999). 1999. *Standard Practice for Preparing, Cleaning, and Evaluating Corrosion Test Specimens.* West Conshohocken, Pennsylvania: American Society for Testing and Materials. TIC: 238771.

2.2.5. ASM International 1990. *Properties and Selection: Irons, Steels, and High-Performance Alloys*. Volume 1 of *Metals Handbook.* 10th Edition. Materials Park, Ohio: ASM International. TIC: 245666. ISBN: 0-87170-377-7.

2.2.6. Boyer, H.E., ed. 2000. *Atlas of Stress-Strain Curves*. Metals Park, Ohio: ASM International. TIC: 248901. ISBN: 0-87170-240-1.

2.2.7. LL020603612251.015. Slow Strain Rate Test Generated Stress Corrosion Cracking Data. Submittal date: 08/27/2002.

2.2.8. Haynes International. 1997. Hastelloy C-22 Alloy. Kokomo, Indiana: Haynes International. TIC: 238121.

2.2.9. Avallone, E.A. and Baumeister, T., III, eds. 1987. *Marks' Standard Handbook for Mechanical Engineers*. 9th Edition. New York, New York: McGraw-Hill. TIC: 206891. ISBN: 0-07-004127-X.

2.2.10. Meriam, J.L. and Kraige, L.G. 1987. *Statics*. Volume 1 of *Engineering Mechanics*. 2nd Edition. Pages 441, 443. New York, New York: John Wiley & Sons. TIC: 241293.

2.2.11. Beer, F.P. and Johnston, E.R., Jr. 1977. *Vector Mechanics for Engineers, Statics*. 3rd Edition. New York, New York: McGraw-Hill Book Company. TIC: 247391. ISBN: 0-07-004278-0.

2.2.12. BSC (Bechtel SAIC Company) 2004. *Drip Shield Structural Response to Rock Fall*. 000-00C-SSE0-00300-000-00A. Las Vegas, Nevada: Bechtel SAIC Company. ACC: ENG.20040405.0019; ENG.20050817.0026.

2.2.13. Roark, R.J. and Young, W.C. 1975. *Formulas for Stress and Strain*. 5th Edition. New York, New York: McGraw-Hill. TIC: 240746. ISBN: 0-07-053031-9.

2.2.14. Nicholas, T. 1980. *Dynamic Tensile Testing of Structural Materials Using A Split Hopkinson Bar Apparatus*. AFWAL-TR-80-4053. Wright-Patterson Air Force Base, Ohio: Air Force Wright Aeronautical Laboratories. TIC: 249469.

2.2.15. DOE (U.S. Department of Energy) 2007. *Transportation, Aging and Disposal Canister System Performance Specification*. WMO-TADCS-000001, Rev. 0. DOE/RW-0585. Washington D.C.: U.S. Department of Energy, Office of Civilian Radioactive Waste Management. ACC: DOC.20070614.0007.

2.2.16. BSC 2007. *Basis of Design for the TAD Canister-Based Repository Design Concept*. 000-3DR-MGR0-00300-000-001. Las   Vegas,   Nevada: BSC.   ACC: ENG.20071002.0042; ENG.20071026.0033.

2.2.17. BSC 2007. *IED GEOTECHNICAL AND THERMAL PARAMETERS IV*. 800-IED-MGR0-00404-000-00A. Las Vegas, Nevada: BSC. ACC: ENG.20070125.0018.

2.2.18. BSC 2004. *Design and Engineering, Stress Intensity Classification: Waste Package Outer Corrosion Barrier Stresses Due to Horizontal Drop Event*. 000-00C-MGR0-01600-000-00A. Las Vegas, Nevada: BSC. ACC: ENG.20041122.0001.

2.2.19. BSC 2007. *Naval Long Waste Package Vertical Impact on Emplacement Pallet and Invert*.   000-00C-DNF0-00100-000-00C. Las Vegas, Nevada: BSC. ACC: ENG.20071017.0001.

2.2.20. Naples, E.M. 1999. Bounding Source Term for Naval Spent Nuclear Fuel (SNF) for Use by the Yucca Mountain Site Characterization Office. Letter from E.M. Naples (Department of the Navy) to D.C. Haught (DOE/YMSCO), July 1, 1999. ACC: MOL.19990806.0047.

2.2.21. Chen, W.F. 1982. *Plasticity in Reinforced Concrete.* New York, New York: McGraw-Hill. TIC: 240453. ISBN: 0-07-010687-8.

2.2.22. Jaeger, J.C. and Cook, N.G.W. 1979. *Fundamentals of Rock Mechanics.* 3rd Edition. New York, New York: Chapman and Hall. TIC: 218325. ISBN: 0-41222010-5.

2.2.23. LS-DYNA V.970.3858 D MPP. 2003. HP-UX 11.22. STN:10300-970.3858 D MPP-00.

2.2.24. LS-DYNA D MPP V971.7600.2.1116. 2007. HP-UX 11.23. 10300-971.7600.2.1116-00.

2.2.25. BSC 2005. *IED WASTE PACKAGE PROCESSES, GROUND MOTION TIME HISTORIES, AND TESTING AND MATERIALS [Sheet 1 of 1].* 800-IED-WIS0-00501-000-00A. Las Vegas, Nevada: BSC, ACC: ENG.20050406.0004.

2.2.26. DOE 2007. *"High-Level Radioactive Waste and U.S. Department of Energy and Naval Spent Nuclear Fuel to the Civilian Radioactive Waste Management System*." Volume 1 of *Integrated Interface Control Document.* DOE/RW-0511, Rev. 3. Washington, D.C.: DOE, Office of Civilian Radioactive Waste Management. ACC: DOC.20070125.0002.

2.2.27. DOE 2003. *Validation Test Report for LS-DYNA Version 970.3858 D MPP.* 10300-VTR-970.3858 D MPP-00. Las Vegas, Nevada: DOE, Office of Repository Development. ACC: MOL.20031218.0337.

2.2.28. BSC 2007. *Probabilistic Characterization of Preclosure Rockfalls in Emplacement Drifts.* 800-00C-MGR0-00300-000-00A. Las Vegas, Nevada: BSC. ACC: ENG.20070329.0009.

2.2.29. DOE 2007. *Software Validation Report for: LS-DYNA D MPP 971.7600.2.1116.* 10300-SVR-971.7600.2.1116-00-HPUX 11.23. Las Vegas, Nevada: DOE, Office of Repository Development. ACC: MOL.20070921.0254.

2.2.30. BSC 2007. *TAD Waste Package Configuration.* 000-MW0-DSC0-00101-000 REV 00B. Las Vegas, Nevada: BSC. ACC: ENG.20070301.0010.

2.2.31. BSC 2007. *TAD Waste Package Configuration.* 000-MW0-DSC0-00102-000 REV 00B. Las Vegas, Nevada: BSC. ACC: ENG.20070301.0011.

2.2.32. BSC 2007. *TAD Waste Package Configuration.* 000-MW0-DSC0-00103-000 REV 00B. Las Vegas, Nevada: BSC. ACC: ENG.20070301.0012.

2.2.33. BSC 2004. *Design and Engineering, Emplacement Pallet Assembly Exploded [Sheet 2 of 15].* 000-M00-SSE0-00302-000-00A. Las Vegas, Nevada: BSC. ACC: ENG.20040224.0006.

2.2.34. BSC 2004. *Design and Engineering, Emplacement Pallet Waste Package Support Assembly Exploded [Sheet 3 of 15].* 000-M00-SSE0-00303-000-00A. Las Vegas, Nevada: BSC. ACC: ENG.20040224.0007.

2.2.35.   BSC 2004. *Design and Engineering, Emplacement Pallet Assembly Plate 1 [Sheet 4 of 15]*. 000-M00-SSE0-00304-000-00A. Las Vegas, Nevada: BSC. ACC: ENG.20040224.0008.

2.2.36.   BSC 2004. *Design and Engineering, Emplacement Pallet Assembly Plate 2 [Sheet 5 of 15]*. 000-M00-SSE0-00305-000-00A. Las Vegas, Nevada: BSC. ACC: ENG.20040224.0009.

2.2.37.   BSC 2004. *Design and Engineering Emplacement Pallet Assembly Plate 3 [Sheet 6 of 15]*. 000-M00-SSE0-00306-000-00A. Las Vegas, Nevada: BSC. ACC: ENG.20040224.0010.

2.2.38.   BSC 2004. *Design and Engineering, Emplacement Pallet Assembly Plate 4 [Sheet 7 of 15]*. 000-M00-SSE0-00307-000-00A. Las Vegas, Nevada: BSC. ACC: ENG.20040224.0011.

2.2.39.   BSC 2004. *Design and Engineering, Emplacement Pallet Assembly Plate 5 [Sheet 8 of 15]*. 000-M00-SSE0-00308-000-00A. Las Vegas, Nevada: BSC. ACC: ENG.20040224.0012.

2.2.40.   BSC 2004. *Design and Engineering, Emplacement Pallet Assembly Plate 6 [Sheet 9 of 15]*. 000-M00-SSE0-00309-000-00A. Las Vegas, Nevada: BSC. ACC: ENG.20040224.0013.

2.2.41.   BSC 2004. *Design and Engineering, Emplacement Pallet Assembly Plate 7 [Sheet 10 of 15]*. 000-M00-SSE0-00310-000-00A. Las Vegas, Nevada: BSC. ACC: ENG.20040224.0014.

2.2.42.   BSC 2004. *Design and Engineering, Emplacement Pallet Assembly Plate 8 [Sheet 11 of 15]*. 000-M00-SSE0-00311-000-00A. Las Vegas, Nevada: BSC. ACC: ENG.20040224.0015.

2.2.43.   BSC 2004. *Design and Engineering, Emplacement Pallet Assembly Plate 9 [Sheet 12 of 15]*. 000-M00-SSE0-00312-000-00A. Las Vegas, Nevada: BSC. ACC: ENG.20040224.0016.

2.2.44.   BSC 2004. *Design and Engineering, Emplacement Pallet Assembly Tube 1 [Sheet 13 of 15]*. 000-M00-SSE0-00313-000-00A. Las Vegas, Nevada: BSC. ACC: ENG.20040224.0017.

2.2.45.   BSC 2004. *Design and Engineering, Emplacement Pallet Assembly Tube 2 [Sheet 14 of 15]*. 000-M00-SSE0-00314-000-00A. Las Vegas, Nevada: BSC. ACC: ENG.20040224.0018.

2.2.46.   BSC 2004. *Design and Engineering, Emplacement Pallet Assembly Tube 3 [Sheet 15 of 15]*. 000-M00-SSE0-00315-000-00A. Las Vegas, Nevada: BSC. ACC: ENG.20040224.0019.

2.2.47. BSC 2007. *5-DHLW/DOE SNF - Short Co-Disposal Waste Package Configuration.* 000-MW0-DS00-00101-000-00D. Las Vegas, Nevada: BSC. ACC: ENG.20070719.0002.

2.2.48. BSC 2007. *5-DHLW/DOE SNF - Short Co-Disposal Waste Package Configuration.* 000-MW0-DS00-00102-000-00C. Las Vegas, Nevada: BSC. ACC: ENG.20070719.0003.

2.2.49. BSC 2007. *5-DHLW/DOE SNF - Short Co-Disposal Waste Package Configuration.* 000-MW0-DS00-00103-000-00C. Las Vegas, Nevada: BSC. ACC: ENG.20070719.0004.

2.2.50. Special Metals 2006. *Inconel Alloy 22*. Publication Number SMC-049. Huntington, West Virginia: Special Metals Corporation. TIC: 259169.

2.2.51. Inco 1995. *Product Handbook*. Huntington, West Virginia: Inco Alloys International. TIC: 242681.

2.2.52. BSC 2007. *Waste Package Component Design Methodology Report.* 000-30R-WIS0-00100-000-003. Las Vegas, Nevada: BSC. ACC: ENG.20070927.0034; ENG.20071018.0026.

2.2.53. BSC 2007. *Nonlithophysal Rock Fall on Waste Packages*. 000-00C-MGR0-01400-000-00B. Las Vegas, Nevada: BSC. ACC: ENG.20070724.0015.

2.2.54. BSC 2007. *Repository Subsurface Emplacement Drifts Steel Invert Structure Plan & Elevation*. 800-SS0-SSE0-00201-000-00C. Las Vegas, Nevada: BSC. ACC: ENG.20071002.0056.

2.2.55. BSC 2007. *Material Modeling of Alloy 22 Test Specimen Data*. 000-00C-WIS0-03200-000-00A. Las Vegas, Nevada: BSC. ACC: ENG.20070711.0001.

2.2.56. Allegheny Technologies 2004. *Nickel-Based Alloy Filler Material and Base Metal Composition Test Program*. 004223-0069-001-2. Albany, Oregon: Allegheny Technologies. ACC: ENG.20040507.0005.

2.2.57. Not used.

2.2.58. BSC 2007. *Preliminary Preclosure Nuclear Safety Design Bases*. 000-PSA-MGR0-01000-000-001. Las Vegas, Nevada: Bechtel SAIC Company. ACC: ENG.20071015.0008.

2.2.59. BSC 2004. *Drift Degradation Analysis*. ANL-EBS-MD-000027 REV 03. Las Vegas, Nevada: Bechtel SAIC Company. ACC: DOC.20040915.0010; DOC.20050419.0001; DOC.20051130.0002; DOC.20060731.0005.

2.3   DESIGN CONSTRAINTS

None

2.4   DESIGN OUTPUTS

Results from this calculation will be used by Subsurface Engineering Organization in other calculations and analyses.

Results from this calculation are expected to be used in future iterations of the *HLW/DOE SNF Co-disposal Waste Package Design Report*, 000-00C-DS00-00600-000-00, and in the *TAD Waste Package Design Report*, 000-00C-DSC0-00100-000-00. Also, results from this calculation will support the Preclosure Safety Analysis Group's PRA activities as described in Reference 2.2.58.

3.   ASSUMPTIONS

3.1   ASSUMPTIONS REQUIRING VERIFICATION

3.1.1   Waste Package and Emplacement Pallet Dimensions and Materials

The dimensions, masses, materials and load paths of the WP and EP used in the development of this calculation, corresponding to the drawings of References 2.2.30 to 2.2.49, are assumed to be reasonably the same in the regions of high stress and load transfer as the final definitive design.

Rationale–The rationale for this assumption is that the design of References 2.2.30 to 2.2.49 in the region of high stress is representative of the design created for the LA. This assumption is used in Sections 6.1 and 6.4 and will require verification at completion of the final definitive design. This assumption is being tracked in CalcTrac.

3.1.2   TAD Canister Dimensions and Materials

The geometry, dimensions and mass of the loaded TAD Spent Nuclear Fuel (SNF) canister are assumed to be the same as the loaded Naval SNF Long canister. The material used to model the TAD SNF canister is Type 316L Stainless Steel (SS), which is a 300 Series SS as specified in Reference 2.2.15, Section 3.1.8.

Rationale- The rationale for this assumption is that the specified dimensions of the TAD SNF and Naval SNF Long canisters are the same (Section 33.2.2.1 of Reference 2.2.16, and Figure C-17 of Reference 2.2.26) and the mass of the loaded canisters will have negligible effect on the results of this calculation. Which 300 Series SS the TAD canister will be constructed of has not been finalized, and it cannot be predetermined that 316L SS (the material specified for the Naval Long canister, Reference 2.2.26, Figure C-17) would be a conservative material selection or not. However, because the TAD canister is surrounded by the 2 inch thick inner vessel and the 1 inch thick OCB, the sensitivity of the OCB structural response to rock impact due to which 300 Series SS the TAD canister is constructed of is expected to be small. This assumption is used in Sections 6.1 and 6.2 and will require verification at completion of the final definitive design. This assumption is being tracked in CalcTrac.

3.2   ASSUMPTIONS NOT REQUIRING VERIFICATION

3.2.1   Material Properties and Temperature Dependency

Room temperature (RT) (20 *°C* (68 *°F*)) material property values are assumed for the OCB, Inner Vessel, and EP for all analyses. The impact on calculated ETF values using RT structural material properties is anticipated to be small.

Rationale– All temperature dependent event sequence Deterministic results to date show slightly higher damage (stress intensity ratio to allowable) in the OCB when using the RT property values compared to property values for temperatures up to 300 *°C* (572 *°F*), e.g. Section 7.3.1 of Reference 2.2.19.   Further, Deterministic sensitivity studies in Reference 2.2.18, Section 6 indicate that temperature has negligible effect on the results of this type of calculation. Section 7.5.1 of Reference 2.2.19 provides a temperature sensitivity study for a Capability calculation that shows the same trend. Therefore this assumption does not require verification. This assumption is used in Section 6.1.

3.2.2   Material Properties for the Rock

The temperature-dependent material properties are not available for TSw2 (Topopah Spring welded tuff, nonlithophysal) rock except at RT. The RT material properties are assumed for this material. The impact of using RT material properties is anticipated to be small.

Rationale– The rock material properties do not have dominant impact on the calculation results except for the compressive strength of the rock, which decreases with increasing temperature. Thus, the representation of the rock as an elastic-ideally-plastic solid with RT compressive strength as the yield strength is conservative. Therefore this assumption does not require verification. This assumption is used in Section 6.1 and corresponds to Section 6.1.1.17 in Reference 2.2.52.

3.2.3   Metallic Material Properties and Rate Dependency

Some of the rate-dependent material properties are not available for the metallic materials used at any strain rate. The material properties obtained under the static loading conditions are assumed for all materials. The impact of using material properties obtained under static loading conditions is anticipated to be small.

Rationale– The mechanical properties of subject materials do not significantly change at the maximum wall-averaged strain rates that occur during the one of the highest kinetic energy rock impact scenarios. Figure 1 is a time plot in seconds (*s*) of the wall-averaged effective strain in a Co-disposal Short WP at the OCB location with the highest wall-averaged stress intensity during the 40.8 *MT* (45 *ton*) at 20.1 *m/s* (65.9 *ft/s*) rock impact scenario (see section 7.2). From Figure 1 the maximum wall-averaged effective strain rate (maximum slope of the effective strain curve) is seen to be $= 0.0722/0.002 \ s = 36.1 \ s^{-1}$. For this value of strain rate, Reference 2.2.14 Figures 27 and 30, pages 42 and 45, respectively, indicates only a minor strengthening of 300 Series SS and high alloy steels, i.e. less than 20%. Therefore, the impact of using material properties obtained under static loading conditions will be small and this assumption will not require verification. This assumption is used in Section 6.1 and corresponds to Section 6.1.1.2 in Reference 2.2.52.
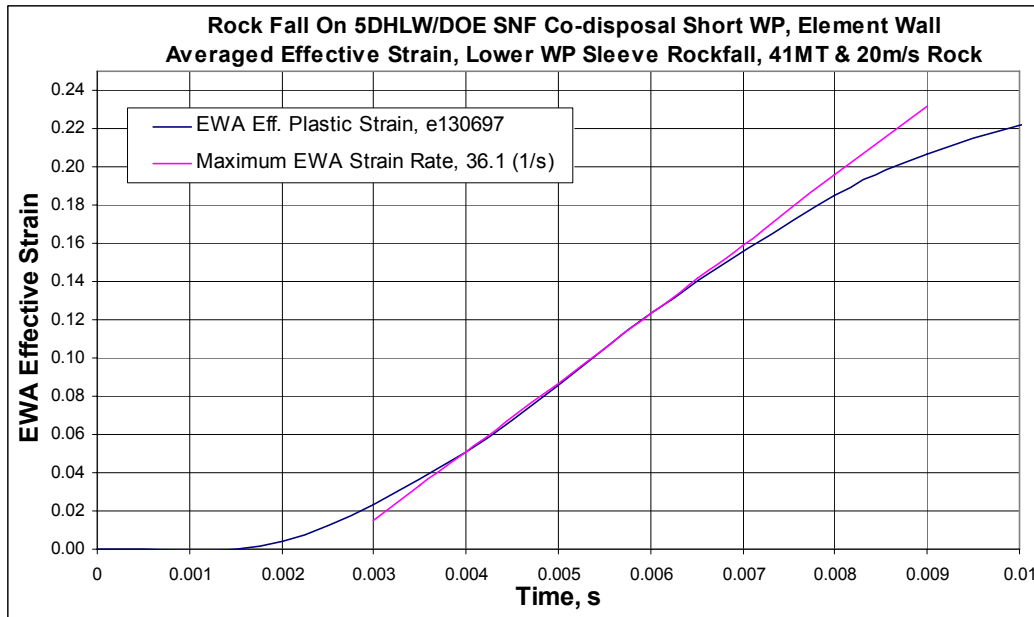
Figure 1.   EWA Effective Strain Rock-WP Impact on Lower Sleeve

3.2.4   Poisson's Ratio of Alloy 22

The RT Poisson's ratio of Alloy 22 is not published in traditional sources. Therefore, the RT Poisson's ratio of Alloy 625 (SB-443 N06625) is assumed for Alloy 22. The impact of this assumption is anticipated to be negligible.

Rationale– The chemical compositions of Alloy 22 and Alloy 625 are similar since they are both 600 Series nickel-base alloys (Reference 2.2.3 [Section II, Part B, SB-575, Table 1] and Reference 2.2.2 [p. 143], respectively). Therefore, the difference in their Poisson's ratio is expected to be small. Furthermore, there are only small differences in RT Poisson's ratio values for the family of 600 Series nickel-based alloys:

  Alloy 600 [UNS N06600] = 0.290 (Reference 2.2.2, p.141)
  Alloy 625 [UNS N06625] = 0.278 (Reference 2.2.2, p.143)
  Alloy 690 [UNS N06690] = 0.289 (Reference 2.2.2, p.145)

The impact on stress results of small differences in Poisson's ratio is anticipated to be negligible. Stress formulas for cylindrical shells (Reference 2.2.13, Table 30) indicate insensitivity to Poisson's ratio. For the loading case of uniform radial shear loads, the maximum hoop circumferential membrane stress, the key breaching stress, is proportional to Poisson's ratio, υ, through the term $(1-\upsilon^2)^{1/4}$. Using the lowest and highest υ values of the three 600 Series nickel-base alloys, 0.278 and 0.290, the difference in maximum hoop circumferential membrane stress values is a negligible 0.2%. Therefore, the study of parametric variations provides verification of this assumption per Reference 2.1.1 page 4 ("*Verification may include . . . studies of parametric variations*") and further verification of this assumption is not required. This assumption is used in Section 6.1 and corresponds to Section 6.1.1.7 in Reference 2.2.52.

3.2.5   Poisson's Ratio of 316L Stainless Steel

The RT Poisson's ratio of 316L SS is not published in traditional sources. Therefore the RT Poisson's ratio of 316 SS is assumed for 316L SS. The impact of this assumption is anticipated to be negligible.

Rationale– The chemical compositions of 316L SS and 316 SS are similar (see Reference 2.2.3, Section II, Part A, SA-240, Table 1) because they are both 300 Series (austenitic) SS. Therefore the differences in their Poisson's ratio values are expected to be small. The 300 Series SSs have a relatively small range of RT Poisson ratio values:

> Type 304 SS [UNS S304000] = 0.290 (Reference 2.2.2, p. 755, Figure 15)
> Type 316 SS [UNS S316000] = 0.298 (Reference 2.2.2, p. 755, Figure 15)
> Type 310 SS [UNS S310000] = 0.308 (Reference 2.2.2, p. 755, Figure 15)

The impact on stress results of small differences in Poisson's ratio is anticipated to be negligible. Stress formulas for cylindrical shells (Reference 2.2.13, Table 30) indicate insensitivity to Poisson's ratio. For the loading case of uniform radial shear loads, the maximum hoop circumferential membrane stress, the key breaching stress, is proportional to Poisson's ratio, υ, through the term $(1-\upsilon^2)^{1/4}$. Using the lowest and highest υ values of the three 300 Series SSs, 0.290 and 0.308, the difference in maximum hoop circumferential membrane stress values is a negligible 0.3%. Therefore, the study of parametric variations provides verification of this assumption per Reference 2.1.1 page 4 ("*Verification may include . . . studies of parametric variations*") and further verification of this assumption is not required. This assumption is used in Section 6.1 and corresponds to Section 6.1.1.9 in Reference 2.2.52.

3.2.6   Not Used

3.2.7   The Uniform Strain of 316L Stainless Steel

The RT uniform strain (strain corresponding to tensile strength) of 316L SS is not listed in traditional sources. Therefore, it is assumed that the RT uniform strain is 60% of the RT minimum specified elongation (strain corresponding to rupture point in tensile test).

Rationale– The shape of the stress-strain curve for 316L SS that leads to the 60% selection is based on testing of "as-received" 316L SS material at a moderate strain rate, 8 *s⁻¹* (see Reference 2.2.6, p. 305). Therefore this assumption does not require verification. This assumption is used in Section 6.1.1 and corresponds to Section 6.1.1.4 in Reference 2.2.52.

3.2.8   The Uniform Strain of Alloy 22

The RT uniform strain of Alloy 22 is not listed in traditional sources. Therefore, it is assumed that the RT uniform strain is 90% of the RT minimum specified elongation for Alloy 22.

Rationale– The rationale for this assumption is based on measurements of RT engineering stress-strain curves for Alloy 22 (DTN: LL020603612251.015, Reference 2.2.7). The use of Reference 2.2.7 was approved as the appropriate data for the intended use in an Information Exchange Document (Reference 2.2.25).   Therefore this assumption does not require verification. This assumption is used in Section 6.1.1 and corresponds to Section 6.1.1.5 in Reference 2.2.52.

3.2.9   The Uniform Strain of 316 Stainless Steel

The uniform strain of 316 SS is not listed in traditional sources. Therefore, it is assumed that the RT uniform strain is 90% of the RT minimum specified elongation.

Rationale– The rationale for this assumption is the shape of the stress-strain curve for 316 SS from a qualified source (Reference 2.2.6, p. 304). Therefore this assumption does not require verification. This assumption is used in Section 6.1.1 and corresponds to Section 6.1.1.5 in Reference 2.2.52.

3.2.10   Friction Coefficient between 316 and 316L Stainless Steel

The friction coefficient for contacts occurring between the 316 SS and 316L SS is not available in traditional sources. It is, therefore, assumed that the dynamic (sliding) friction coefficient for this contact is 0.4.

Rationale– The rationale for this assumption is that this friction coefficient represents the lower (conservative – less energy lost due to WP internal component sliding contact) bound for the steel-on-steel contacts (Reference 2.2.9, Table 3.2.1, p. 3-26 and Reference 2.2.10, p. 441). Therefore this assumption does not require verification. This assumption is used in Section 6.4 and corresponds to Section 6.1.1.14 in Reference 2.2.52.

3.2.11   Friction Coefficient between Alloy 22 and Other Metallic Materials

The friction coefficients for contacts among the Alloy 22 components, or the contacts involving Alloy 22 and 316 SS, are not available in traditional sources. It is, therefore, assumed that the dynamic (sliding) friction coefficient for both of these contacts is 0.4.

Rationale– This friction coefficient represents the lower (conservative – less energy lost due to WP component sliding contact) bound for most dry nickel-on-steel and nickel-on-nickel contacts (Reference 2.2.9, Table 3.2.1, p. 3-26); nickel being the dominant component in Alloy 22 (Reference 2.2.3, Section II, Part B, SB-575, Table 1). Therefore this assumption does not require verification. This assumption is used in Section 6.4 and corresponds to Section 6.1.1.15 in Reference 2.2.52.

3.2.12   Friction Coefficient between Metal and Rock

The friction coefficient for contacts occurring between the rock and Alloy 22 (OCB) is not available in traditional sources. It is, therefore, assumed that the dynamic (sliding) friction coefficient for this contact is 0.525.

Rationale– For an estimate of the dynamic metal-on-stone friction coefficient values it is recommended (Reference 2.2.11, p. 306) that the static metal-on-stone friction values be reduced by 25%. Reducing the upper bound static metal-on-stone friction value in Reference 2.2.11 (Table 8.1, p. 306) by 25% leads to 0.525. This estimated dynamic friction value represents the upper (conservative – less rock spread) end of the range of dynamic friction and therefore does not require verification. This assumption is used in Section 6.4 and corresponds to Section 6.1.1.21 in Reference 2.2.52.

3.2.13   Variation of Functional Friction Coefficients

The variation of functional friction coefficient between the static and dynamic values as a function of relative velocity of the surfaces in contact is not available in traditional sources for the materials used in this calculation. Therefore, the effect of relative velocity of the surfaces in contact is neglected in these calculations by assuming that the functional friction coefficient and static friction coefficient are both equal to the dynamic friction coefficient. The impact of this assumption on results presented in this document is anticipated to be negligible.

Rationale– This assumption provides a conservative bounding set of results by minimizing the friction coefficient within the given finite element analysis framework (the lone exception being the use of the upper bound of the estimated dynamic friction between metal and rock as discussed in Assumption 3.2.12). Therefore this assumption does not require verification. This assumption is used in Section 6.4 and corresponds to Section 6.1.1.16 in Reference 2.2.52.

3.2.14   Rock Shape

The rock shape is assumed to be a rectangular prism.

Rationale– The rock blocks geometry data in *Drift Degradation Analysis* (Reference 2.2.59, Appendix I) shows that some of the rock blocks are essentially rectangular prisms. A finite element representation (FER) of the rock with an inclined rectangular prism provides a conservative approach from the point of view that the rock center of gravity is located directly above the point of impact, transferring the maximum linear momentum to the WP. Therefore this assumption does not require verification. The sharp edge of the prism also results in maximum stresses in the WP. This assumption is used in Sections 6.3 and 6.4.

3.2.15   Material Properties of Rock Not Adjusted for Nominal PRA Analysis

The recommended material property set of the TSw2 nonlithophysal rock does not need to be nominally-adjusted for the mean Alloy 22 Capability analyses.

Rationale– The rationale for this assumption is that the TSw2 rock material strength is data derived and there is no known amount of margin in the reported compressive strength value. Additionally, the TSw2 rock material is modeled as an elastic-ideally-plastic material so the stress level in the rock will be limited to the compressive strength of the rock material. An incremental strength increase, e.g. a 10% increase like the one applied to the materials of the inner vessel, of the rock material will have only a limited and small affect on the structural response of the OCB. Therefore this assumption does not require verification. This assumption is used in Section 6.1.2. Section 7.4.2 and Appendix II describe the analysis of the rock compressive strength variability.

3.2.16   Material Properties of Invert Lattice Not Adjusted for PRA Analysis

The material property set of the steel in the invert lattice structure, A 588 alloy steel (Reference 2.2.54), does not need to be 10% strength adjusted for the Capability analyses.

Rationale– The rationale for this assumption is that any small strength adjustments to the invert lattice material will have an insignificant effect on the OCB structural response. Therefore this assumption does not require verification. This assumption is used in Section 6.1.2.

3.2.17   Material Properties of Co-disposal WP Internals Not Adjusted for PRA Analysis

The material properties for the basket structure and DHLW canisters in the Co-disposal Short WP do not need to be strength adjusted for the Capability analysis. The same material properties used in the deterministic analyses (Reference 2.2.53, Section 7.2) can be used in the Capability analyses.

Rationale– This assumption is based on the small to negligible difference to OCB structural response that is be expected if the material properties of the basket structure and DHLW canisters are adjusted to account for a "best-estimate" increase in strength over Code minimums, e.g. 10% strength increase (Reference 2.2.52, I-3.1). Because vendor averaged data is used for the material properties of the OCB, which is 1 *in*. (0.0254 *m*) thick, and 10% strength adjusted properties values are used for the inner vessel, which is 2 *in*. (0.0508 *m*) thick, the affect of a 10% strength increase in the material of the Co-disposal Short WP basket structure and the DHLW canisters is not expected to be significant. This assumption is used in 6.1.2

3.2.18   Mean Compressive Strength of Rock

A recommended value of the nonlithophysal rock block compressive strength, 70 *MPa* (10 *ksi*), is provided in Reference 2.2.17, Figure 1. Therefore, for the purpose of the present calculation, the mean compressive strength of the rock blocks is assumed to be 70 *MPa* (10 *ksi*).

Rationale– This assumption is based on the recommended compressive strength value for nonlithophysal rock blocks of significant size (3000 *mm* (118 *in*), Reference 2.2.17, Figure 1). The compressive strength value is the stress point in the rock after which the constitutive behavior of the rock is assumed to be ideally perfectly plastic with constant stress as strain increases. This assumption is used in Sections 6.1 and 7.4.2 and corresponds to Section 6.1.1.18 in Reference 2.2.52.

3.2.19   Poisson's Ratio and Modulus of Elasticity of Rock

The mean values of the modulus of elasticity and Poisson's ratio of the TSw2 rock are given in Reference 2.2.17, Table 2. For the purpose of the present calculation, the mean values of modulus of elasticity, 33.6 *GPa* ($4.87 * 10^6$ *psi*), and Poisson's ratio, 0.20, are used.

Rationale– The mean values for Poisson's ratio and modulus of elasticity agree well with typical values of said properties for the nonlithophysal rocks in which some of the emplacement drifts are expected to be placed. These material parameters are insignificant in comparison to the compressive strength chosen. Therefore this assumption will have negligible effect on the calculation results and does not require verification. This assumption is used in Section 6.1 and corresponds to Section 6.1.1.19 in Reference 2.2.52.

3.2.20   Rock Density

The density of the TSw2 rock is assumed to be 2411 *kg/m³* (0.0871 *lb/in³*).

Rationale– The density value is the mean density value of all Topopah Spring Welded rocks in Reference 2.2.17, Table 1. It should be noted though that this assumption has no significant effect on the calculation results since the important input parameter is the mass of the rock regardless of the density. Therefore this assumption does not require verification. The rock

shape is discussed in Assumption 3.2.14. Small adjustments to the density are made in the LS-DYNA input to provide an accurate rock mass. This assumption is used in Sections 6.1 and 6.3 and corresponds to Section 6.1.1.20 in Reference 2.2.52.

3.2.21   Poisson's Ratio for 304L Stainless Steel

Poisson's ratio for 304L SS is not published in traditional sources. Therefore, it is assumed to be the same as Poisson's ratio for 304 SS (Reference 2.2.2, Figure 15, p. 755).

Rationale– The rationale for this assumption is that the chemical compositions of 304L SS and 304 SS are similar (Reference 2.2.3, Section II, Part A, SA-240, Table 1) because they are both 300 Series (austenitic) SSs. Therefore the differences in their Poisson's ratio values are expected to be small. The 300 Series SSs have a relatively small range of RT Poisson ratio values:

> Type 304 SS [UNS S304000] = 0.290 (Reference 2.2.2, p. 755, Figure 15)
> Type 316 SS [UNS S316000] = 0.298 (Reference 2.2.2, p. 755, Figure 15)
> Type 310 SS [UNS S310000] = 0.308 (Reference 2.2.2, p. 755, Figure 15)

The impact on stress results of small differences in Poisson's ratio is anticipated to be negligible. Stress formulas for cylindrical shells (Reference 2.2.13, Table 30) indicate insensitivity to Poisson's ratio. For the loading case of uniform radial shear loads, the maximum hoop circumferential membrane stress, the key breaching stress, is proportional to Poisson's ratio, υ, through the term $(1-\upsilon^2)^{1/4}$. Using the lowest and highest υ values of the three 300 Series SSs, 0.290 and 0.308, the difference in maximum hoop circumferential membrane stress values is a negligible 0.3%. Therefore, the study of parametric variations provides verification of this assumption per Reference 2.1.1 page 4 ("*Verification may include . . . studies of parametric variations*") and further verification of this assumption is not required. This assumption is used in Section 6.1 and corresponds to Section 6.1.1.10 in Reference 2.2.52.

3.2.22   Uniform Strain of A 516 Carbon Steel

The uniform strain of A 516 carbon steel (CS) is not listed in traditional sources. Therefore, it is conservatively assumed that the uniform strain is 50 percent of the elongation.

Rationale– The rationale for this assumption is based on measurements of the stress-strain curve for A 36 CS (Reference 2.2.6, p. 186), which has a similar chemical composition as A 516 CS (Reference 2.2.3, Section II, Part A, SA-516/SA-516M, Table 1 and SA-36/SA-36M, Table 2). Use of this assumption is limited to the waste form basket structure whose behavior will have an insignificant effect on the OCB structural response. Therefore this assumption does not require verification. This assumption is used in Section 6.1.1 and corresponds to Section 6.1.1.3 in Reference 2.2.52.

3.2.23   Strain Rate Dependent Properties of Rock

The strain rate-dependent properties of the TSw2 rock block are not published in traditional sources. The properties obtained under the static loading conditions are assumed for the rock block. The impact of using properties obtained under static loading conditions is anticipated to be small.

Rationale– The rationale for this assumption is that "the properties of most rocks can be regarded as being virtually independent of strain rate in the range covered by the usual laboratory tests" (Reference 2.2.22, p. 144) and that the strain rates in the rock are low at the time of maximum stress in the OCB. Therefore this assumption does not require verification. This assumption is used in Section 6.1.

3.2.24   Simplification of Loaded Internals of the WP

The geometries of the loaded commercial waste form and basket internals of the WPs are simplified for the purpose of efficient structural calculations. For all TAD bearing WP cases except cases involving mid WP rock impacts, the TAD canistered SNF are developed as thick shell cylinders in the TAD canister with the appropriate mass values to account for the waste forms and internal structures that are not explicitly modeled. The maximum recordable weight, 49,320 *kg* (54.25 *ton*) (Reference 2.2.26, Figure C-17, Note 3), is assumed to be distributed evenly in a thick-walled (9.1 *in* (23 *cm*) – see Section 6.2.1) cylinder with a 15 *in* (38 *cm*) top plug and 3.5 *in* (8.9 *cm*) bottom lid (Reference 2.2.20, Drawing 6253E73) and properties of 316L SS (Reference 2.2.26, Figure C-17, Note 1). Additionally, the overall center of gravity of the total mass of the canister is located 110.6 *in* (2.81 *m*) from the bottom external surface and satisfies the Reference 2.2.26, Figure C-17 specification to be between 103 and 123 *in* (2.62 and 3.12 *m*).

For rock impact on the middle of the TAD bearing WP the wall of the TAD canister was represented with a 1 *in* (2.54 *cm*) thickness and the total mass of the TAD canister was maintained by increasing the density of the TAD canister material.

Rationale– The rationale for modeling the TAD canister as a thick shelled cylinder is that it simplifies the FER while preserving the mass effects that a fully loaded canister could impart on the OCB structural response to rock impact. Note that the use of information from Reference 2.2.26, Figure C-17 is suitable since the reference document has been established as a requirement (Reference 2.2.16, Section 12.2.1.2). This assumption is used in Section 6.2.

3.2.25   The Uniform Strain of A 588 Alloy Steel

The RT uniform strain of A 588 alloy steel [UNS K11430] is not listed in traditional sources. Therefore, it is assumed that the uniform strain is 66% of the minimum specified elongation.

Rationale– The rationale for this assumption is based on measurements of RT engineering stress-strain curves for structural steels (Reference 2.2.6, p. 186 and 189). Therefore this assumption does not require verification. This assumption is used in Section 6.1.

3.2.26   The Uniform Strain of 304L Stainless Steel

The uniform strain of 304L SS is not listed in traditional sources. Therefore, it is assumed that the uniform strain is 75% of the minimum specified elongation.

Rationale– The rationale for this assumption is based on measurements of RT engineering stress-strain curves for 304 SS (Reference 2.2.6, p. 294), which has a similar chemical composition to 304L SS (Reference 2.2.3, Section II, Part A, SA-240, Table 1). Therefore this assumption does not require verification. This assumption is used in Section 6.1.2.

4. METHODOLOGY

4.1 QUALITY ASSURANCE

This calculation was prepared in accordance with EG-PRO-3DP-G04B-00037, *Calculations and Analyses* (Reference 2.1.1). The WPs are classified as Safety Category items (important to safety [ITS] and important to waste isolation [ITWI]) (Reference 2.2.16, Section 11.1.2). The EP is classified as ITWI (Reference 2.2.16, Section 8.1.2). Therefore, the approved version of this document is designated as QA: QA.

The emplacement drift steel invert structure drawing (Reference 2.2.54) is a QA: N/A document. However, the use of this source as an input is justified because emplacement drift steel invert is classified as non-ITS and non-ITWI (Reference 2.2.16, Section 8.1.2).

4.2 USE OF SOFTWARE

The computer code used for dynamic structural analysis in this calculation is the commercially available LS-DYNA finite element analysis package. Two versions of the LS-DYNA code were use to perform the structural analysis. LS-DYNA V.970.3858 D MPP (Software Tracking Number [STN]: 10300-970.3858 D MPP-00, Reference 2.2.23) and LS_DYNA V.971.7600.2.1116 D MPP (STN: 10300-971.7600.2.1116-00, Reference 2.2.24). LS-DYNA is obtained from Software Configuration Management in accordance with appropriate procedures. Each version of the LS-DYNA code has an available validation test report (Reference 2.2.27 and 2.2.29). LS-DYNA is a commercially available FEA code and is appropriate for the WP structural analyses performed in this calculation. The simulations that use LS-DYNA V.970.3858 D MPP are performed on a Hewlett-Packard (HP) Itanium2 platform cluster which uses the HP-UX 11.22 operating system. The HP Itanium2 platform computer cluster used with LS-DYNA V.970.3858 D MPP is identified with one tag number: 501711. The simulations performed with LS-DYNA V.971.7600.2.1116 D MPP are on a Hewlett-Packard (HP) Itanium2 platform cluster which uses the HP-UX 11.23 operating system. The HP Itanium2 platform computer cluster used with LS-DYNA V.971.7600.2.1116 D MPP is identified with one tag number: YMP005000. All workstations are located in Las Vegas, Nevada. The LS-DYNA evaluations performed for this calculation are fully within the range of the validation tests (References 2.2.27 and 2.2.29) performed for the LS-DYNA code. Access to the code is granted by Software Configuration Management in accordance with the appropriate procedures. LS-DYNA is listed in the *Repository Project Management Automation Plan* (Reference 2.1.3, Table 6-1). The results of this calculation are provided in terms of effective stresses (VM stresses) and expended toughness fractions (ETF).

The finite element mesh, which is subsequently used in the LS-DYNA solver, is developed using TrueGrid Version 2.3 (hereinafter referred to as "TrueGrid"). TrueGrid is a pre-processing tool for graphical and geometrical representation and therefore is Level 2 software as defined in *Software Management* (Reference 2.1.2, Section 4 and Attachment 12).   The meshing is executed on two HP 9000 series UNIX workstations (Operating System HP-UX 11.0), identified with Yucca Mountain Project tag numbers 150691 and 151324, and located in Las Vegas, Nevada. The suitability and adequacy of the mesh generated using TrueGrid is based on visual examination, engineering judgment, and the results of the mesh verification exercise performed

in section 7.1. TrueGrid is listed in the *Repository Project Management Automation Plan* (Reference 2.1.3, Table 6-1).

LS-PREPOST V1.0 (Livermore Software Technology Corporation) is the postprocessor used only for visual display and graphical representation of LS-DYNA FERs and results and therefore is Level 2 software as defined in Reference 2.1.2, Attachment 12. The suitability and adequacy of the displayed results is based on visual examination and engineering judgment. The post processing is performed on either the HP Itanium2 (IA64) series UNIX servers (Operating System HP-UX 11.22), collectively identified with the Yucca Mountain Project tag number 501711, or on the HP Itanium2 (IA64) series UNIX servers (Operating System HP-UX 11.23), collectively identified with the Yucca Mountain Project tag number YMP005000. Both clusters of servers are located in Las Vegas, Nevada.

The commercially available Microsoft Office Excel 2003 (11.8105.8107 SP2) spreadsheet code, which is a component of Microsoft Office 2003 Professional, is used to perform simple data conversion (maximum shear stress to stress intensity) and plotting. These results were verified by checks using hand calculations and plots were verified by visual inspection. Usage of Microsoft Office 2003 Professional in this calculation constitutes Level 2 software usage, as defined in IT-PRO-0011 (Reference 2.1.2, Section 4 and Attachment 12). Microsoft Office 2003 Professional is listed in the current controlled Software Report, as well as the Repository Project Management Automation Plan (Reference 2.1.3, Table 6-1). Microsoft Office Excel 2003 was executed on a PC with X86 architecture running the Microsoft Windows XP Professional operating system, Version 5.1.2600, Service Pack 2, Build 2600.

Due to the size of the files associated with this calculation, both input and output, some files have been electronically compressed using commercially available software packages. On the HP-UX platform computers the GZIP command is used to compress or uncompress files, this command comes packaged with the HP-UX 11.22 operating system. The HP-UX platform computer cluster where use of the GZIP command was performed is identified with one tag number: 501711. The files that were compressed were verified to uncompress correctly by hand check and visual inspection.

All other calculations reported in this document are performed by hand.

The LS-DYNA input files, identified by .k and .inc file extensions, and LS-DYNA output files ("d3hsp") are provided in Attachment I. The input files for TrueGrid, identified by .tg file extensions are provided in Attachment I. The TrueGrid output files have the .inc extensions.

4.3 APPROACH

This is a summary description of the methodology used to conduct this calculation.

1. Using the TrueGrid software package, discretize a finite element representation (FER) of a TAD bearing WP that is formatted for the LS-DYNA "keyword" input. Hand calculations are performed to calculate the wall thickness of the simplified loaded TAD canister (see Assumption 3.2.24 and Section 6.2.1) and to adjust dimensions of the variously sized falling rocks (see Section 6.3). Modify the TAD bearing WP FER to create a FER for the Co-disposal Short WP, replacing the TAD canister with the

Co-disposal Short WP basket and internals. The TAD bearing WP FER, Co-disposal Short WP FER, and EP FER are based on the drawings and sketches in References 2.2.30 through 2.2.49.

2. Set up LS-DYNA input deck to simulate the WP being struck by an emplacement drift rock fall (Nonlithophysal zone). Selection of material properties and rock impact event sequence parameters are described in the *Waste Package Component Design Methodology Report* (Reference 2.2.52, Sections 6.1 and 7.1.2.5). Hand calculations are performed to derive the Tangent Moduli of the materials used in the LS-DYNA models, see Sections 6.1.1 and 6.1.2. The OCB material strength properties used for the Capability analysis are based on best estimate values derived from published vendor expected strength values (References 2.2.8, 2.2.50, and 2.2.51) and adjusted, using a worst case triaxiality factor per Section 7.1.7.2.4 of Reference 2.2.52. The best estimate material properties for WP components other than the OCB and Co-disposal Short WP internals (see Assumption 3.2.17) are based on 1.1 times the ASME Code minimum strength values, also, per Section 7.1.7.2.4 of Reference 2.2.52.

3. Verify the level of mesh discretization that is adequate for this analysis using the mesh optimization technique described in the *Waste Package Component Design Methodology Report* (Reference 2.2.52, Section 7.1.3).

4. Simulate rock impacts on two locations that will capture the maximum effective stresses that could be generated in the OCB due to preclosure rock impacts. The impact locations considered are: a point at the middle of the WP length, and the lower WP sleeve. These locations exhibited the highest primary membrane stress intensities in the OCB during the deterministic rock impact calculation (Reference 2.2.53, Section 7.2). Modify each FER so that the level of mesh discretization is adequate at each of the impact locations.

5. Analyze the Co-disposal Short WP and TAD bearing WP using both the lower WP sleeve impact location and the middle WP impact location. The simulations will analyze the primary membrane effective stresses (VM) generated in the OCB of a Co-disposal Short WP or TAD bearing WP due to the full range of rock masses and impact velocities (Reference 2.2.28, Table 2 and Table 6). Additionally, impacts by rocks of mass equal to a maximum loaded Co-disposal Short WP or a TAD bearing WP are simulated for each of those respective WP types to fully capture the Capability of the OCB. For the Capability analysis to support the PRA the OCB material's Toughness Index (I_T) and Expended Toughness Fraction (ETF) for each rock impact scenario is calculated per Section 7.1.7.2.2 of Reference 2.2.52.

5. LIST OF ATTACHMENTS

		Number of Pages
Attachment I.	Figures obtained from LS-DYNA	6
Attachment II.	Plots of Capability Variability Including Rock Compressive Strength Variability	4
Attachment III.	Directory Listing of (Data DVD) Electronic Files	12
Attachment IV.	Data DVD Attachment	Electronic file, 1 disk

6. BODY OF CALCULATION

6.1 MATERIAL PROPERTIES

The RT material properties for the metals listed below are obtained under static loading conditions (see Assumptions 3.1.1, 3.2.1 and 3.2.3). Also, RT material properties obtained under static loading conditions are used for TSw2 rock (see Assumptions 3.2.2 and 3.2.23).

Stress units are Pascal (*Pa*), Mega Pascal (*MPa* = 10^6 *Pa*), Giga Pascal (*GPa* = 10^9 *Pa*), lb/in^2 (*psi*) and *ksi* = 10^3 *psi*.

6.1.1 Listing of ASME Material Properties

Unless noted, the material properties listed in this section are at room temperature.

Alloy 22 [ASME SB-575 UNS N06022] (EP):

- Density = 8690 *kg/m*^{3} (0.314 *lb/in*^{3})
  (Reference 2.2.3, Section II, Part B, SB-575, Section 7.1)
- Poisson's ratio = 0.278
  (Assumption 3.2.4)
- Elongation = 0.45
  (Reference 2.2.3, Section II, Part B, SB-575, Table 4)
- Modulus of Elasticity = 206 *GPa* (29.9 x 10^6 *psi*)
  (Reference 2.2.8, p.14, Table "Average Dynamic Modulus of Elasticity")
  This data is the best available and suitable for its use in this calculation.
- Yield Strength = 310 *MPa* (45.0 *ksi*)
  (Reference 2.2.3, Section II, Part D, Subpart 1, Table Y-1)
- Tensile Strength = 689 *MPa* (100 *ksi*)
  (Reference 2.2.3, Section II, Part D, Subpart 1, Table U)

316 SS [ASME SA-240 UNS S31600] (EP Tube 1, Interface Ring, Inner Vessel and Shear Ring):

- Density = 7980 kg/m^3 (0.288 lb/in^3)
    (Reference 2.2.4, Table X1.1, p. 7)
- Poisson's ratio = 0.298
    (Reference 2.2.2, Figure 15, p. 755)
- Elongation = 0.40
    (Reference 2.2.3, Section II, Part A, SA-240, Table 2)
- Modulus of elasticity = 195 GPa (28.3·10^6 psi)
    (Reference 2.2.3, Section II, Part D, Subpart 2, Table TM-1)
- Yield strength = 207 MPa (30.0 ksi)
    (Reference 2.2.3, Section II, Part D, Subpart 1, Table Y-1)
- Tensile strength = 517 MPa (75.0 ksi)
    (Reference 2.2.3, Section II, Part D, Subpart 1, Table U)

316L SS [ASME SA-240 UNS S31603]
    (TAD Canister (Assumption 3.1.2) and DOE SNF Canister (Ref. 2.2.16, Section 11.2.2.8)):

- Density = 7980 kg/m^3 (0.288 lb/in^3)
    (Reference 2.2.4, Table X1.1, p. 7)
- Poisson's ratio = 0.298
    (Assumption 3.2.5)
- Elongation = 0.40
    (Reference 2.2.3, Section II, Part A, SA-240, Table 2)
- Modulus of elasticity = 195 GPa (28.3·10^6 psi)
    (Reference 2.2.3, Section II, Part D, Subpart 2, Table TM-1)
- Yield strength = 172 MPa (25.0 ksi)
    (Reference 2.2.3, Section II, Part D, Subpart 1, Table Y-1)
- Tensile strength = 483 MPa (70.0 ksi)
    (Reference 2.2.3, Section II, Part D, Subpart 1, Table U)

304L SS [ASME SA-240 UNS S30403]
    (HLW canisters, Reference 2.2.16, Section 11.2.2.7):

- Density = 7980 kg/m^3 (0.288 lb/in^3)
    (Reference 2.2.4, Table X1.1, p. 7)
- Poisson's ratio = 0.29
    (Assumption 3.2.21)
- Elongation = 0.40
    (Reference 2.2.3, Section II, Part A, SA-240, Table 2)
- Modulus of elasticity = 195 GPa (28.3·10^6 psi)
    (Reference 2.2.3, Section II, Part D, Subpart 2, Table TM-1)

- Yield strength = 172 *MPa* (25.0 *ksi*)
      (Reference 2.2.3, Section II, Part D, Subpart 1, Table Y-1)
- Tensile strength = 483 *MPa* (70.0 *ksi*)
      (Reference 2.2.3, Section II, Part D, Subpart 1, Table U)

A 516 CS [ASME SA-516 UNS K02700]
      (Divider Plate Assembly (Reference 2.2.47)):

- Density = 7850 *kg/m*^{3} (0.284 *lb/in*^{3})
      (Reference 2.2.3, Section II, Part A, SA-20/SA20M, Section 14.1)
- Poisson's ratio = 0.30
      (Reference 2.2.5, p. 374)
- Elongation = 0.21
      (Reference 2.2.3, Section II, Part A, SA-516/SA-516M, Table 2)
- Modulus of elasticity = 203 *GPa* (29.5·10^6 *psi*)
      (Reference 2.2.3, Section II, Part D, Subpart 2, Table TM-1)
- Yield strength = 262 *MPa* (38.0 *ksi*)
      (Reference 2.2.3, Section II, Part D, Subpart 1, Table Y-1)
- Tensile strength = 483 *MPa* (70.0 *ksi*)
      (Reference 2.2.3, Section II, Part D, Subpart 1, Table U)

A 588 alloy steel [ASTM A 588, Grade 50 [UNS K11430]]; A 36 CS density, Poisson's ratio and modulus of elasticity used (Invert steel lattice (Assumption 3.2.25 and Reference 2.2.54)):

- Density = 7860 *kg/m*^{3} (0.284 *lb/in*^{3})
      (Reference 2.2.4, Table X1.1, page 7)
- Poisson's ratio = 0.30
      (Reference 2.2.5, p. 374)
- Elongation = 0.21
      (Reference 2.2.3, Section II, Part A, Table 2)
- Modulus of elasticity = 203 *GPa* (29.5·10^6 *psi*)
      (Reference 2.2.3, Section II, Part D, Subpart 2, Table TM-1)
- Yield strength = 345 *MPa* (50.0 *ksi*)
      (Reference 2.2.3, Section II, Part D, Subpart 1, Table Y-1)
- Tensile strength = 483 *MPa* (70.0 *ksi*)
      (Reference 2.2.3, Section II, Part D, Subpart 1, Table U)

TSw2 Rock (used in all simulations):

- Density = 2411 *kg/m*^{3} (0.0871 *lb/in*^{3})
      (Assumption 3.2.20)
- Poisson's ratio = 0.20
      (Assumption 3.2.19)
- Modulus of elasticity = 33.66 *GPa* (4.87 x 10^6 *psi*)
      (Assumption 3.2.19)

- Unconfined compressive strength = 70 *MPa* (10.0 *ksi*)
  (Assumption 3.2.18)

Calculation of True Measures of Ductility for the ASME Material Properties

The material properties in Section 6.1.1 refer to engineering stress and strain definitions: $S = P / A_0$ and $e = (L - L_0) / L_0$ (see Reference 2.2.1, Chapter 9). Where P stands for the force applied during a static tensile test, L is the length of the deformed specimen, and L_0 and A_0 are the original length and cross-sectional area of the specimen, respectively. The engineering stress-strain curve does not give a true indication of the deformation characteristics of a material during plastic deformation since it is based entirely on the original dimensions of the specimen. Hence, the constitutive relation in LS-DYNA is defined in terms of true stress and strain: $\sigma = P / A$ and $\varepsilon = \ln(L / L_0)$ where A is the deformed area (Reference 2.2.1, Chapter 9).

The relationships between the true stress and strain definitions and the engineering stress and strain definitions, $\sigma = S(1 + e)$ and $\varepsilon = \ln(1 + e)$, can be readily derived based on constancy of volume ($A_0 L_0 = AL$) and strain homogeneity during plastic deformation (Reference 2.2.1, Chapter 9). These expressions are applicable only in the hardening region of the stress-strain curve that is limited by the onset of necking.

The following parameters are used in the subsequent calculations:

$S_y \cong \sigma_y$ = yield strength
S_u = engineering tensile strength
σ_u = true tensile strength
$e_y \cong \varepsilon_y$ = strain corresponding to yield strength
e_u = engineering strain corresponding to tensile strength (engineering uniform strain)
ε_u = true strain corresponding to tensile strength (true uniform strain)

In absence of data on the uniform strain in traditional sources, the uniform strain needs to be estimated based on the character of stress-strain curves and elongation (strain corresponding to rupture of the tensile specimen).

For Alloy 22 and 316 SS, a reduction in elongation by 10% is assumed for the RT uniform strain (see Assumptions 3.2.8 and 3.2.9).

For Alloy 22;
$e_u = 0.9 * \text{Elongation} = 0.9 * 0.45 = 0.41$
$\varepsilon_u = \ln(1 + e_u) = \ln(1 + 0.41) = 0.34$
$\sigma_u = S_u(1 + e_u) = 689(1 + 0.41) = 971$ *MPa* (141 *ksi*)
Therefore, the true tensile strength of Alloy 22 at RT is 971 *MPa* (141 *ksi*).

For 316 SS;
$e_u = 0.9 * \text{Elongation} = 0.9 * 0.40 = 0.36$
$\varepsilon_u = \ln(1 + e_u) = \ln(1 + 0.36) = 0.31$
$\sigma_u = S_u(1 + e_u) = 517(1 + 0.36) = 703$ *MPa* (102 *ksi*)

Therefore, the true tensile strength of 316 SS at RT is 703 *MPa* (102 *ksi*).

For 316L SS the RT uniform strain is assumed to be 60% of RT elongation (see Assumption 3.2.7).

For 316L SS;
e_u = 0.6 * Elongation = 0.6 * 0.40 = 0.24
ε_u = ln (1 + e_u) = ln (1 + 0.24) = 0.22
σ_u = S_u (1 + e_u) = 483 (1 + 0.24) = 599 *MPa* (86.9 *ksi*)
Therefore, the true tensile strength of 316L SS at RT is 599 *MPa* (86.9 *ksi*).

For A 516 CS the RT uniform strain is assumed to be 50% of RT elongation value for A 36 CS (see Assumption 3.2.22).
e_u = 0.5 * Elongation = 0.5 * 0.21 = 0.105
ε_u = ln (1 + e_u) = ln (1 + 0.105) = 0.10
σ_u = S_u (1 + e_u) = 483 (1 + 0.105) = 534 *MPa* (77.4 *ksi*)
Therefore, the true tensile strength of A 516 CS at RT is 534 *MPa* (77.4 *ksi*).

For 304L SS the RT uniform strain is assumed to be 75% of the RT elongation value for 304 SS (Assumption 3.2.26).
e_u = 0.75 * Elongation = 0.75 * 0.40 = 0.30
ε_u = ln (1 + e_u) = ln (1 + 0.30) = 0.26
σ_u = S_u (1 + e_u) = 483 (1 + 0.30) = 628 *MPa* (91.1 *ksi*)
Therefore, the true tensile strength of 304L SS at RT is 628 *MPa* (91.1 *ksi*).

Calculations for Tangent Moduli for the ASME Material Properties

The results of this simulation are required to include elastic and plastic deformations for all materials. When the materials are driven into the plastic range, the slope of the stress-strain curve continuously changes. A ductile failure is preceded by a protracted regime of hardening and substantial accumulation of inelastic strains. Thus, a simplification for the stress-strain curve is needed to incorporate plasticity into the FEA. A standard approximation commonly used in engineering is to use a straight line that connects the yield point and the tensile strength point of the material. The parameters used in the subsequent calculations in addition to those defined in Section 6.1.2 are modulus of elasticity (E) and tangent (hardening) modulus (E_1). The tangent modulus represents the slope of the stress-strain curve in the plastic region.

For Alloy 22 (used in OCB, WP Sleeves, and Pallet Base), the tangent modulus at RT is calculated using the true stress and strain values derived in Sections 6.1.1 and 6.1.2:
E_1 = (σ_u - σ_y) / (ε_u - σ_y / E) = (0.971 - 0.310) / (0.34 - 0.310 / 206) = 1.95 *GPa* (283 *ksi*)

For 316 SS (used in Inner Vessel and Pallet Longitudinal Posts) at RT:
E_1 = (σ_u - σ_y) / (ε_u - σ_y / E) = (0.703 - 0.207) / (0.31 - 0.207 / 195) = 1.60 *GPa* (232 *ksi*)

For 316L SS (used in TAD Canister and DOE SNF Canister in the Co-disposal Short WP) at RT:
E_1 = (σ_u - σ_y) / (ε_u - σ_y / E) = (0.599 - 0.172) / (0.22 - 0.172 / 195) = 1.95 *GPa* (283 *ksi*)

For A 516 CS (used in Co-disposal Short WP Basket Divider Plates) at RT:
$E_1 = (\sigma_u - \sigma_y) / (\varepsilon_u - \sigma_y / E) = (0.534 - 0.262) / (0.10 - 0.262 / 203) = 2.76$ *GPa* (400 *ksi*)

For 304L SS (used in HLW Canister Conceptualization in the Co-disposal Short WP) at RT:
$E_1 = (\sigma_u - \sigma_y) / (\varepsilon_u - \sigma_y / E) = (0.628 - 0.172) / (0.262 - 0.172 / 195) = 1.74$ *GPa* (253 *ksi*)

The steel invert structure is modeled as an elastic surface; therefore the Tangent Modulus of A 588 alloy steel is not required.

6.1.2   Listing of Vendor Supplied Material Properties

The Capability calculation uses adjusted material strength properties values from Section 6.1.1 for all WP components except the OCB. Vendor supplied material strength data is used for the OCB components of the WP. Furthermore, the vendor supplied material strength data used for the OCB is adjusted to account for material triaxiality affects. In the Capability calculation the material properties taken from 6.1.1 are adjusted by increasing the S_y, S_u, and elongation values by 10% (Reference 2.2.52, Section 7.1.7.2.4). The EP uses the same vendor supplied material strength data as the OCB, but no material triaxiality affects are incorporated.

The following vendor averaged Alloy 22 RT material properties values and PRA adjustments are taken directly from Reference 2.2.52, Table I-2 and Equations I-5 through I-9.

Vendor Averaged Alloy 22 RT Properties:

- Uniaxial yield strength, S_y and σ_y'$= 356$ *MPa* (52 *ksi*)

- Uniaxial engineering tensile strength, S_u'$= 764$ MPa (111 ksi)

- Uniform strain, e_u'$= 0.61$

- True strain, $\varepsilon_u = \ln(1 + e_u') = \ln(1 + 0.61) = 0.476$

- True stress, $\sigma_u = S_u \cdot (1 + e_u') = 764 \cdot (1 + 0.61) = 1230$ *MPa* (178 *ksi*)

Evaluations of the governing locations indicate the presence of more severe triaxiality gradients than VM stress and strain gradients, with some triaxiality ratios near the worst case value of 0.05. Therefore, the worst case triaxiality adjustment, ADJ=0.519 (Reference 2.2.52, Table I-3) is used to obtain triaxiality-adjusted vendor-averaged true ultimate strain, ε_u', and true ultimate (tensile) strength, σ_u', values:

$\varepsilon_u' = \ln(1 + ADJ \cdot e_u') = \ln (1 + 0.519 \cdot 0.61) = 0.275$

$\sigma_u' = S_u \cdot (1 + ADJ \cdot e_u') = 764 \cdot (1 + 0.519 \cdot 0.61) = 1006$ *MPa* (146 *ksi*)

Because a tri-linear representation of the stress-strain curve for Alloy 22 will be used for the OCB (Reference 2.2.52, Section 7.1.7.2.4, Figure 9) no stresses will be carried by the OCB above σ_u', as the onset of void formation is conceptualized.

Calculations for Tangent Moduli for the Vendor Supplied Material Properties

When the materials are driven into the plastic range, the slope of the stress-strain curve continuously changes. A simplification for the stress-strain curve is needed to incorporate plasticity into the FERs. A standard post-yield approximation commonly used in engineering is to use a straight line between the yield point and the ultimate tensile strength point of the material (bilinear elastoplastic representation). The tangent modulus represents the slope of the stress-strain curve in the plastic region.

LS-DYNA solutions are conducted using true stress and true strain. Therefore, a bilinear true stress – true strain curve is constructed. The only new parameter in the subsequent calculations is the tangent (hardening) modulus (E_1), the plastic region slope of this bilinear true stress – true strain curve.

For RT Capability analyses using vendor supplied average data Alloy 22 material properties (used in Pallet Base), the tangent modulus at RT is calculated using the true stress and strain values derived at the beginning of this Section:

$$E_1 = (\sigma_u - \sigma_y) / (\varepsilon_u - \sigma_y / E) = (1.230 - 0.356) / (0.476 - 0.356 / 206) = 1.84 \; GPa \; (267 \; ksi)$$

For RT Capability analyses with worst case triaxiality adjusted vendor supplied average data Alloy 22 material properties (used in OCB and WP Sleeves), the material vendor average data tangent modulus at RT with a triaxiality adjustment factor of 0.519 is calculated using the modified true stress and strain values, σ_u' and ε_u':

$$E_1 = (\sigma_u' - \sigma_y) / (\varepsilon_u' - \sigma_y / E) = (1.006 - 0.356) / (0.275 - 0.356 / 206) = 2.38 \; GPa \; (345 \; ksi)$$

In actuality, the adjusted Alloy 22 material properties model conceptualization used for the true stress-strain curve applied to the RT Capability analyses is input point-by-point to create a tri-linear curve and the E_1 value calculated above is not used.

In the case of 316 SS for the RT Capability calculations the 10% adjusted strength values are:

$\sigma_y \approx S_y = 1.1 \cdot 207 \; MPa = 228 \; MPa$
$S_u = 1.1 \cdot 517 \; MPa = 569 \; MPa$
$elongation \; = 1.1 \cdot 0.4 = 0.44$

This leads to:

$e_u = 0.9 \cdot elongation = 0.9 \cdot 0.44 = 0.396$
$\varepsilon_u = \ln(1 + e_u) = \ln(1 + 0.396) = 0.334$
$\sigma_u = S_u \cdot (1 + e_u) = 569 \cdot (1 + 0.396) = 794 \; MPa$
$\varepsilon_y = \sigma_y / E = (228 / 195) \cdot 10^{-3} = 1.17 \cdot 10^{-3}$
$E_1 = (\sigma_u - \sigma_y)/(\varepsilon_u - \varepsilon_y) = (0.794 - 0.228)/(0.334 - 1.17 \cdot 10^{-3}) = 1.70 \; GPa \; (0.246 \cdot 10^6 \; psi)$

In the case of 316L SS for the RT Capability calculations (used in TAD Canister and DOE SNF Canister in the Co-disposal Short WP), the 10% adjusted strength values are:

$\sigma_y \approx S_y = 1.1 \cdot 172 \; MPa = 189 \; MPa$
$S_u = 1.1 \cdot 483 \; MPa = 531 \; MPa$
$elongation = 1.1 \cdot 0.4 = 0.44$

This leads to:

$e_u = 0.6 \cdot elongation = 0.9 \cdot 0.44 = 0.264$
$\varepsilon_u = \ln(1 + e_u) = \ln(1 + 0.264) = 0.234$
$\sigma_u = S_u \cdot (1 + e_u) = 531 \cdot (1 + 0.264) = 671 \; MPa$
$\varepsilon_y = \sigma_y / E = (189 / 195) \cdot 10^{-3} = 0.97 \cdot 10^{-3}$
$E_1 = (\sigma_u - \sigma_y)/(\varepsilon_u - \varepsilon_y) = (0.671 - 0.189)/(0.234 - 0.97 \cdot 10^{-3}) = 2.07 \; GPa \; (0.300 \cdot 10^6 \; psi)$

For the purposes of the Capability analyses the material properties of the rock, the invert steel lattice (A 588 alloy steel), and the Co-disposal Short WP internals do not have their strength or elongation values increased by 10% (Assumptions 3.2.15, 3.2.16, and 3.2.17, respectively).

6.1.3   Constitutive Representation of Rock Behavior

In general, the constitutive representation of rock behavior (i.e., stress-strain relation) needs to address various complexities of rock deformation. In contrast to the brittle behavior of rock under tension, the stress-strain behavior of rock under compression can take numerous forms depending on the loading conditions (lateral confinement is a notable example), geometry (i.e., the slenderness ratio of the test specimen), and size. Brittle materials in general, when subjected to compression, exhibit a wide range of nonlinear stress-strain behaviors due to the nucleation, propagation, and coalescence of micro cracks under different boundary conditions (see Reference 2.2.22, Sections 4.2 through 4.5). Moreover, the compressive strength of brittle materials (including rock) is significantly higher than their tensile strength. Finally, unlike engineering metals, the rocks may exhibit nonlinear behavior even under moderate hydrostatic compression, and there is a significant effect of size on strength (see Reference 2.2.22; Sections 4, 6, and 7, for detailed discussion). A variety of constitutive representations have been developed to address the most prominent features of the behavior of brittle materials (for example, see Reference 2.2.21, pages 362 and 363). These complex constitutive representations require a large number of input parameters. Some of these are not available at present for TSw2, while others are not intrinsic properties of rock but rather fitting parameters whose estimation requires test data currently unavailable for TSw2. Thus, a reasonable simplification of rock constitutive behavior is necessary. Fortunately, the stress state of the rocks is of no interest in this analysis and the rock deformation is important only in as much as it affects the stresses and strains in the WP OCB, which is the objective of this calculation.

As a first approximation, the constitutive representation of rock behavior should appropriately capture local crushing of the rock at the point of impact, resulting in a reasonable distribution of impact energy across an enlarging contact area. It is, therefore, considered appropriate to simplistically represent the rock behavior as elastic-ideally-plastic (Figure 2 and Reference 2.2.22, Section 9). This representation of nonlinear behavior offers obvious advantages compared to the elastic representation for the given loading conditions. The unconfined compressive strength of rock, used as the yield strength in the constitutive representation, is the most important rock material property parameter in this study that affects the results. A

reasonable value of the unconfined compressive strength is, therefore, used to provide a mean set of results. Keeping in mind the large size of the rocks, 70 *MPa* is chosen as the representative mean rock strength (Assumption 3.2.18).
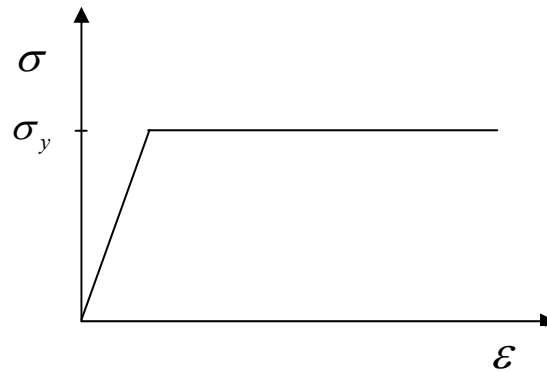
Figure 2.　　Elastic-Ideally-Plastic Constitutive Representation

6.2 MASS AND GEOMETRIC DIMENSIONS OF SPENT NUCLEAR FUEL CANISTERS

The following design parameters are used for the DHLW canisters to be loaded into a Co-disposal Short WP: mass = 2,500 *kg* (5512 *lb*), length = 3.0 *m* (118 *in*), outside diameter = 0.61 *m* (24 *in*), canister shell material is 304L SS (Reference 2.2.16, Section 11.2.2.7). In addition to these parameters: neck height = 0.21336 *m* (8.4 *in*), neck diameter = 0.1684 *m* (6.63 *in*) (Reference 2.2.26, Figure C-20). Note that the use of information from Reference 2.2.26, Figure C-20 is suitable since this has been established as a requirement (Reference 2.2.16, Section 11.2.2.2)

The following design parameters are used for the DOE SNF canisters (nominally 18 *in* x 10 *ft* (0.457 *m* x 3.048 *m*)) to be loaded into a Co-disposal Short WP: mass = 2,270 *kg* (5004 *lb*), length = 3.0 *m* (118 *in*), outside diameter = 0.4742 *m* (18.67 *in*), canister shell material is 316L SS (Reference 2.2.16, Section 11.2.2.8).

For the TAD canister, this calculation is performed by using the bounding mass and geometric dimensions of the Naval SNF long canister (Assumption 3.1.2) obtained from Reference 2.2.26, Figure C-17: maximum recordable total mass = 49,320 *kg* (54.25 *tons*), maximum outside diameter = 1.689 *m* (66.5 *in*), maximum length = 5.385 *m* (212 *in*), canister shell material is 316L SS (Assumption 3.1.2 and Reference 2.2.26, Figure C-17, Note 1). For the purposes of this calculation, the mass of the Naval SNF long canister is modeled as the maximum recordable total mass but the outside diameter is modeled as 1.679 *m* (66.12 *in*), and the length is modeled as 5.350 *m* (210.63 *in*). The internal structure of the WP is simplified in the FER by reducing the structure of the Naval SNF long canister to a thick walled (0.231 *m* (9.1 *in*) – see Section 6.2.1)

hollow cylinder with a 0.381 *m* (15 *in*) top shield and 0.089 *m* (3.5 *in*) bottom lid (Assumption 3.2.24)(Reference 2.2.20, Drawing 6253E73). The density of 316L SS is held constant as the cylinder wall thickness of the canister is back-calculated to closely match the maximum recordable mass of the Naval SNF long canister, See Section 6.2.1. Note that the overall center of gravity of the modeled canister is located 2.81 *m* (110.6 *in*) from the canister's bottom external surface (see Section 6.2.2) which satisfies the requirement that the center of gravity be located between 2.62 *m* and 3.12 *m* (103 *in* and 123 *in*)(Reference 2.2.26, Figure C-17).

In the rock impact on mid package scenario the distortions caused by the rock will include an inward deflection of the TAD canister side wall. In order to capture representative deflections of the TAD side wall, in the mid TAD bearing WP rock impact scenarios, the thickness of the TAD canister's side walls are reduced to 0.0254 *m* (1 *in*) thickness (Assumption 3.1.2) and the total mass of the TAD canister is maintained by increasing the density of the 316L SS used for the shell wall of the TAD canister cavity. The 316L SS density used for the TAD canister 0.0254 *m* (1 *in*) thick shell wall is back calculated to be ρ=63,784 *kg/m³* (2.304 *lb/in³*) in order to maintain the same over-all mass of the simplified TAD canister, see Section 6.2.3.

6.2.1   Calculations for TAD Canister Wall Thickness

Total length of Canister

= 210.63 *in*
= (210.63)/(12*3.281) *m*
= 5.3497 *m*

Top Lid (Plug) thickness

= 15 *in*
= (15)/(12*3.281) *m*
= 0.381 *m*

Bottom Lid thickness

= 3.5 *in*
= (3.5)/(12*3.281) *m*
= 0.0889 *m*

Canister outer diameter

= 66.12 *in*
= (66.12)/(12*3.281) *m*
= 1.6794 *m*

Canister Shell length

= (210.63) – (15 + 3.5) *in*
= 192.13 *in*
= (192.13)/(12*3.281) *m*
= 4.88 *m*

Canister weight

= 49.32 *Metric Ton*
= 49,320 *kg*
= (49,320*2.2046) *lb*
= 108,731 *lb*
= (108,731/2000) = 54.37 *Ton (Eng.)*

Canister material (316L SS) density = 7980 kg/m^3

Top Lid (Plug) weight   = $(\pi/4)*(dia^2)*(length)*density$
                                       = $(\pi/4)*(1.6794^2)*(0.381)*(7980)$ kg
                                       = 6,735 kg
                                       = (6,735*2.2046) lb
                                       = 14,848 lb

Bottom Lid weight   = $(\pi/4)*(dia^2)*(length)*density$
                                       = $(\pi/4)*(1.6794^2)*(0.0889)*(7980)$ kg
                                       = 1572 kg
                                       = (1572*2.2046) lb
                                       = 3465 lb

Shell weight   = (total wt.) – wt. of (top plug + bottom plate)
                                       = (49,320) – (6735 + 1572) kg
                                       = 41, 013 kg
                                       = (41,013*2.2046) lb
                                       = 90,417 lb

Shell length   = (Total length) – length of (Top Plug + Bottom Plate)
                                       = (5.3497) – (0.381 + 0.0889) m
                                       = 4.8798 m

Shell weight (ID Formula)   = $(\pi/4)*(OD^2 - ID^2)*(shell\ length)*(density)$
                                       = $(\pi/4)*(1.6794^2 - ID^2)*(4.8798)*(7980)$ kg
                                       = 41,013 kg

Shell internal diameter (ID):

$$(1.6794^2 - ID^2) = \{(41,013)/(7980*4.8798)*(\pi)\}*(4)$$
$$= 1.341$$
$$ID = (1.6794^2 – 1.341)^{0.5}\ m$$
$$= 1.2163\ m$$
$$= (1.2163 * 3.281 * 12)\ in$$
$$= 47.89\ in$$

Shell wall thickness   = (OD – ID)/2
                                       = (1.6794 – 1.2163)/2 m
                                       = 0.2315 m
                                       = (0.2315 * 3.281 * 12) in
                                       = 9.1165 in

6.2.2   Calculations for TAD Canister Center of Gravity Location

Center of Gravity locations (along the z-axis) relative to the bottom external surface of the SNF canister.

Bottom Lid Center of Gravity (z-axis)   = (3.5 in)/2 = 1.75 *in*
                                          = (1.75)/(12*3.281) m = 0.0444 *m*

Shell Center of Gravity (z-axis)   = 3.5 in + (192.13 in)/2 = 99.57 *in*
                                          = (99.57)/(12*3.281) m = 2.529 *m*

Top Lid (Plug) Center of Gravity   = 3.5 in + 192.13 in. + (15 in)/2 = 203.13 *in*
                                          = (203.13)/(12*3.281) m = 5.159 *m*

Total Canister Center of Gravity (z-axis)   =
          = [(1.75 *in**3,465 *lb*)+(99.57 *in**90,417 *lb*)+(203.13 *in**14,848 *lb*)]/108,731 *lb*
                                          = 110.6 *in*
                                          = (110.6)/(12*3.281) *m* = 2.809 *m*

Bounding CG location (distance from bottom external surface of the loaded canister) between 103 in. and 123 in. (Reference 2.2.26, Figure C-17)

                                          = (103/12*3.281) *m* and (123/12*3.281) *m*
                                          = 2.6161 *m* and 3.124 *m*

6.2.3   Calculations for TAD Canister Wall Density for Mid WP Rock Impact

Canister shell weight   = (total wt.) – wt. of (top plug + bottom plate)
                               = (49,320) – (6735 + 1572) *kg*
                               = 41, 013 *kg*
                               = 90,417 *lb*

Shell length   = (Total length) – length of (Top Plug + Bottom Plate)
                               = (5.3497) – (0.381 + 0.0889) *m*
                               = 4.8798 *m*

Canister outer diameter   = 66.12 *in*
                               = (66.12)/(12*3.281) *m*
                               = 1.67936 *m*

Canister inner diameter   = 66.12-(2*1.00) *in*
                               = (64.12)/(12*3.281) *m*
                               = 1.6286 *m*

Volume of 1" canister shell   = $(\pi/4)*(OD^2 - ID^2)*$(shell length)
                               = $(\pi/4)*(1.67936^2 – 1.6286^2)*(4.8798)$
                               = 0.643 m^3

Density of shell wall   = (Shell Weight)/(Shell Volume)
                                            = (41,013)/(0.643) = 63784 kg/m^3
                                            = 2.304 lb/in^3

6.3   CALCULATION FOR ROCK DIMENSIONS

The rock shape used in this calculation is that of a rectangular prism (see Assumption 3.2.14). The rock dimensions for this analysis have been derived by scaling the rectangular prism dimensions of a simple 1.0 *m* (3.28 *ft*) by 2.5 *m* (8.20 *ft*) by 2.5 *m* (8.20 *ft*), 14.5 *MT* (31,967 *lbs*) rock consistent with Reference 2.2.12 as follows:

$\rho = m_2 / v_2$
$\rho = m_1 / v_1$

Therefore:
$v_2 / v_1 = m_2 / m_1$

Where:
ρ = rock density (Assumption 3.2.20), m = rock mass, and v = rock volume
a, b, c = three different side lengths of a rectangular prism
Subscripts 1 and 2 indicate two rocks of different sizes

The dimensions of a 20.0 *MT* (44,092 *lbs*) rock are calculated below:

$v_2 / v_1 = m_2 / m_1 = 20.0 / 14.5 = 1.379$

$v_2 = 1.379 * v_1 = [(1.379)^{1/3} * a_1] [(1.379)^{1/3} * b_1] [(1.379)^{1/3} * c_1]$
$v_2 = [1.113\ a_1] [1.113\ b_1] [1.113\ c_1]$

The dimensions of the 14.5 *MT* (31,967 *lbs*) rock are:
a_1 = 2.5 *m* (98.4 *in*)
b_1 = 2.5 *m* (98.4 *in*)
c_1 = 1.0 *m* (39.4 *in*)

Therefore, the dimensions of the 20.0 *MT* (44,092 *lbs*) rock are:
a_2 = 1.113 * a_1 = 1.113 * 2.5 = 2.783 *m* (109.6 *in*)
b_2 = 1.113 * b_1 = 1.113 * 2.5 = 2.783 *m* (109.6 *in*)
c_2 = 1.113 * c_1 = 1.113 * 1.0 = 1.113 *m* (43.82 *in*)

Each rock is positioned such that its center of gravity lies directly above the point of impact. The position of the rock is centered over the top of the WP (x = 0) with symmetry about the YZ plane which goes through the WP centerline. Therefore the rock inclination is determined using two dimensions of the rectangular prism:

Rock angle of inclination = arctan (c_1 / b_1) = arctan (1.0 / 2.5) = 21.8°

Repeating the calculation for a 0.43 *MT* (948 *lbs*) rock yields the following rock dimensions: $a_2 = 0.7738$ *m* (30.5 *in*), $b_2 = 0.7738$ *m* (30.5 *in*), $c_2 = 0.3095$ *m* (12.2 *in*).

Repeating the calculation for a 2.72 *MT* (5,997 *lbs*) rock yields the following rock dimensions: $a_2 = 1.431$ *m* (56.3 *in*), $b_2 = 1.431$ *m* (56.3 *in*), $c_2 = 0.572$ *m* (22.5 *in*).

Repeating the calculation for a 28.22 *MT* (62,214 *lbs*) rock yields the following rock dimensions: $a_2 = 3.121$ *m* (122.9 *in*), $b_2 = 3.121$ *m* (122.9 *in*), $c_2 = 1.249$ *m* (49.2 *in*).

Repeating the calculation for a 40.8 *MT* (89,950 *lbs*) rock yields the following rock dimensions: $a_2 = 3.529$ *m* (138.9 *in*), $b_2 = 3.529$ *m* (138.9 *in*), $c_2 = 1.412$ *m* (55.6 *in*).

Repeating the calculation for a 73.5 *MT* (162,000 *lbs*) rock yields the following rock dimensions: $a_2 = 4.295$ *m* (169.1 *in*), $b_2 = 4.295$ *m* (169.1 *in*), $c_2 = 1.718$ *m* (67.6 *in*).

6.4   FINITE ELEMENT REPRESENTATION

Rock impacts may occur both in the preclosure and post-closure periods. For the preclosure period, the drip shields have not yet been emplaced, so rocks may fall onto the emplaced WPs. Two WP configurations for are investigated in this calculation to determine their structural response to rock impact sequences: the TAD bearing WP and a Co-disposal Short WP (See Assumption 3.1.1). A finite element analysis is performed by using the commercially available LS-DYNA finite element code. Two different axial regions of rock impacts are evaluated in this study (Figure 3). The first impact region (A) is selected at the WP lower end, directly above the lower WP sleeve in the region of the support ring; the second impact region (C) is at mid-length along the WP top. These two regions that a falling rock could hit the top of a WP present the most structurally challenging locations to the OCB as determined from previous deterministic rock impact analyses (Reference 2.2.53, Section 7.2). Because of the significant differences in structural response to rock impact seen at these two locations (Reference 2.2.53, Section 7.2) they provide encompassing locations in which to analyze the Capability of the OCB.

C   A

WP   WP
Upper End   Lower End
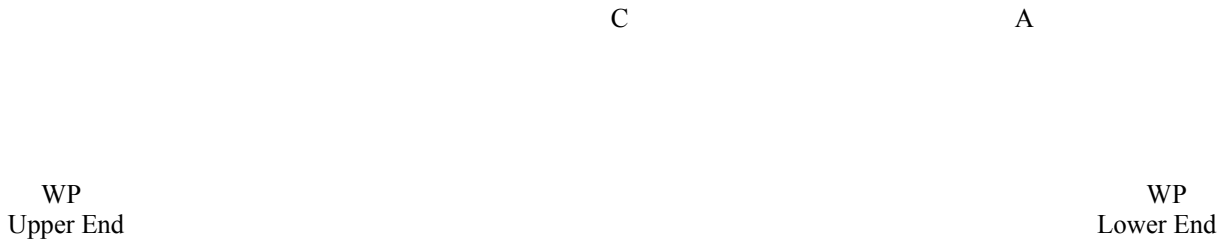
Figure 3.   A Simplified Illustration of Rock-WP Impact Regions
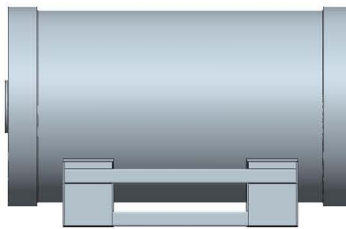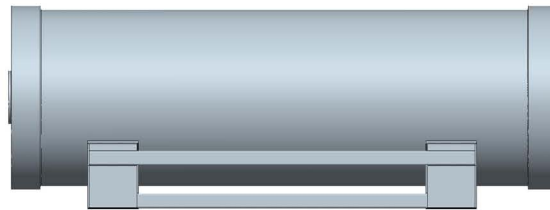
Figure 4.   General Illustration of a TAD bearing WP and a Co-Disposal Short WP

For the purposes of the Capability analyses, both the TAD bearing WP and the Co-disposal Short WP were simulated not only for both impact regions but also for the full range of rock impact scenarios. A list of all LS-DYNA simulations, their corresponding WP configurations, rock impact types, WP regions of impact, rock masses, velocities, and kinetic energy values are presented in Tables 1 and 2.

Tables 1 and 2 provide a quick-reference summary of the cases that were simulated in Attachment IV including the file names associated with the case numbers.

The impacting rock block is prone to large deformations in the FER due to its low yield strength and no strain hardening compared to Alloy 22. For any impact scenario that causes the rock to impact onto the WP sleeve, the rock is anticipated to locally crumble as it transfers its energy onto the sleeve.

The rock impact evaluations do not result in significant interaction of the inner vessel structure with the contents of the inner vessel, such as the canisters or the basket structure. Therefore, only one configuration for the internals of a Co-disposal Short WP is considered and the TAD bearing WP is conceptualized with simplified TAD canisters (see Section 6.2). The thick wall simplified TAD canister is used with the simulations involving rock impact on the lower WP sleeve, while the simplified TAD canister with the 1 *in* (0.0254 *m*) wall and density adjustment is used in the rock impact on mid WP simulations. The effects of different canisters or basket types and orientations are not studied in this calculation.

For single rock impact evaluations, a total of 36 three-dimensional half-symmetry FERs of the WP emplaced on the EP, and the rock (also half-symmetry), are developed in LS-DYNA (see Figure 5 for a typical FER). Of these 36 single rock impact evaluations, 18 simulations used a TAD bearing WP configuration (Reference 2.2.30 thru 2.2.32), see Figures 5 and 7, and 18 simulations used a Co-disposal Short WP configuration (Reference 2.2.47 thru 2.2.49), see Figures 6 and 8. The FER described in Case 22 was the scenario used to verify the mesh objectivity. Four versions of the FER for Case 22 were developed with progressively refined meshing in the region of interest. As detailed in Section 7.1 the "Fine" level of mesh refinement was selected as the optimal level and all other FERs were constructed to the same level of refinement. The mesh of the FER (see Figure 5 for example) is appropriately generated and refined in the contact region according to standard engineering practice and the methodology described in Section 7.1.3 of Reference 2.2.52.

FERs are developed by using the dimensions provided in Section 6.2, Section 6.3, and References 2.2.30 thru 2.2.49. To reduce the computer execution time while preserving all features of the problem relevant to the structural calculation, the rock is set in a position just before impact and given an initial impact velocity equal to the kinetic energy level being analyzed. The input values for rock impact velocity and rock block size for each of the single rock impact simulations are specified in Tables 1 and 2. An example of the impact velocity calculation using a 20.0 *MT* (44,092 *lbs*) rock is as follows: using the relation kinetic energy = mass*(velocity)^2/2, a 20.0 *MT* (44,092 *lbs*) rock with maximum $1.0 * 10^6$ *J* (737,560 *ft·lb$_f$*) kinetic energy results in a velocity of 10.0 *m/s* (32.8 *ft/s*) (this rock impact scenario is used in Cases 4, 13, 22, and 31). In English units a gravitational constant must be included in the denominator to perform the same calculation, kinetic energy = mass*(velocity)^2/(2*32.2 *ft/s^2*).

A loaded TAD bearing WP has a mass of 73.5 *MT* (81 *ton*) (Reference 2.2.30) so this was the mass selected as the bounding mass for the falling rocks simulated. Two impact velocities were selected to use with the 73.5 *MT* (81 *ton*) rocks arbitrarily at 10 *m/s* (32.8 *ft/s*) and 15 *m/s* (49.2 *ft/s*). A fully loaded Co-disposal Short WP has a mass bound of 40.8 *MT* (45 *ton*) (Reference 2.2.47). For consistency purposes, the impact velocities used with the 40.8 *MT* (45 *ton*) rocks in the Co-disposal Short WP simulations were selected in order to maintain a comparable kinetic energy level with the 73.5 MT (81 *ton*) rock simulations, so the highest energy impacts on the Co-disposal Short WP were at 13.4 *m/s* (44.0 *ft/s*) and 20.1 *m/s* (65.9 *ft/s*).

In the high kinetic energy rock impact scenarios on the lower WP sleeve it is possible for the end of the WP to be pushed downward past the invert surface level. To account for the invert surface a plate of A 588 alloy steel (Reference 2.2.54) was modeled under the WP sleeve. The invert plate was modeled as an elastic material with boundary conditions along the bottom side that prevented movement in any direction.

Table 1.   List of LS-DYNA Simulations for TAD Bearing WPs

Case #	WP configuration	Type of rock impact	Rock Impact Region	Rock mass	Rock Velocity	Rock Kinetic Energy	Notes on FER mesh size	Filename used in LS-DYNA simulations
1	TAD bearing	Single rock	Case A	0.43 *MT* (0.47 *ton*)	3.74 *m/s* (12.3 *ft/s*)	3,000 *J* (2213 *ft·lb$_f$*)	Fine	tada4m1_pra05_3000J.k
2	TAD bearing	Single rock	Case A	2.72 *MT* (3.0 *ton*)	3.32 *m/s* (10.9 *ft/s*)	15,000 *J* (11,063 *ft·lb$_f$*)	Fine	tada5m1s_pra05.k
3	TAD bearing	Single rock	Case A	20 *MT* (22 *ton*)	7.07 *m/s* (23.2 *ft/s*)	0.5 * 10^6 *J* (368,780 *ft·lb$_f$*)	Fine	tada2m3c_pra05_500000J.k
4	TAD bearing	Single rock	Case A	20 *MT* (22 *ton*)	10.0 *m/s* (32.8 *ft/s*)	1.0 * 10^6 *J* (737,560 *ft·lb$_f$*)	Fine	tada2m2c_pra05.k
5	TAD bearing	Single rock	Case A	20 *MT* (22 *ton*)	11.8 *m/s* (38.7 *ft/s*)	1.4 * 10^6 *J* (1.0 * 10^6 *ft·lb$_f$*)	Fine	tada2m3c_pra05_1400000J.k
6	TAD bearing	Single rock	Case A	28.2 *MT* (31.1 *ton*)	11.3 *m/s* (37.1 *ft/s*)	1.8 * 10^6 *J* (1.3 * 10^6 *ft·lb$_f$*)	Fine	tada3m1a_pra05_18J.k
7	TAD bearing	Single rock	Case A	28.2 *MT* (31.1 *ton*)	12.5 *m/s* (41.0 *ft/s*)	2.2 * 10^6 *J* (1.6 * 10^6 *ft·lb$_f$*)	Fine	tada3m1a_pra05_2200000J.k
8	TAD bearing	Single rock	Case A	73.5 *MT* (81 *ton*)	10.0 *m/s* (32.8 *ft/s*)	3.7 * 10^6 *J* (2.7 * 10^6 *ft·lb$_f$*)	Fine	tada4m2a_pra05.k
9	TAD bearing	Single rock	Case A	73.5 *MT* (81 *ton*)	15.0 *m/s* (49.2 *ft/s*)	8.3 * 10^6 *J* (6.1 * 10^6 *ft·lb$_f$*)	Fine	tada4m2a_pra05_8MJ.k
10	TAD bearing	Single rock	Case C	0.43 *MT* (0.47 *ton*)	3.74 *m/s* (12.3 *ft/s*)	3,000 *J* (2213 *ft·lb$_f$*)	Fine	tada3m2s_pra05_mid.k
10s	*TAD bearing*	*Single rock*	*Case C*	*0.43 MT (0.47 ton)*	*3.74 m/s (12.3 ft/s)*	*3,000 J (2213 ft·lb$_f$)*	*Fine*	*tada3m2s_pra05_mid140.k*
11	TAD bearing	Single rock	Case C	2.72 *MT* (3.0 *ton*)	3.32 *m/s* (10.9 *ft/s*)	15,000 *J* (11,063 *ft·lb$_f$*)	Fine	tada5m1s_pra05_mid.k
12	TAD bearing	Single rock	Case C	20 *MT* (22 *ton*)	7.07 *m/s* (23.2 *ft/s*)	0.5 * 10^6 *J* (368,780 *ft·lb$_f$*)	Fine	tada2m8_pra05_mid_0.5MJ.k
13	TAD bearing	Single rock	Case C	20 *MT* (22 *ton*)	10.0 *m/s* (32.8 *ft/s*)	1.0 * 10^6 *J* (737,560 *ft·lb$_f$*)	Fine	tada2m8_pra05_mid.k
13s	*TAD bearing*	*Single rock*	*Case C*	*20 MT (22 ton)*	*10.0 m/s (32.8 ft/s)*	*1.0 * 10^6 J (737,560 ft·lb$_f$)*	*Fine*	*tada2m8_pra05_mid140.k*
14	TAD bearing	Single rock	Case C	20 *MT* (22 *ton*)	11.8 *m/s* (38.7 *ft/s*)	1.4 * 10^6 *J* (1.0 * 10^6 *ft·lb$_f$*)	Fine	tada2m8_pra05_mid_1.4MJ.k
15	TAD bearing	Single rock	Case C	28.2 *MT* (31.1 *ton*)	11.3 *m/s* (37.1 *ft/s*)	1.8 * 10^6 *J* (1.3 * 10^6 *ft·lb$_f$*)	Fine	tada3m2_pra05_mid_1.8MJ.k
16	TAD bearing	Single rock	Case C	28.2 *MT* (31.1 *ton*)	12.5 *m/s* (41.0 *ft/s*)	2.2 * 10^6 *J* (1.6 * 10^6 *ft·lb$_f$*)	Fine	tada3m2_pra05_mid_2.2MJ.k
16s	*TAD bearing*	*Single rock*	*Case C*	*28.2 MT (31.1 ton)*	*12.5 m/s (41.0 ft/s)*	*2.2 * 10^6 J (1.6 * 10^6 ft·lb$_f$)*	*Fine*	*tada3m2_pra05_mid_2.2MJ140.k*
17	TAD bearing	Single rock	Case C	73.5 *MT* (81 *ton*)	10.0 *m/s* (32.8 *ft/s*)	3.7 * 10^6 *J* (2.7 * 10^6 *ft·lb$_f$*)	Fine	tada3m2_pra05_mid_3.7MJ.k
17s	*TAD bearing*	*Single rock*	*Case C*	*73.5 MT (81 ton)*	*10.0 m/s (32.8 ft/s)*	*3.7 * 10^6 J (2.7 * 10^6 ft·lb$_f$)*	*Fine*	*tada3m2_pra05_mid_3.7MJ140.k*
18	TAD bearing	Single rock	Case C	73.5 *MT* (81 *ton*)	15.0 *m/s* (49.2 *ft/s*)	8.3 * 10^6 *J* (6.1 * 10^6 *ft·lb$_f$*)	Fine	tada3m2_pra05_mid_8.3MJ.k
18s	*TAD bearing*	*Single rock*	*Case C*	*73.5 MT (81 ton)*	*15.0 m/s (49.2 ft/s)*	*8.3 * 10^6 J (6.1 * 10^6 ft·lb$_f$)*	*Fine*	*tada3m2_pra05_mid_8.3MJ140.k*

Note: Case numbers ending with 's' are part of the Rock Compressive Strength Variability Study, Section 7.4.2

Table 2.   List of LS-DYNA Simulations for Co-disposal Short WPs

Case #	WP configuration	Type of rock impact	Rock Impact Region	Rock mass	Rock Velocity	Rock Kinetic Energy	Notes on FER mesh size	Filename used in LS-DYNA simulations
19	Co-disposal Short	Single rock	Case A	0.43 MT (0.47 ton)	3.74 m/s (12.3 ft/s)	3,000 J (2213 ft·lb_f)	Fine	5dhlwa1m1_newSlv_3000J.k
19s	*Co-disposal Short*	*Single rock*	*Case A*	*0.43 MT (0.47 ton)*	*3.74 m/s (12.3 ft/s)*	*3,000 J (2213 ft·lb_f)*	*Fine*	*5dhlwa1m1_newSlv_3000J140.k*
20	Co-disposal Short	Single rock	Case A	2.72 MT (3.0 ton)	3.32 m/s (10.9 ft/s)	15,000 J (11,063 ft·lb_f)	Fine	5dhlwa2m1s_newSlv_15000J.k
21	Co-disposal Short	Single rock	Case A	20 MT (22 ton)	7.07 m/s (23.2 ft/s)	0.5 * 10⁶ J (368,780 ft·lb_f)	Fine	5dhlwa2m1s_newSlv_0.5MJ.k
22	Co-disposal Short	Single rock	Case A	20 MT (22 ton)	10.0 m/s (32.8 ft/s)	1.0 * 10⁶ J (737,560 ft·lb_f)	Fine	5dhlwa2m1s_newSlv.k
22a	*Co-disposal Short*	*Single rock*	*Case A*	*20 MT (22 ton)*	*10.0 m/s (32.8 ft/s)*	*1.0 * 10⁶ J (737,560 ft·lb_f)*	*Coarse*	*5dhlwa2m1s_newSlv_Crs.k*
22b	*Co-disposal Short*	*Single rock*	*Case A*	*20 MT (22 ton)*	*10.0 m/s (32.8 ft/s)*	*1.0 * 10⁶ J (737,560 ft·lb_f)*	*Standard*	*5dhlwa2m1s_newSlv_Std.k*
22d	*Co-disposal Short*	*Single rock*	*Case A*	*20 MT (22 ton)*	*10.0 m/s (32.8 ft/s)*	*1.0 * 10⁶ J (737,560 ft·lb_f)*	*Very Fine*	*5dhlwa2m1s_newSlv_vFine.k*
22s	*Co-disposal Short*	*Single rock*	*Case A*	*20 MT (22 ton)*	*10.0 m/s (32.8 ft/s)*	*1.0 * 10⁶ J (737,560 ft·lb_f)*	*Fine*	*5dhlwa2m1s_newSlv140.k*
23	Co-disposal Short	Single rock	Case A	20 MT (22 ton)	11.8 m/s (38.7 ft/s)	1.4 * 10⁶ J (1.0 * 10⁶ ft·lb_f)	Fine	5dhlwa2m1s_newSlv_1.4MJ.k
24	Co-disposal Short	Single rock	Case A	28.2 MT (31.1 ton)	11.3 m/s (37.1 ft/s)	1.8 * 10⁶ J (1.3 * 10⁶ ft·lb_f)	Fine	5dhlwa2m1s_newSlv_1.8MJ.k
25	Co-disposal Short	Single rock	Case A	28.2 MT (31.1 ton)	12.5 m/s (41.0 ft/s)	2.2 * 10⁶ J (1.6 * 10⁶ ft·lb_f)	Fine	5dhlwa2m1s_newSlv_2.2MJ.k
25s	*Co-disposal Short*	*Single rock*	*Case A*	*28.2 MT (31.1 ton)*	*12.5 m/s (41.0 ft/s)*	*2.2 * 10⁶ J (1.6 * 10⁶ ft·lb_f)*	*Fine*	*5dhlwa2m1s_newSlv_2.2MJ140.k*
26	Co-disposal Short	Single rock	Case A	40.8 MT (45 ton)	13.4 m/s (44.0 ft/s)	3.7 * 10⁶ J (2.7 * 10⁶ ft·lb_f)	Fine	5dhlwa5m1_newSlv_3.7MJ.k
26s	*Co-disposal Short*	*Single rock*	*Case A*	*40.8 MT (45 ton)*	*13.4 m/s (44.0 ft/s)*	*3.7 * 10⁶ J (2.7 * 10⁶ ft·lb_f)*	*Fine*	*5dhlwa5m1_newSlv_3.7MJ140.k*
27	Co-disposal Short	Single rock	Case A	40.8 MT (45 ton)	20.1 m/s (65.9 ft/s)	8.3 * 10⁶ J (6.1 * 10⁶ ft·lb_f)	Fine	5dhlwa5m1_newSlv_8.3MJ.k
27s	*Co-disposal Short*	*Single rock*	*Case A*	*40.8 MT (45 ton)*	*20.1 m/s (65.9 ft/s)*	*8.3 * 10⁶ J (6.1 * 10⁶ ft·lb_f)*	*Fine*	*5dhlwa5m1_newSlv_8.3MJ140.k*
28	Co-disposal Short	Single rock	Case C	0.43 MT (0.47 ton)	3.74 m/s (12.3 ft/s)	3,000 J (2213 ft·lb_f)	Fine	5dhlwa1m1_newSlv_mid_3000J.k
29	Co-disposal Short	Single rock	Case C	2.72 MT (3.0 ton)	3.32 m/s (10.9 ft/s)	15,000 J (11,063 ft·lb_f)	Fine	5dhlwa2m1_newSlv_midHit_15000J.k
30	Co-disposal Short	Single rock	Case C	20 MT (22 ton)	7.07 m/s (23.2 ft/s)	0.5 * 10⁶ J (368,780 ft·lb_f)	Fine	5dhlwa2m1_newSlv_midHit_0.5MJ.k
31	Co-disposal Short	Single rock	Case C	20 MT (22 ton)	10.0 m/s (32.8 ft/s)	1.0 * 10⁶ J (737,560 ft·lb_f)	Fine	5dhlwa2m1_newSlv_midHit.k
32	Co-disposal Short	Single rock	Case C	20 MT (22 ton)	11.8 m/s (38.7 ft/s)	1.4 * 10⁶ J (1.0 * 10⁶ ft·lb_f)	Fine	5dhlwa2m1_newSlv_midHit_1.4MJ.k
33	Co-disposal Short	Single rock	Case C	28.2 MT (31.1 ton)	11.3 m/s (37.1 ft/s)	1.8 * 10⁶ J (1.3 * 10⁶ ft·lb_f)	Fine	5dhlwa2m1_newSlv_midHit_1.8MJ.k
34	Co-disposal Short	Single rock	Case C	28.2 MT (31.1 ton)	12.5 m/s (41.0 ft/s)	2.2 * 10⁶ J (1.6 * 10⁶ ft·lb_f)	Fine	5dhlwa2m1_newSlv_midHit_2.2MJ.k
35	Co-disposal Short	Single rock	Case C	40.8 MT (45 ton)	13.4 m/s (44.0 ft/s)	3.7 * 10⁶ J (2.7 * 10⁶ ft·lb_f)	Fine	5dhlwa5m1_newSlv_mid3.7MJ.k
36	Co-disposal Short	Single rock	Case C	40.8 MT (45 ton)	20.1 m/s (65.9 ft/s)	8.3 * 10⁶ J (6.1 * 10⁶ ft·lb_f)	Fine	5dhlwa5m1_newSlv_mid8.3MJ.k

Note: Case numbers ending with 'a', 'b', and 'd' are part of the Mesh Verification Study, Section 7.1
Note: Case numbers ending with 's' are part of the Rock Compressive Strength Variability Study, Section 7.4.2
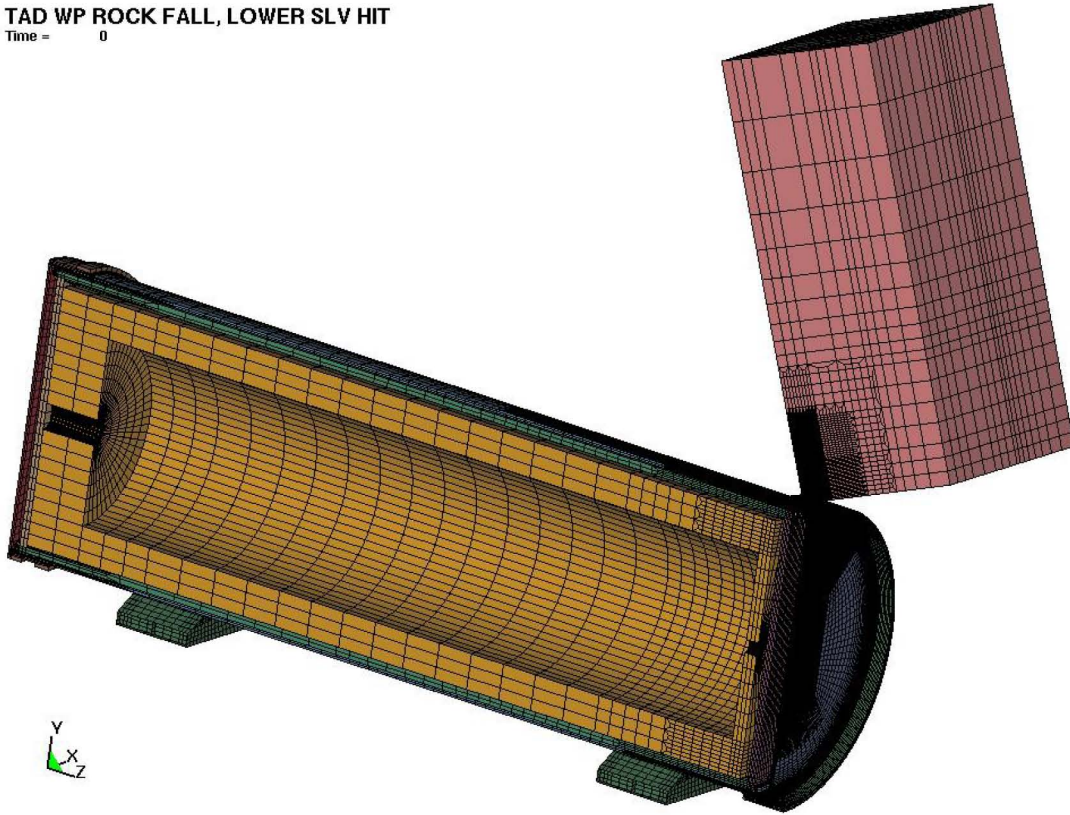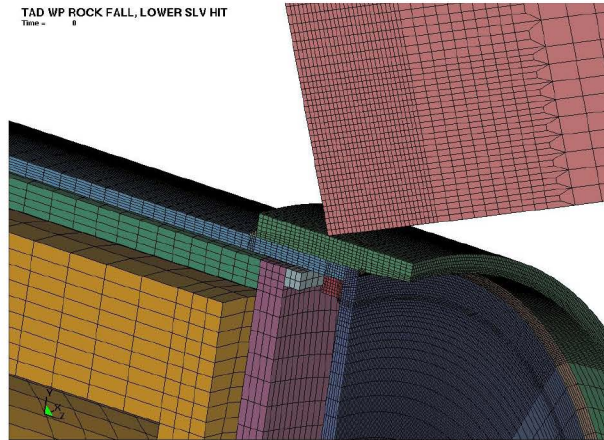
Figure 5.   Finite Element Representation of a Rock Impact on the Lower Sleeve of a TAD Bearing WP

5 DHLW/DOE SNF-SHORT WP ROCK FALL, LOWE
Time =   0
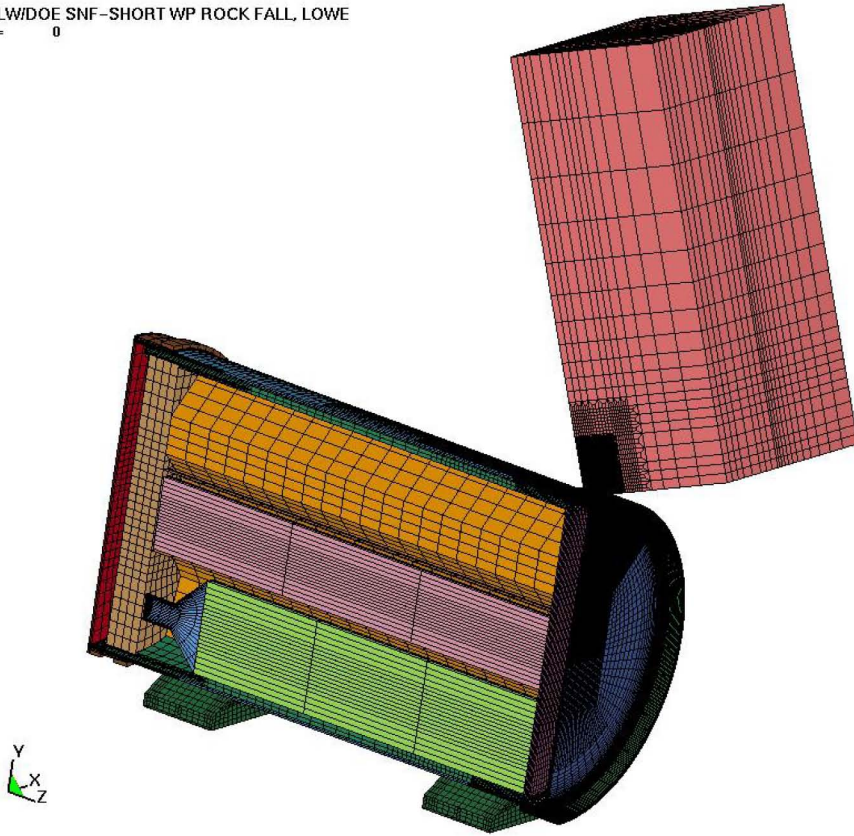
5 DHLW/DOE SNF-SHORT WP ROCK FALL, LOWE
Time =   0
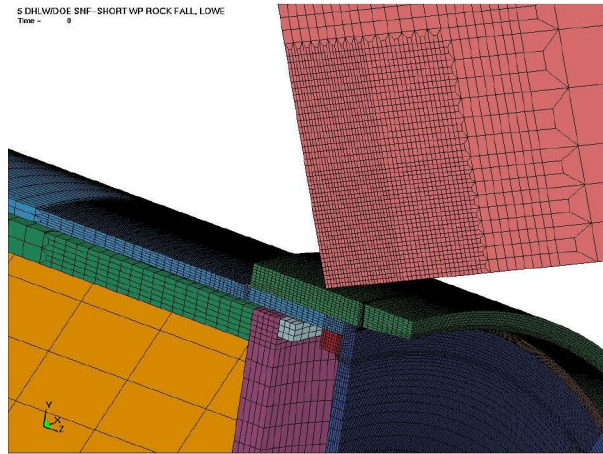
Figure 6.   Finite Element Representation of a Rock Impact on the Lower Sleeve of a Co-disposal Short WP
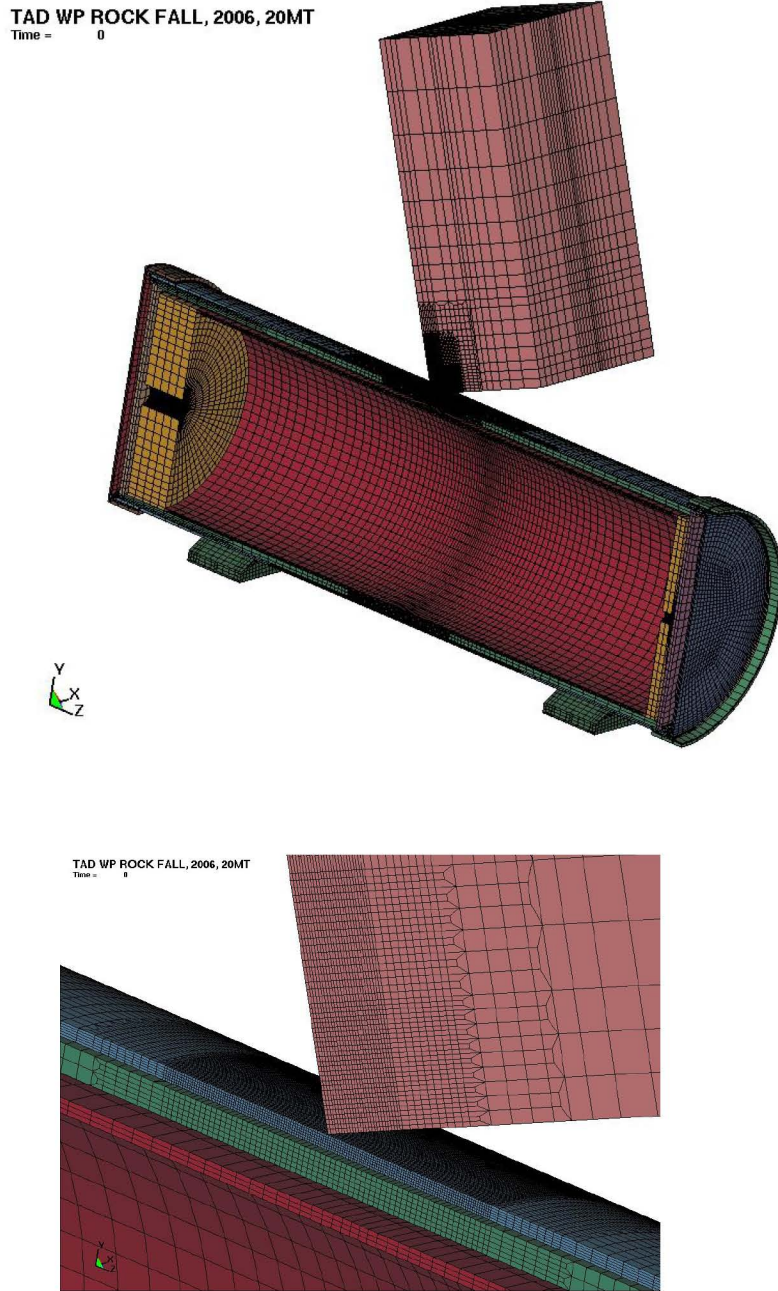
Figure 7.   Finite Element Representation of a Rock Impact on the mid section of a TAD Bearing WP
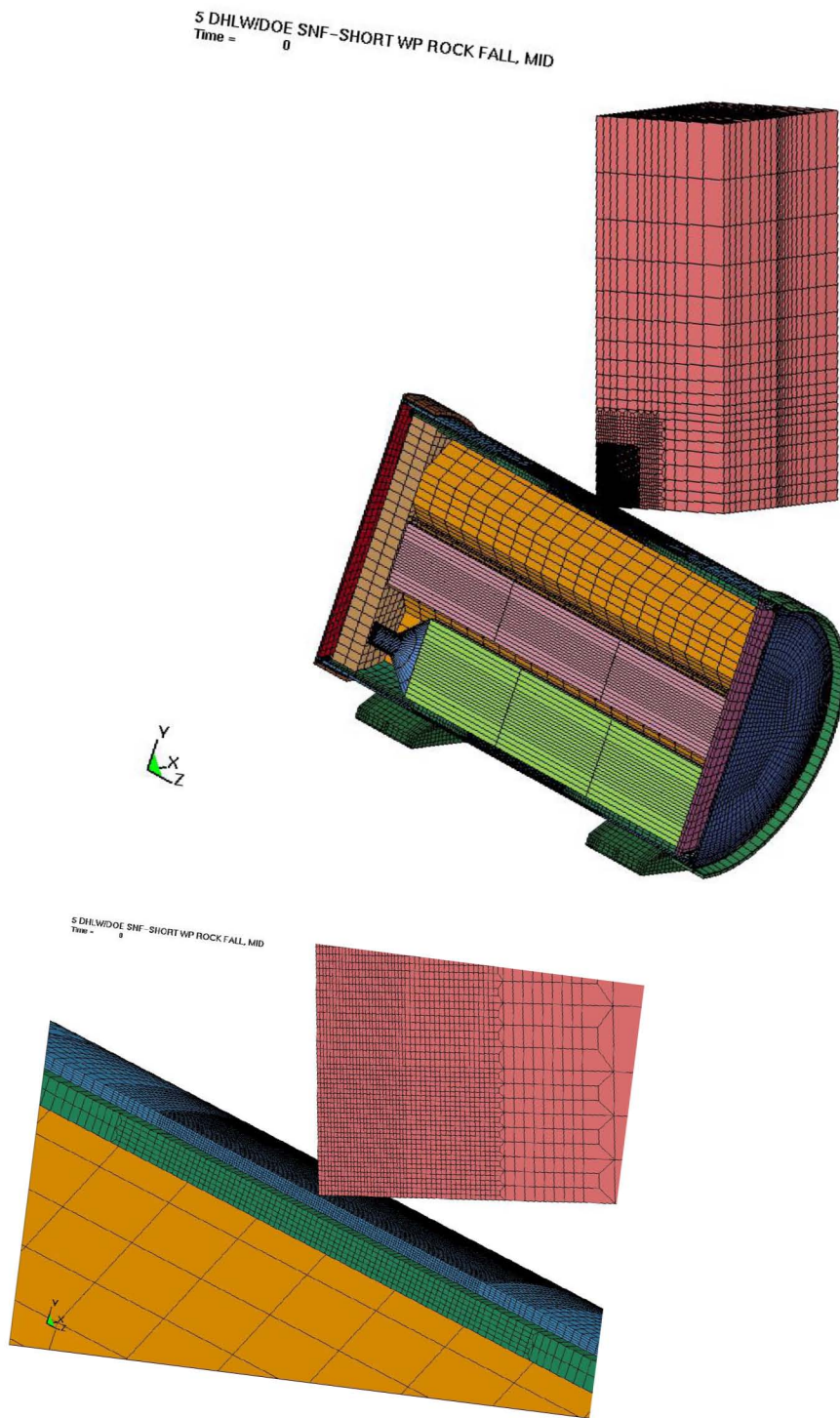
Figure 8.   Finite Element Representation of a Rock Impact on the mid section of a Co-disposal Short WP

Depending on the rock impact region, the inner vessel is repositioned axially within the OCB to maximize the stresses the rock strike will produce in the OCB. When the rock impact region is on the lower WP sleeve then the inner vessel and TAD canister are positioned at the upper end of the WP cavity, only a loose fit gap distance (11.1 *mm* (0.437 *in*)) away from the upper lid of the OCB at the top of the WP. The mid package rock impact region scenario should have no sensitivity to the position of the inner vessel, in these cases the inner vessel and TAD canister are simply placed in the middle of the OCB cavity. The Co-disposal Short WP internals do not have any significant space to shift to within the inner vessel cavity so they are modeled in the same position for both rock impact locations analyzed. During a simulation the inner vessel is free to move within the OCB interior, as well as the TAD canister within the inner vessel cavity.

These FERs are used in LS-DYNA to perform a transient dynamic analysis of rock impact. The rock shape used in this analysis is consistent with the rock geometry and dimensions obtained and used in previous rock impact structural analyses (Assumption 3.2.14). The angle of rock inclination with respect to the WP is adjusted such that the center of gravity of the rock is directly above the initial contact region (see Assumption 3.2.14). This configuration is conservative, since the kinetic energy of the rock is transferred to WP strain energy over a relatively small impact volume. The FER of the falling rock is divided into three regions: a small finely-meshed impact region, and intermediate region of less mesh refinement, and a large coarsely-meshed region for the remaining portion of the rock. These three regions of the rock have a tied-node interface with each other to ensure that the rock will behave as one continuous part during the simulations. The finely-meshed portion of the rock is necessary to capture the deformation of the rock in the localized region of impact and simulate the crushing of the rock expected in that region.

LS-DYNA "standard" contact algorithms are used to represent contacts between: rock and WP, OCB and inner vessel, OCB and EP, inner vessel and TAD canister, and any contact interactions between the TAD canister contents if they are modeled. In the absence of more appropriate data, the dynamic friction coefficients for all WP component contacts are assumed to be 0.4 (see Assumptions 3.2.10 and 3.2.11). It is assumed that the functional friction coefficient and the static friction coefficient are equal to the dynamic friction coefficient (see Assumption 3.2.13). For the rock on WP contact, the dynamic friction coefficients are assumed to be 0.525 (Assumption 3.2.12). For the rock on WP contact, again, the functional friction coefficient and the static friction coefficient are assumed equal to the dynamic friction coefficient (see Assumption 3.2.13). To increase solution stability, the contact stiffnesses are doubled and the contact viscous damping is set to 30%. A very small amount of structural damping (*DAMPING_PART_STIFFNESS, Coef = 0.0001) was used to stabilize any high frequency response without any expected affect on the major (low frequency) responses sought after in the OCB.

7. RESULTS AND CONCLUSIONS

7.1 MESH VERIFICATION

An initial study of the FER mesh for the 20 *MT* (44,092 *lb*), 10 *m/s* (32.8 *ft/s*) rock impact on a Co-disposal Short WP at location A (See Figure 3) is performed to verify the objectivity of the mesh, i.e., that the calculation results are not mesh-sensitive. Table 3 shows the element wall-averaged (EWA) stress intensity (SI) of comparable wall sections for four different FER meshes. The EWA SIs presented in Table 3 are each from the same relative location on the OCB bottom lid (identified by surface element number) in the region of maximum structural response.

The first (coarse) mesh in Table 3 is developed by following the guidance in *Waste Package Component Design Methodology* (Reference 2.2.52, Section 7.1.3). The standard mesh is a refined version of the coarse mesh, where in the region of interest (OCB lower lid) the mesh is refined in the angular coordinate direction. The lower lid of the OCB is the critical structural component for reporting maximum structural response for the governing loading. The volumes and stress values for each element are obtained from the post-processing of LS-DYNA simulations. The change in the WP element volume between the coarse and standard mesh is 67%. The change in EWA SI for the elements in the same location is 0.4%, which indicates that the change in EWA SI is within the tolerance described in the Reference 2.2.52, Section 7.1.3. The mesh is again refined to obtain a "fine" mesh, this time the refinement is performed in the radial (outward from the center of the circular lid) direction. In the region of interest, the change in volume and EWA stress magnitudes between the standard and fine mesh simulations are 30% and 0.8%, respectively. The "fine" mesh is further refined, this time in the axial (lid thickness) direction to make a "very fine" mesh. In the region of interest, the change in volume and EWA stress magnitudes between the fine and very fine mesh simulations are 25% and 0.2%, respectively. In accordance with the methodology described in Reference 2.2.52, Section 7.1.3, the "fine" mesh is deemed the optimal mesh and a similar mesh density is used for all simulations.

Table 3.   Mesh Sensitivity Study Comparisons

Coarse Mesh (Case 22a)		Standard Mesh (Case 22b)		Change from Coarse Mesh
Element # 55407 (OCB bottom lid, at symmetry plane)	Volume 2.20E-07 m^3 (0.0134 in^3)	Element # 99723 (OCB bottom lid, at symmetry plane)	Volume 7.33E-08 m^3 (0.00447 in^3)	67%
	EWA SI 516 MPa (74.8 ksi)		EWA SI 514 MPa (74.5 ksi)	0.4%
Standard Mesh (Case 22b)		Fine Mesh (Case 22)		Change from Standard Mesh
Element # 99723 (OCB bottom lid, at symmetry plane)	Volume 7.33E-08 m^3 (0.00447 in^3)	Element # 131583 (OCB bottom lid, at symmetry plane)	Volume 5.15E-08 m^3 (0.00314 in^3)	30%
	EWA SI 514 MPa (74.5 ksi)		SI 510 MPa (74.0 ksi)	0.8%
Fine Mesh (Case 22)		Very Fine Mesh (Case 22d)		Change from Fine Mesh
Element # 131583 (OCB bottom lid, at symmetry plane)	Volume 5.15E-08 m^3 (0.00314 in^3)	Element # 138873 (OCB bottom lid, at symmetry plane)	Volume 3.86E-08 m^3 (0.00236 in^3)	25%
	SI 510 MPa (74.0 ksi)		SI 509 MPa (73.8 ksi)	0.2%

SI: Stress intensity

7.2 CAPABILITY CALCULATION

The triaxiality-adjusted vendor average and nominally-adjusted ASME material properties presented in Section 6.1 were used in Capability calculations for two rock impact locations; location A (Lower WP Sleeve), and location C (mid WP).

The maximum stressed OCB location was evaluated in each simulation for the time-maximum of the EWA VM stress, $\sigma_{vm,max}$, and for the EWA VM strain, $\varepsilon_{vm,max}$, in the same location. The string of through-wall elements with the largest value of $\sigma_{vm,max}$ times $\varepsilon_{vm,max}$ is used as the governing wall-section.

The material Toughness Index, I_T, from the triaxiality adjusted vendor average properties in Section 6.1.2 (Reference 2.2.52, Section 7.1.7.2.2, Equation 3) is:

$I_T = \varepsilon_u'(\sigma_y + \sigma_u)/2 = 0.28(356 + 1006)/2 = 191 \ MPa$

When the wall-section toughness Demand, I_T', is below I_T, it is computed as:

$$I_T' = \varepsilon_{vm,tmax} (\sigma_y + \sigma_{vm,max})/2$$

The ratio I_T'/I_T is termed the Expended Toughness Fraction (ETF) and is a measure of the damage. ETF values less than 1.0 do not indicate failure, while ETF values above 1.0 indicate failure.

When the wall-section toughness Demand, I_T', is above I_T (ETF > 1.0), it is computed as:

$$I_T' = I_T + \sigma_{vm,max}(\varepsilon_{vm,unload} - \varepsilon_{vm,flow}), \text{ where}$$

$\varepsilon_{vm,unload}$ is the EWA VM strain at the initiation of unloading, and $\varepsilon_{vm,flow}$ is the EWA VM strain at the time when most, if not all, of the elements in the wall section reach σ_u' and the stress plot runs horizontal in time. This is an indication of incipient failure. In some cases, a surface element on the wall section will be in bearing and/or shear contact with another structure and locally high hydrostatic stress states will prevent that element's VM stress from reaching σ_u'. This local strengthening will not prevent section failure.

At a later time, the horizontal time plots of individual wall element VM stresses begin to separate and retract from σ_u', indicating unloading. The time at initiation of stress plot separation is the time used to determine $\varepsilon_{vm,unload}$.

7.3   EVALUATION

The results presented in Tables 4 and 5 refer to the thirty six simulations specified in Tables 1 and 2, respectively. The corresponding case numbers identify each case in Tables 1 and 2 with the results in Tables 4 and 5. Tables 4 and 5 contain the maximum calculated EWA effective VM stress values in the OCB of the WPs, the EWA effective VM strain at the same time that the maximum EWA effective VM stress occurs, and the corresponding ETF values. Because of the triaxiality adjustment applied to the material properties of the OCB (ADJ=0.519, see Section 6.1.2) these results represent the mean property worst case Capability evaluations of the OCB for the impact orientations analyzed. An ETF value of 1 corresponds to all of the toughness of the OCB material being expended and therefore signaling the onset of failure of the OCB.

Table 4.　　　Maximum ETF values for the TAD Bearing WP OCB

Case #	WP configuration	Rock Kinetic Energy	Element Number[a]	$\sigma_{vm,max}$	$\varepsilon_{vm,max}$ m/m	I_T'	ETF=I_T'/I_T
1	TAD bearing, Lower Sleeve Hit	3,000 J (2213 $ft \cdot lb_f$)	85145	70.4 MPa (10.2 ksi)	0.0003	0.062	0.0003
2	TAD bearing, Lower Sleeve Hit	15,000 J (11,063 $ft \cdot lb_f$)	85055	147 MPa (21.3 ksi)	0.0006	0.152	0.0008
3	TAD bearing, Lower Sleeve Hit	$0.5 * 10^6 J$ (368,780 $ft \cdot lb_f$)	85056	396 MPa (57.5 ksi)	0.0197	7.42	0.0396
4	TAD bearing, Lower Sleeve Hit	$1.0 * 10^6 J$ (737,560 $ft \cdot lb_f$)	91750	430 MPa (62.4 ksi)	0.0336	13.2	0.0706
5	TAD bearing, Lower Sleeve Hit	$1.4 * 10^6 J$ ($1.0 * 10^6 ft \cdot lb_f$)	91750	452 MPa (65.5 ksi)	0.0431	17.4	0.0929
6	TAD bearing, Lower Sleeve Hit	$1.8 * 10^6 J$ ($1.3 * 10^6 ft \cdot lb_f$)	91750	463 MPa (67.1 ksi)	0.0491	20.1	0.1074
7	TAD bearing, Lower Sleeve Hit	$2.2 * 10^6 J$ ($1.6 * 10^6 ft \cdot lb_f$)	91750	492 MPa (71.4 ksi)	0.0674	28.6	0.1527
8	TAD bearing, Lower Sleeve Hit	$3.7 * 10^6 J$ ($2.7 * 10^6 ft \cdot lb_f$)	84555	532 MPa (77.1 ksi)	0.0851	37.8	0.2018
9	TAD bearing, Lower Sleeve Hit	$8.3 * 10^6 J$ ($6.1 * 10^6 ft \cdot lb_f$)	85056	739 MPa (107 ksi)	0.1462	80.0	0.4273
10	TAD bearing, Mid Package Hit	3,000 J (2213 $ft \cdot lb_f$)	99894	251 MPa (36.5 ksi)	0.0013	0.391	0.0021
11	TAD bearing, Mid Package Hit	15,000 J (11,063 $ft \cdot lb_f$)	101190	338 MPa (49.0 ksi)	0.0055	1.92	0.0103
12	TAD bearing, Mid Package Hit	$0.5 * 10^6 J$ (368,780 $ft \cdot lb_f$)	102054	423 MPa (61.3 ksi)	0.0297	11.6	0.0617
13	TAD bearing, Mid Package Hit	$1.0 * 10^6 J$ (737,560 $ft \cdot lb_f$)	101802	458 MPa (66.4 ksi)	0.0331	13.5	0.0719
14	TAD bearing, Mid Package Hit	$1.4 * 10^6 J$ ($1.0 * 10^6 ft \cdot lb_f$)	101748	517 MPa (75.0 ksi)	0.0472	20.6	0.1101
15	TAD bearing, Mid Package Hit	$1.8 * 10^6 J$ ($1.3 * 10^6 ft \cdot lb_f$)	101748	527 MPa (76.4 ksi)	0.0464	20.5	0.1094
16	TAD bearing, Mid Package Hit	$2.2 * 10^6 J$ ($1.6 * 10^6 ft \cdot lb_f$)	103422	564 MPa (81.8 ksi)	0.0514	23.6	0.1261
17	TAD bearing, Mid Package Hit	$3.7 * 10^6 J$ ($2.7 * 10^6 ft \cdot lb_f$)	101199	827 MPa (120 ksi)	0.1474	87.2	0.4655
18	TAD bearing, Mid Package Hit	$8.3 * 10^6 J$ ($6.1 * 10^6 ft \cdot lb_f$)	100764	894 MPa (130 ksi)	0.1553	97.0	0.5180

[a] Element number of solid element on outer surface of OCB for selected through-wall section.

Table 5.   Maximum ETF values for the Co-disposal Short WP OCB

Case #	WP configuration	Rock Kinetic Energy	Element Number[a]	$\sigma_{vm,max}$	$\varepsilon_{vm,max}$ m/m	I_T'	ETF=I_T'/I_T
19	Co-disposal Short, Lower Sleeve Hit	3,000 J (2213 ft·lb$_f$)	131582	81.5 MPa (11.8 ksi)	0.0003	0.074	0.0004
20	Co-disposal Short, Lower Sleeve Hit	15,000 J (11,063 ft·lb$_f$)	131583	159 MPa (23.1 ksi)	0.0007	0.170	0.0009
21	Co-disposal Short, Lower Sleeve Hit	$0.5 * 10^6$ J (368,780 ft·lb$_f$)	131583	404 MPa (58.7 ksi)	0.0223	8.48	0.0453
22	Co-disposal Short, Lower Sleeve Hit	$1.0 * 10^6$ J (737,560 ft·lb$_f$)	131583	451 MPa (65.5 ksi)	0.0461	18.6	0.0993
23	Co-disposal Short, Lower Sleeve Hit	$1.4 * 10^6$ J ($1.0 * 10^6$ ft·lb$_f$)	140114	514 MPa (74.6 ksi)	0.0744	32.4	0.1728
24	Co-disposal Short, Lower Sleeve Hit	$1.8 * 10^6$ J ($1.3 * 10^6$ ft·lb$_f$)	131583	559 MPa (81.1 ksi)	0.0920	42.1	0.2246
25	Co-disposal Short, Lower Sleeve Hit	$2.2 * 10^6$ J ($1.6 * 10^6$ ft·lb$_f$)	131582	687 MPa (99.6 ksi)	0.1308	68.2	0.3642
26	Co-disposal Short, Lower Sleeve Hit	$3.7 * 10^6$ J ($2.7 * 10^6$ ft·lb$_f$)	131583	735 MPa (107 ksi)	0.1549	84.5	0.4511
27	Co-disposal Short, Lower Sleeve Hit	$8.3 * 10^6$ J ($6.1 * 10^6$ ft·lb$_f$)	130697	908 MPa (132 ksi)	0.2544	161	0.8582
28	Co-disposal Short, Mid Package Hit	3,000 J (2213 ft·lb$_f$)	102918	289 MPa (42.0 ksi)	0.0025	0.793	0.0042
29	Co-disposal Short, Mid Package Hit	15,000 J (11,063 ft·lb$_f$)	102054	328 MPa (47.6 ksi)	0.0044	1.51	0.0081
30	Co-disposal Short, Mid Package Hit	$0.5 * 10^6$ J (368,780 ft·lb$_f$)	102054	424 MPa (61.5 ksi)	0.0317	12.3	0.0659
31	Co-disposal Short, Mid Package Hit	$1.0 * 10^6$ J (737,560 ft·lb$_f$)	100908	510 MPa (74.0 ksi)	0.0479	20.7	0.1107
32	Co-disposal Short, Mid Package Hit	$1.4 * 10^6$ J ($1.0 * 10^6$ ft·lb$_f$)	101787	531 MPa (77.0 ksi)	0.0371	16.5	0.0879
33	Co-disposal Short, Mid Package Hit	$1.8 * 10^6$ J ($1.3 * 10^6$ ft·lb$_f$)	100881	546 MPa (79.1 ksi)	0.0555	25.0	0.1335
34	Co-disposal Short, Mid Package Hit	$2.2 * 10^6$ J ($1.6 * 10^6$ ft·lb$_f$)	100881	553 MPa (80.2 ksi)	0.0571	26.0	0.1386
35	Co-disposal Short, Mid Package Hit	$3.7 * 10^6$ J ($2.7 * 10^6$ ft·lb$_f$)	100848	554 MPa (80.4 ksi)	0.0527	24.0	0.1281
36	Co-disposal Short, Mid Package Hit	$8.3 * 10^6$ J ($6.1 * 10^6$ ft·lb$_f$)	101205	850 MPa (123.3 ksi)	0.1537	92.7	0.4949

[a] Element number of solid element on outer surface of OCB for selected through-wall section.

For the rock impact on the lower WP sleeve scenarios, the structural response in the Co-disposal Short WP rock impact simulations are consistently higher than in the TAD bearing WP simulations, but still not expending all of the toughness of the OCB material to cause failure. The significantly higher stresses calculated for the lower WP sleeve impacts on the Co-disposal Short WP as compared to the TAD bearing WP are due to the larger diameter of the Co-disposal Short WP and the EP placement under the Co-disposal Short WP. Figure 4 illustrates how the lower WP sleeve of the Co-disposal Short WP overhangs the ends of the pallet footings a much shorter distance than the overhang observed with the TAD bearing WP. This overhang allows for more energy from the impacting rocks on the lower WP sleeve to be transferred into kinematic rotational energy in the TAD bearing WP than in the Co-disposal Short WP, see Figures 17 through 26 for a comparison of Case #9 with Case #27. In the TAD bearing WP version of the 8.3 *MJ* ($6.1*10^6$ *ft·lb$_f$*) rock impact on the lower WP sleeve, Case #9, the initial EWA VM stress peak rises to ~700 *MPa* (~100 *ksi*) but the maximum EWA VM stress peak of 739 *MPa* (107 *ksi*) occurs at about 50 *ms* as the bottom of the WP sleeve crushes against the invert steel lattice, see Figure 24. Figure 25 shows that the downward movement of a node on the TAD bearing WP OCB lower lid where the peak VM stresses are located stops shortly after the bottom of the WP sleeve has flattened against the top of the invert steel lattice, at about 60 *ms*. None of the elements through the OCB where the peak EWA VM stress was calculated rose to the true ultimate strength level, see Figure 23. By contrast, Figure 19 shows that the maximum EWA VM stress peak for the Co-disposal Short WP, 908 *MPa* (132 *ksi*), occurs during the initial VM stress peak, and from Figure 18 we can see that two of the six OCB through wall elements had reached the true ultimate strength level of the triaxiality adjusted Alloy 22 material properties, σ_u'= 1006 *MPa* (146 *ksi*). Figure 20 shows that the downward movement of a node on the Co-disposal Short WP OCB lower lid where the peak VM stresses are located only slows after the bottom of the WP sleeve has flattened against the top of the invert steel lattice, at about 50 *ms*. Figures 21 and 26 show the VM stress contours at the time of peak VM stress for each case.

In both Figures 19 and 24 the rock impact on the lower sleeve has 8.3 *MJ* ($6.1*10^6$ *ft·lb$_f$*) of kinetic energy. At this level of rock impact energy the VM stress levels in the OCB lower lid rise quickly peaking at 18 *ms* to 21 *ms*. Immediately following this initial rise there is a VM stress drop as the EP foot nearest the rock impact initiates buckling and the WP lower end travels downward. Then, at approximately 30 *ms*, contact is made between the WP lower sleeve and the invert at which point the VM stresses again rise. The Co-disposal Short WP VM stresses shown in Figure 19 do not rise back to the level of their initial high because the contact with the invert primarily deforms the skirt of the WP lower sleeve without transferring much force through the OCB lower lid. By contrast the TAD bearing WP OCB VM stresses shown in Figure 24 show a return to the same high VM stress levels as the WP lower sleeve contacts the invert and significant force is transferred back into the OCB lower lid. The brief dip in VM stress levels seen in Figure 24 near 38 *ms* is due to a buckling of the opposite end of the OCB lower lid. Note that only in the WP lower sleeve rock impact kinetic energy of 8.3 *MJ* ($6.1*10^6$ *ft·lb$_f$*) cases does the WP lower sleeve make contact with the invert and the highly nonlinear structural response associated with that contact occurs.

For the rock impact on the mid WP scenarios, the structural response in the co-disposal WP rock impact simulations are similar (slightly higher in the lower rock kinetic energy cases, slightly

lower in the higher rock kinetic energy cases) to the TAD bearing WP simulations, but once again not expending all of the toughness of the OCB material to cause failure. For the lower kinetic energy rock impact at mid WP cases, the differences in OCB effective stresses calculated for the Co-disposal WP and the TAD bearing WP are due to the Co-disposal WP OCB design having a larger radius than the TAD bearing WP OCB. For the higher kinetic energy rock impact at mid WP cases, the differences in OCB effective stresses calculated for the Co-disposal WP and the TAD bearing WP are due to the modeling of the internals of the Co-disposal WP design while the TAD bearing WP was modeled with the simplified canister conceptualization.

Three Capability analysis cases have equivalent Deterministic analyses (Reference 2.2.53) to compare against; Table 6 shows the comparable analyses. The only difference between the Capability analysis simulations and the Deterministic evaluation simulations is the material properties used to describe the WP. While the Deterministic evaluations used the ASME Code specified minimum material properties (Reference 2.2.53, Section 6.1), the Capability analyses used the average of vendor supplied material properties data, which was then adjusted to account for worst case triaxiality, to describe the OCB and then 10% strength adjusted ASME Code specified minimum material properties for the rest of the WP components (see Section 6.1.2). For the Capability analyses an ETF value of 1 corresponds to all of the toughness of the OCB material being expended and signaling the onset of failure of the OCB, but for the Deterministic evaluations a failure criterion based on the comparison of peak SI to allowable tensile strength was used. For the Deterministic evaluations the first tier level of membrane failure, ductile rupture defined in Table 4 of Reference 2.2.52, is that the time-maximum EWA SI remain below 70% of true tensile strength. The last tiered screening criterion used with the Deterministic evaluations is that the time-maximum EWA SI remain below 90% of true tensile strength, if it is a very localized EWA SI. Further analysis would have to be performed on the Deterministic evaluation results of Reference 2.2.53 to verify if the EWA SI is localized enough so that the last tier screening criterion of 90% true tensile strength is applicable. This criterion is included in Table 6 for benchmark comparison purposes only.

Table 6.   Deterministic Failure Criteria Comparison with Equivalent Capability Analysis ETF Values

		Capability Analysis				Deterministic Evaluation (Reference 2.2.53)		
Case #	WP configuration	Rock Kinetic Energy	EWA SI	$\sigma_{vm,max}$	ETF=I_T'/I_T	EWA SI	EWA SI/0.7σ_u	EWA SI/0.9σ_u
4	TAD bearing, Lower Sleeve Hit	1.0 * 10^6 J (737,560 ft·lb$_f$)	496 MPa (71.9 ksi)	430 MPa (62.4 ksi)	0.0706	573 MPa (83.1 ksi)	0.84	0.66
13	TAD bearing, Mid Package Hit	1.0 * 10^6 J (737,560 ft·lb$_f$)	515 MPa (74.7 ksi)	458 MPa (66.4 ksi)	0.0719	584 MPa (84.7 ksi)	0.86	0.67
22	Co-disposal Short, Lower Sleeve Hit	1.0 * 10^6 J (737,560 ft·lb$_f$)	510 MPa (74.0 ksi)	451 MPa (65.5 ksi)	0.0993	622 MPa (90.2 ksi)	0.91	0.71

7.4   MATERIAL STRENGTH VARIABILITY

7.4.1   Alloy 22 Toughness Variability

The vendor-averaged OCB Alloy 22 material strength data used in the FER simulations represents a mean (expected) value. Information on Alloy 22 strength variability is limited in traditional sources. Reference 2.2.55 processes strength variation data contained in Reference 2.2.56 based on an assumed Normal Distribution. This includes a computation of the variability in Toughness Index, I_T, values computed without triaxiality adjustments (uniaxial test data) and expressed as the standard deviation (σ) from the mean. The average standard deviation of I_T in Table 7-4 of Reference 2.2.55 is 7.3%. This high toughness variability is definitely due in part to the small number of data samples in the Reference 2.2.56 test program. The trend plots of computed ETF values versus rock impact kinetic energy are broadened using this variability in section 7.5.

7.4.2   Rock Compressive Strength Variability

The TSw2 nonlithophysal rock compressive strength data used in the FER simulations represents a mean (recommended) value (Assumption 3.2.18). Information on rock compressive strength variability is limited in traditional sources. Figure 1 of Reference 2.2.17 shows the compressive strength data as a function of nonlithophysal rock block size. Because data for rock compressive strength is extrapolated for rock blocks over the data sample test size of 23 *cm* (9 *in*), and all blocks in this calculation are well over the sampled data size, there is no compressive strength variability data available. To conservatively capture possible variability in compressive strength a value of two times the recommended compressive strength is arbitrarily selected, 140 *MPa* (20 *ksi*). Figures 27 and 28 show the ETF values versus rock impact kinetic energy when rock compressive strength is doubled and mean Alloy 22 vendor material properties with worst case triaxiality are assumed. Figures 27 and 28 show the mid WP rock impact on TAD bearing WP and lower sleeve rock impact on Co-disposal Short WP scenarios, respectively. Figures 29 and 30 include the trend plots of Alloy 22 toughness variability as described in Section 7.4.1. Figures 31 and 32 display the combined ETF values versus rock impact kinetic energy of both the Alloy 22 toughness variability and the rock compressive strength variability. Table 7 summarizes the ETF values for each rock impact scenario and WP type analyzed.

7.5   SUMMARY AND CONCLUSION

The output values are reasonable for the given inputs in this calculation. Where significant material sensitivities are identified, they are taken into account by variability studies. The impact locations and loading orientations are the worst case scenarios and the sensitivity of WP Capability to these is beyond the scope of this calculation. The results are suitable for performing a Capability assessment of the WPs.

The results presented in Tables 4 and 5 indicate that the maximum EWA effective stresses (VM) generated by a rock impact event will not expend the total toughness allowed by the worst case triaxiality adjusted mean strength toughness of Alloy 22 when impacted by a rock of mean compressive strength. The structural response of the TAD bearing WP and the Co-disposal Short WP, in terms of expended toughness fraction, due to rock impact have remained below levels where an OCB breach or WP failure would occur as defined in Reference 2.2.52, section

7.1.7.2.2.   The expected Capability of the OCB, in terms of expended toughness fraction, to respond to the Demand of a preclosure rock impact event is shown in Figures 9 though 12.

The ETF spread due to OCB material strength variability is approximated by linear extrapolation off of the mean ETF trend curves. The linearity of the lower WP sleeve rock impact ETF data mean trends combined with the common zero intercept indicates that the toughness expended for a given rock impact kinetic energy, for this impact location, is roughly linearly related to the Toughness Index value, i.e., a material with twice the Toughness Index of another material will require twice the rock impact kinetic energy to expend the same fraction of available toughness. Therefore, one of the simplest OCB material strength variability adjustments is to proportionately broaden the mean rock impact kinetic energy trends linearly by the Toughness Index variability. The mid WP rock impacts display a non-linear relationship between ETF and kinetic energy due likely to the EP plastic collapse behavior.

By definition, values encompassed by two standard deviations (2σ or 2SD) from the mean on normal Gaussian distributions provide 95% confidence limits. From Section 7.4, the standard deviation from the mean of the Alloy 22 annealed weldment Toughness Index is 7.3%. Therefore, decreasing and increasing the mean rock impact kinetic energy trends by 15% (multiples of 0.85 and 1.15) can provide 95% confidence bounds on the OCB ETF for each of the rock impact kinetic energy levels analyzed. Figures 13 through 16 provide these material properties adjustments and show the Capability of the OCB, including the 95% confidence limits of the expended toughness fraction required to respond to the Demand of a preclosure rock impact event.

It is expected that a more refined statistical handling of the WPs Capability will be employed by Pre-Closure Safety using the impact location, kinetic energy levels, and material strength variability evaluations contained in this calculation.
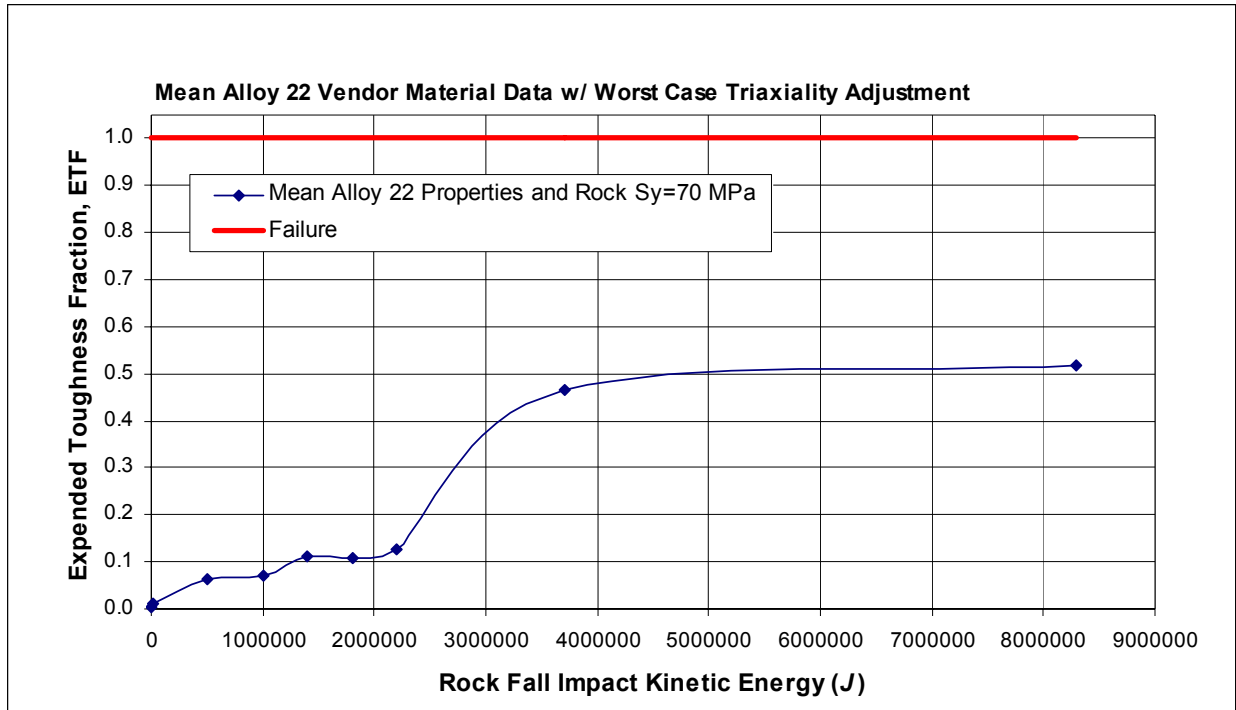
Figure 9.   ETF versus *J* for all Mid WP Rock Impact Cases on TAD Bearing WP
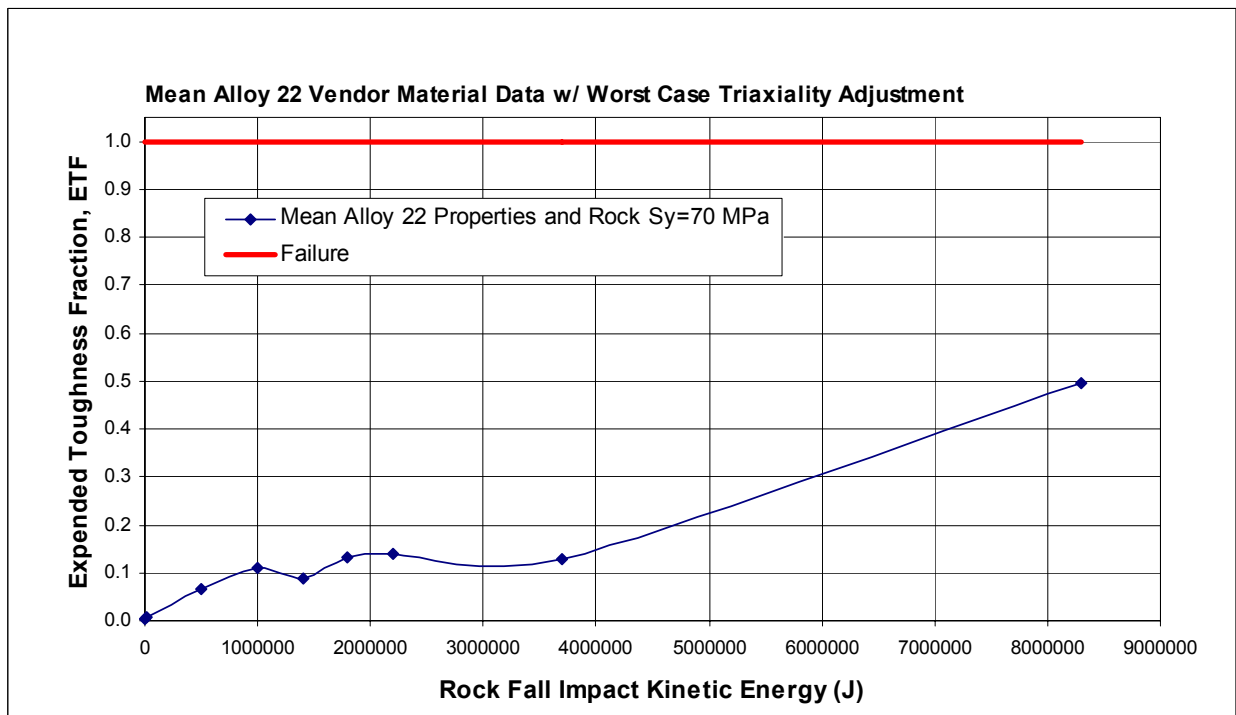
Figure 10.   ETF versus *J* for all Mid WP Rock Impact Cases on Co-disposal Short WP
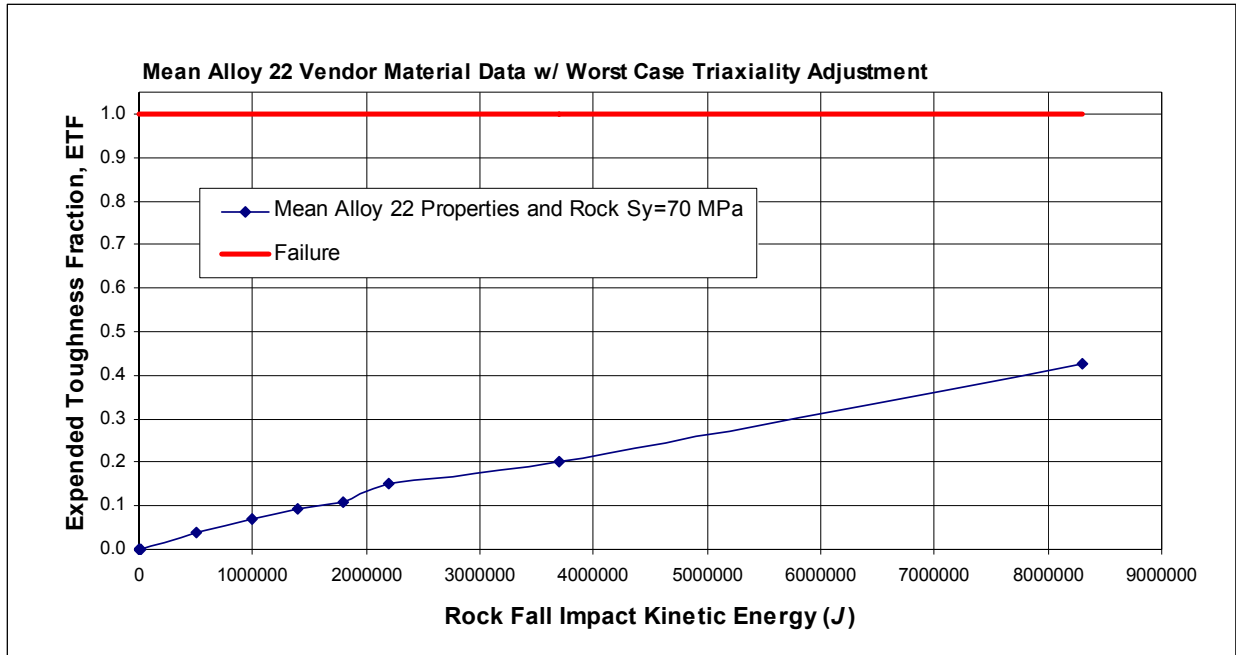
Figure 11.   ETF versus *J* for all Lower WP Sleeve Rock Impact Cases on TAD Bearing WP
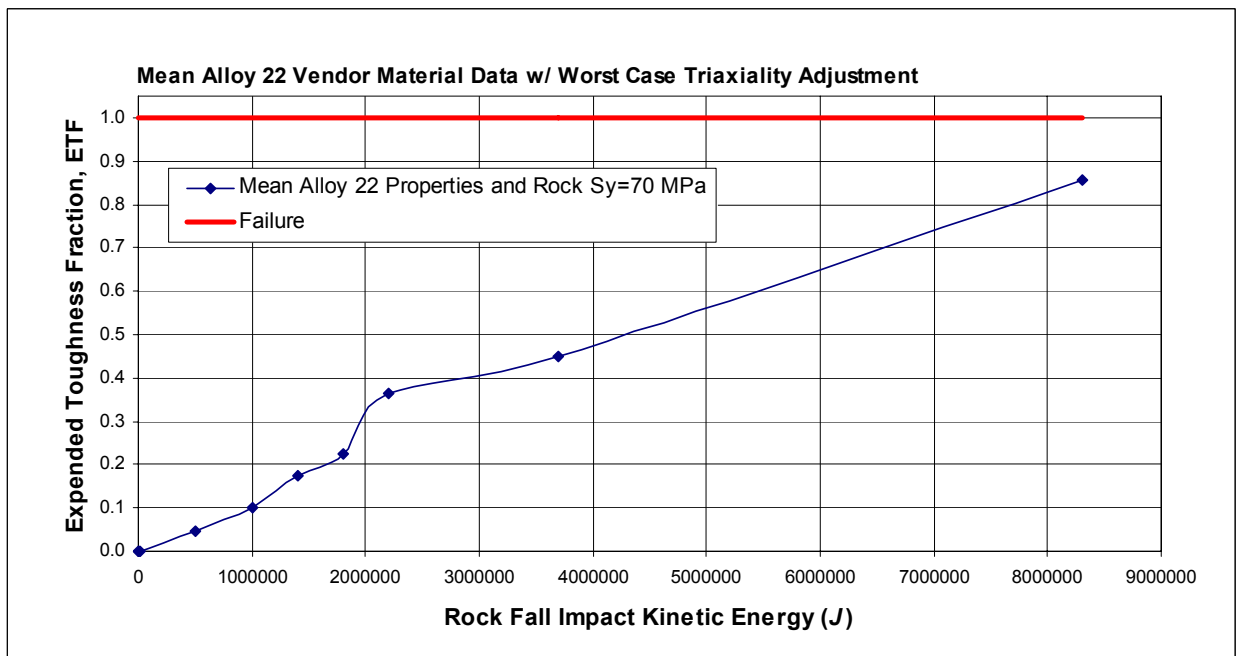
Figure 12.   ETF versus *J* for all Lower WP Sleeve Rock Impact Cases on Co-disposal Short WP
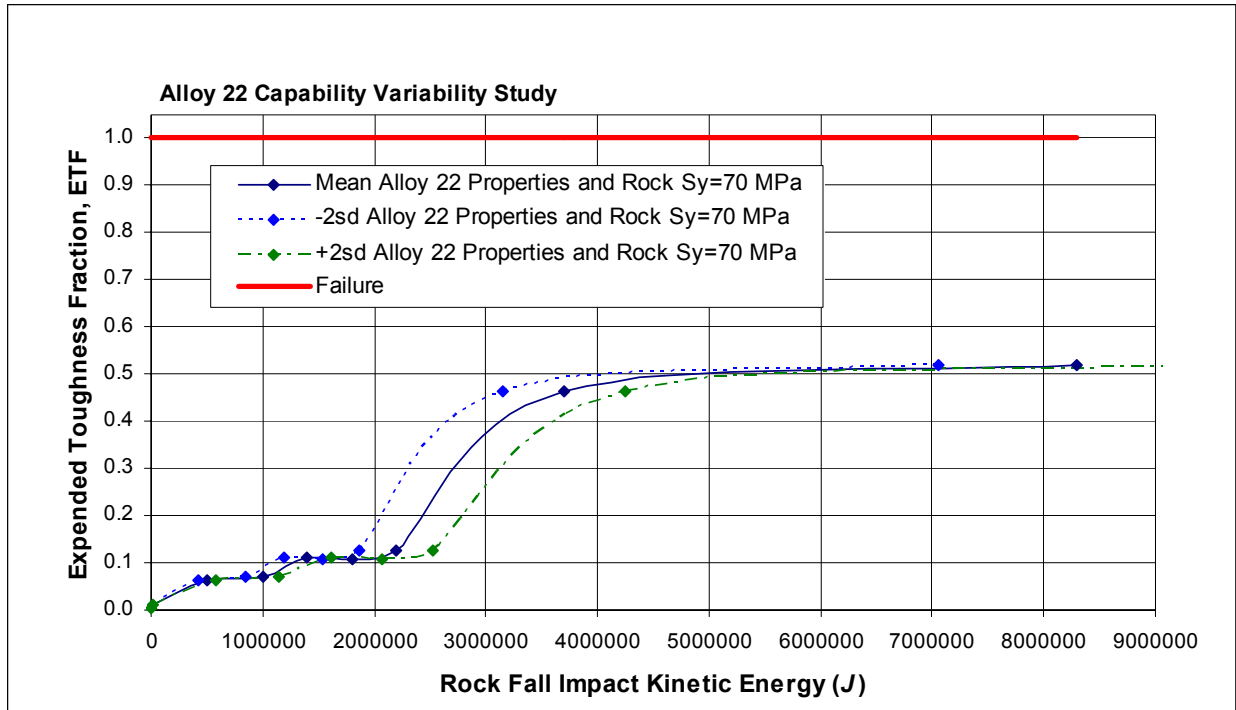
Figure 13.   Mean and 2σ OCB Capability for Mid WP Rock Impacts on TAD Bearing WP
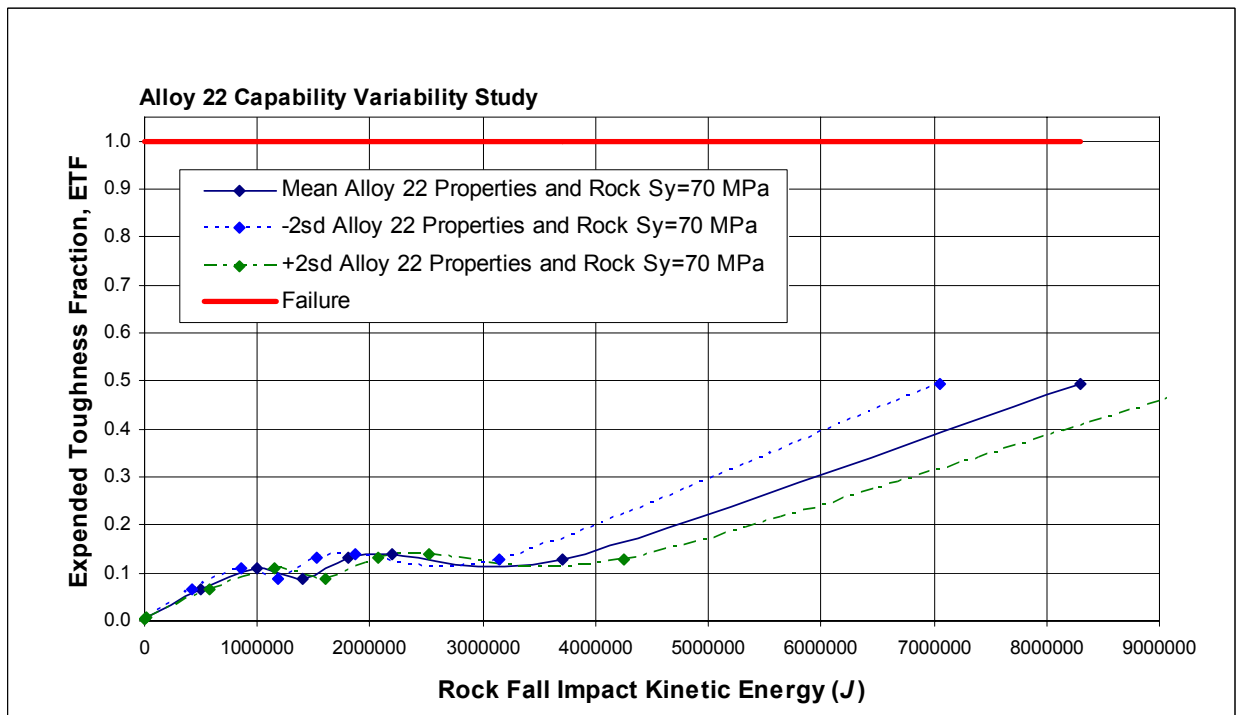
Figure 14.   Mean and 2σ OCB Capability for Mid WP Rock Impacts on Co-disposal Short WP
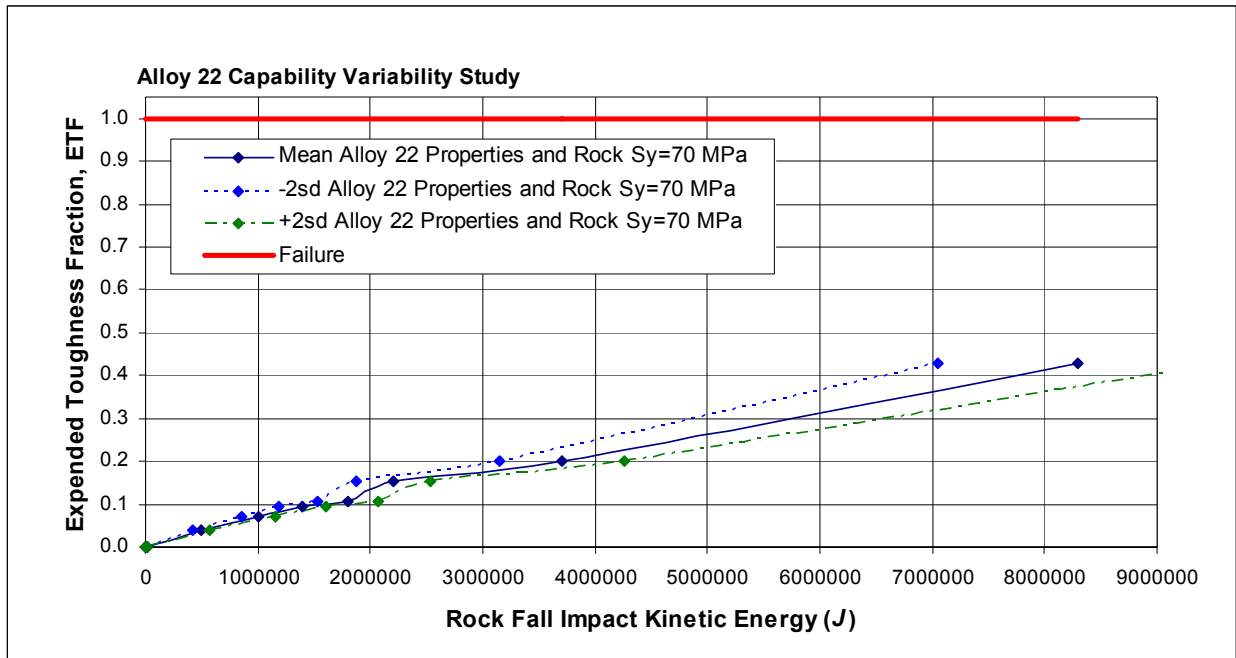
Figure 15.   Mean and 2σ OCB Capability for Lower WP Sleeve Rock Impacts on TAD Bearing WP
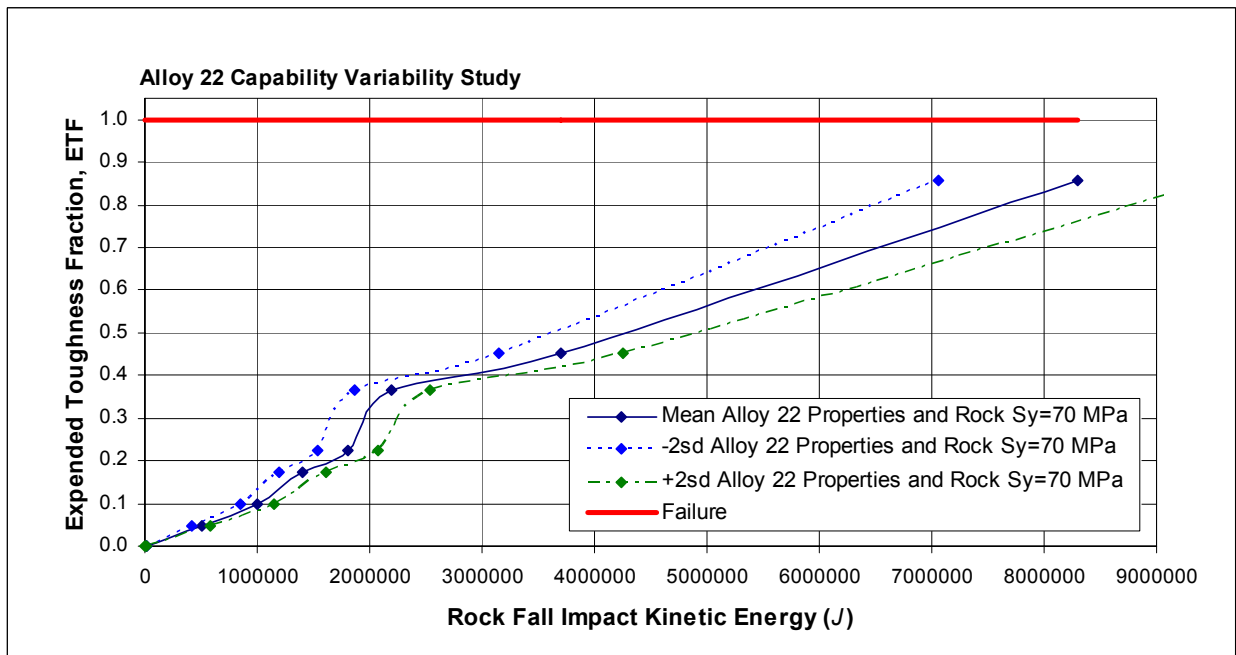
Figure 16.   Mean and 2σ OCB Capability for Lower WP Sleeve Rock Impacts on Co-disposal Short WP

ATTACHMENT I.
FIGURES OBTAINED FROM LS-DYNA
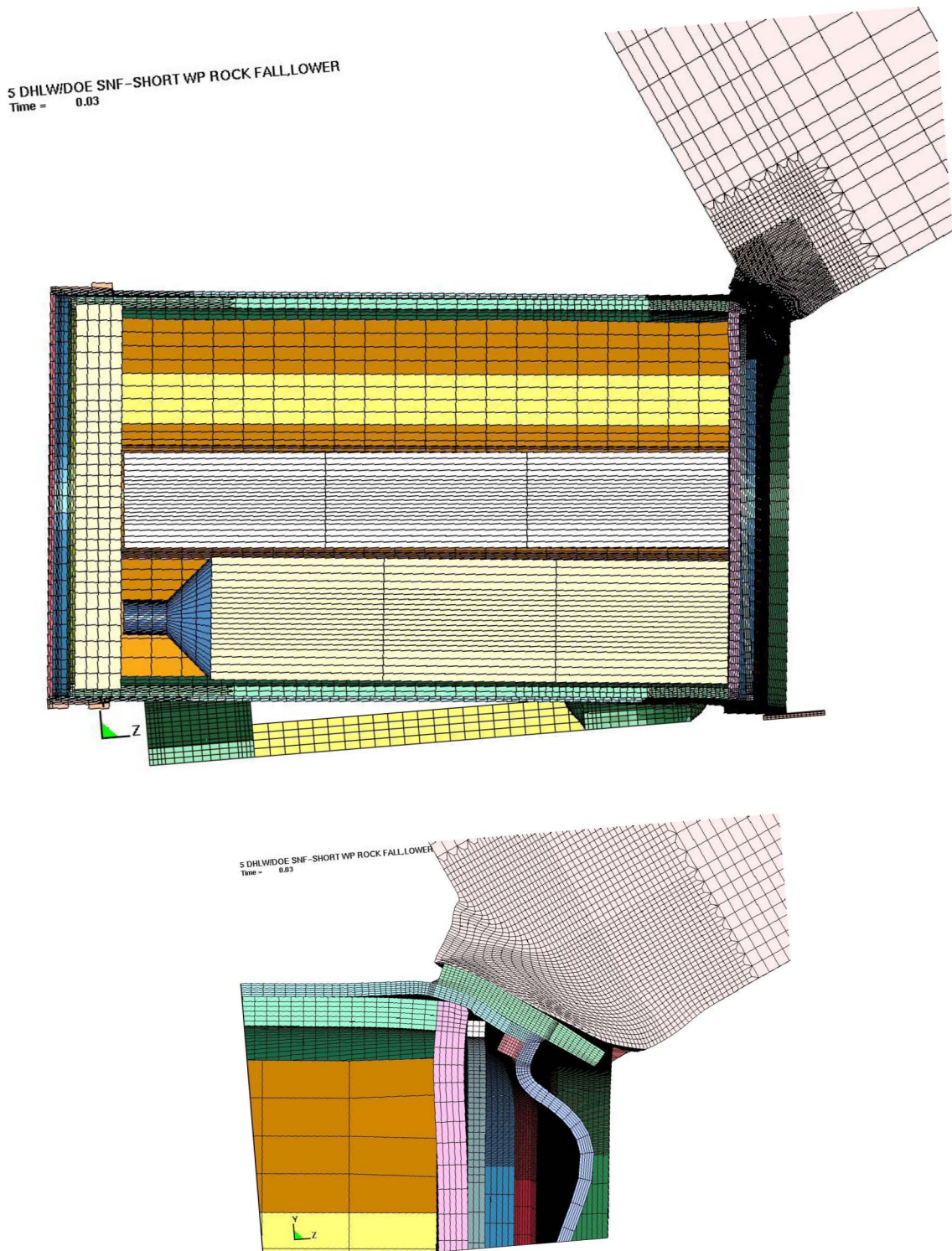
Figure 17.   Co-disposal WP with a 40.8*MT* (45 *ton*), 8.3 *MJ* (6.1*10^6 *ft·lb$_f$*) Rock Impact on the Lower WP Sleeve, 30*ms*
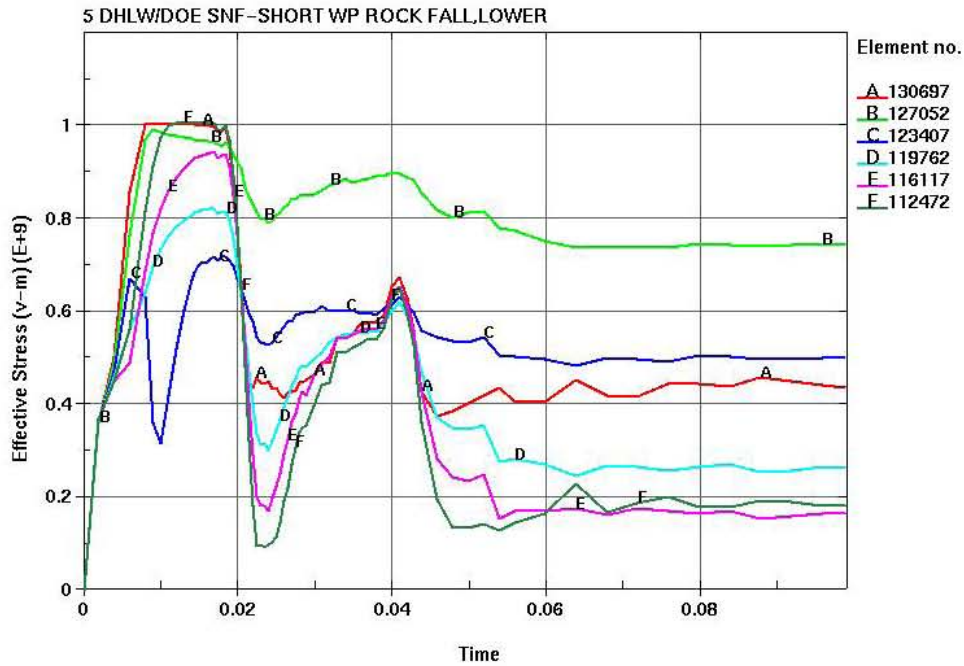
Figure 18.   Co-disposal Short WP, Lower Sleeve Rock Impact, Through-Wall VM Stresses (*Pa*), OCB Lower Lid, 40.8 *MT* (45 *ton*) Rock Impact at 20.1 *m/s* (66.1 *ft/s*) (Case #27)
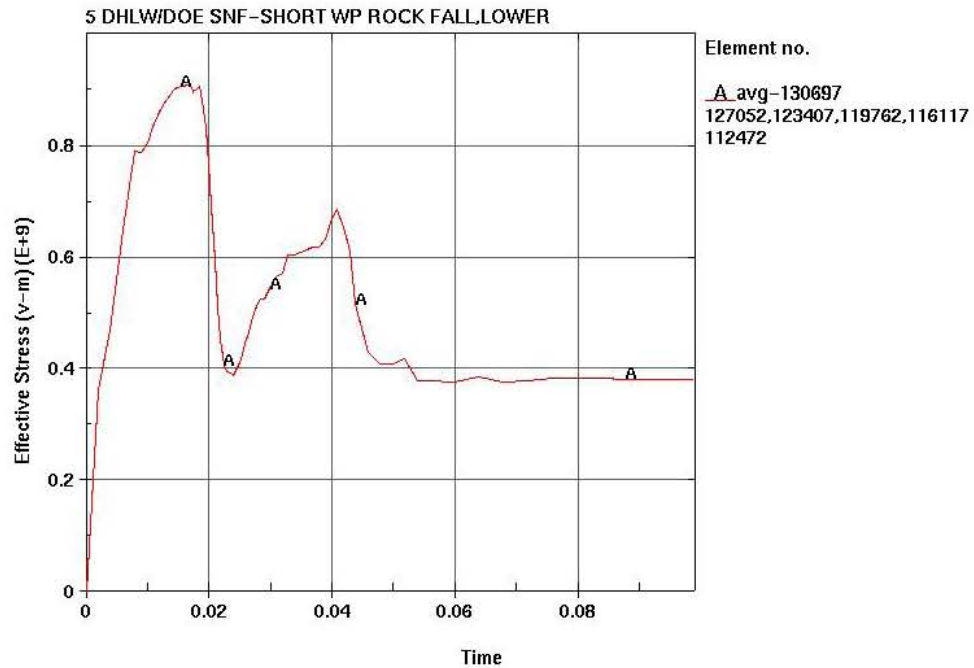
Figure 19.   Co-Disposal Short WP Lower Sleeve Rock Impact, EWA VM Stress (*Pa*), OCB Lower Lid, 40.8 *MT* (45 *ton*) Rock Impact at 20.1 *m/s* (66.1 *ft/s*) (Case #27)
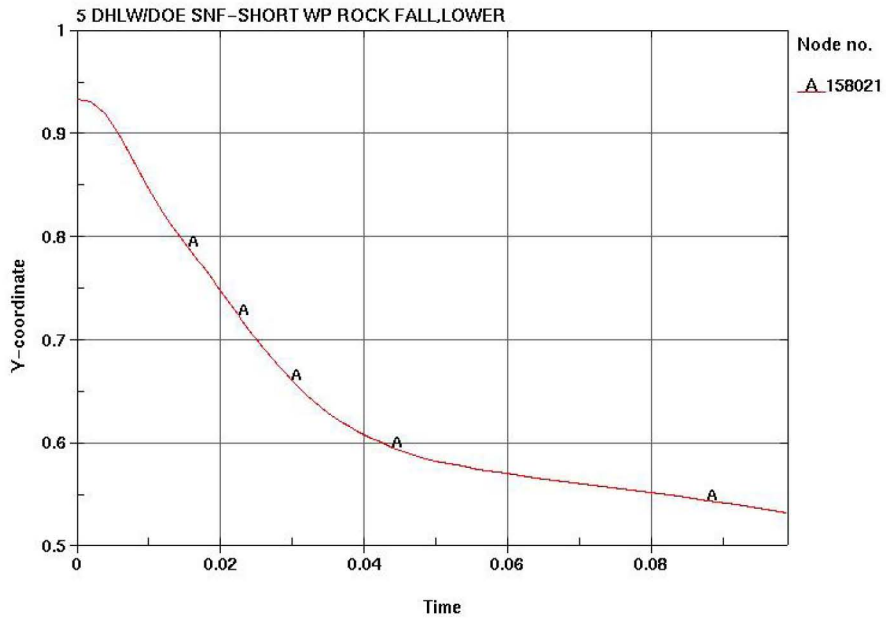
Figure 20.   Co-Disposal Short WP Lower Sleeve Rock Impact, Y-coordinate (*m*) of Node on Element of Peak VM Stress, OCB Lower Lid, 40.8 *MT* (45 *ton*) Rock Impact at 20.1 *m/s* (66.1 *ft/s*) (Case #27)
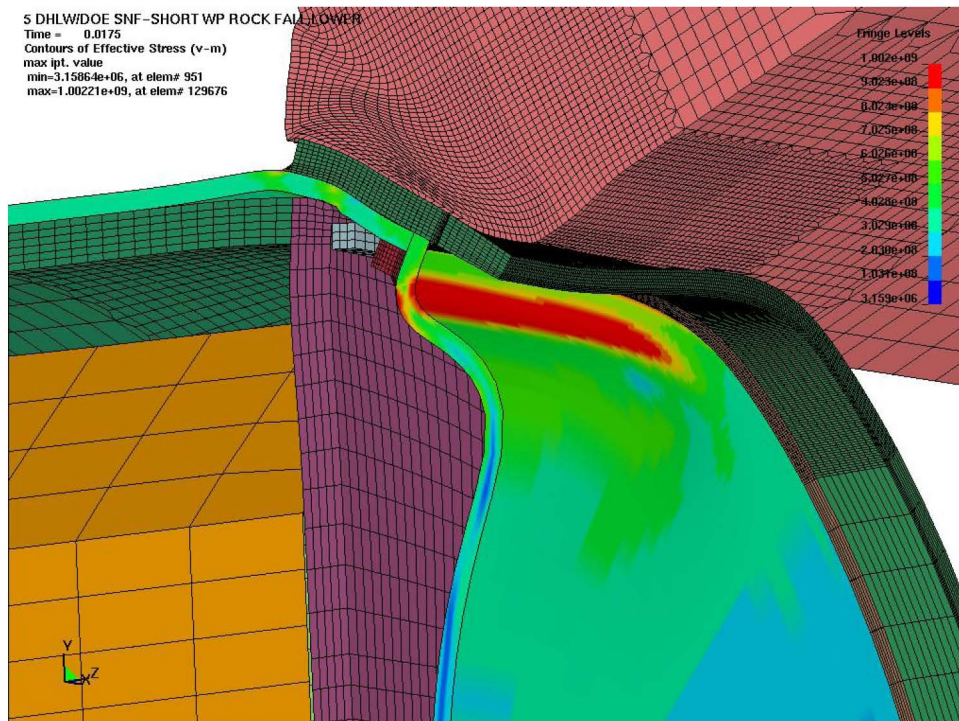
Figure 21.   Co-Disposal Short WP Lower Sleeve Rock Impact, Contour of VM Stress (*Pa*) in the OCB Lower Lid at Peak Time, 40.8 *MT* (45 *ton*) Rock Impact at 20.1 *m/s* (66.1 *ft/s*) (Case #27)
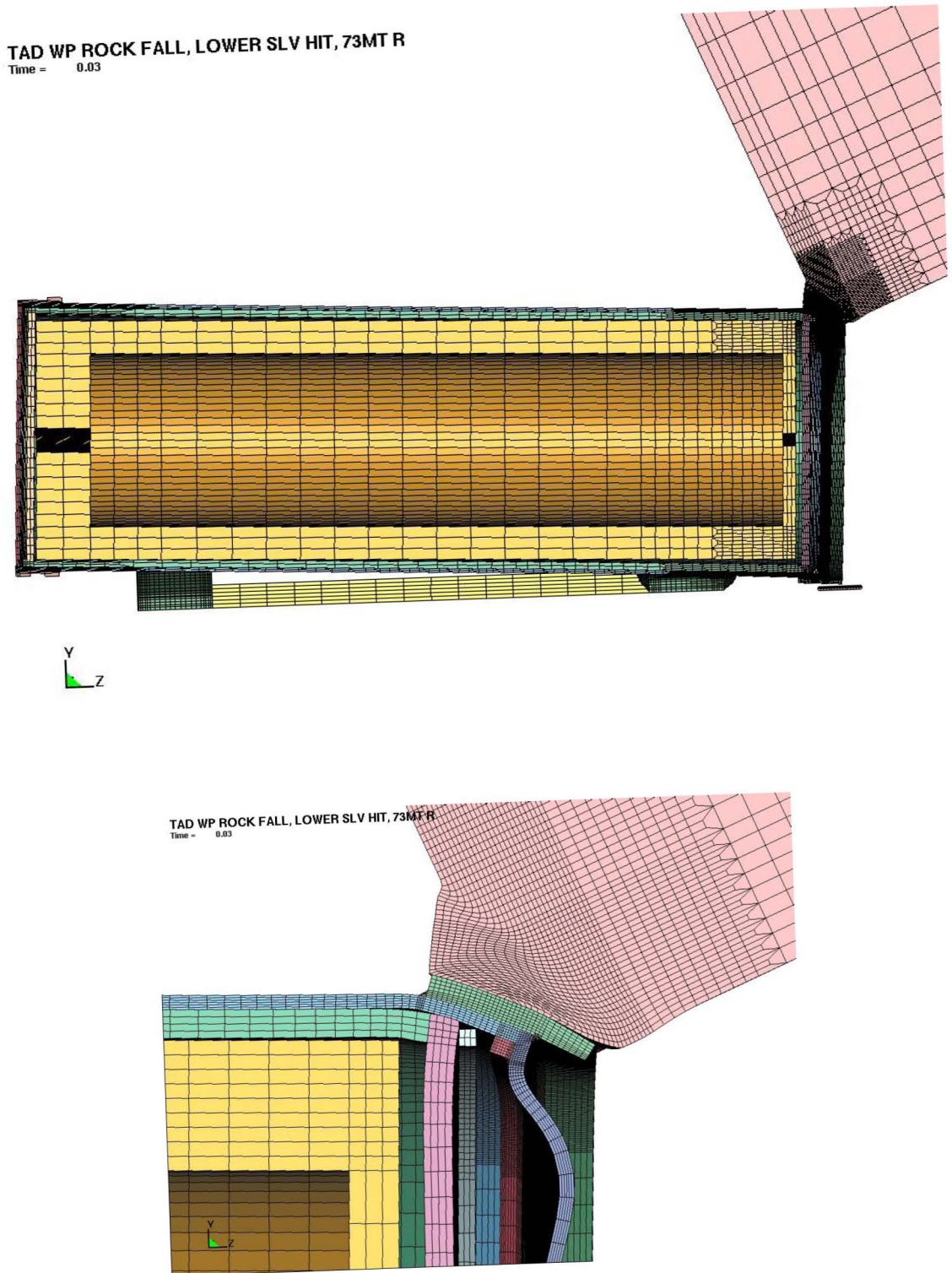
Figure 22.   TAD bearing WP with a 73.5*MT* (81 *ton*), 8.3 *MJ* (6.1*10^6 *ft·lb$_f$*) Rock Impact on the Lower WP Sleeve, 30*ms*
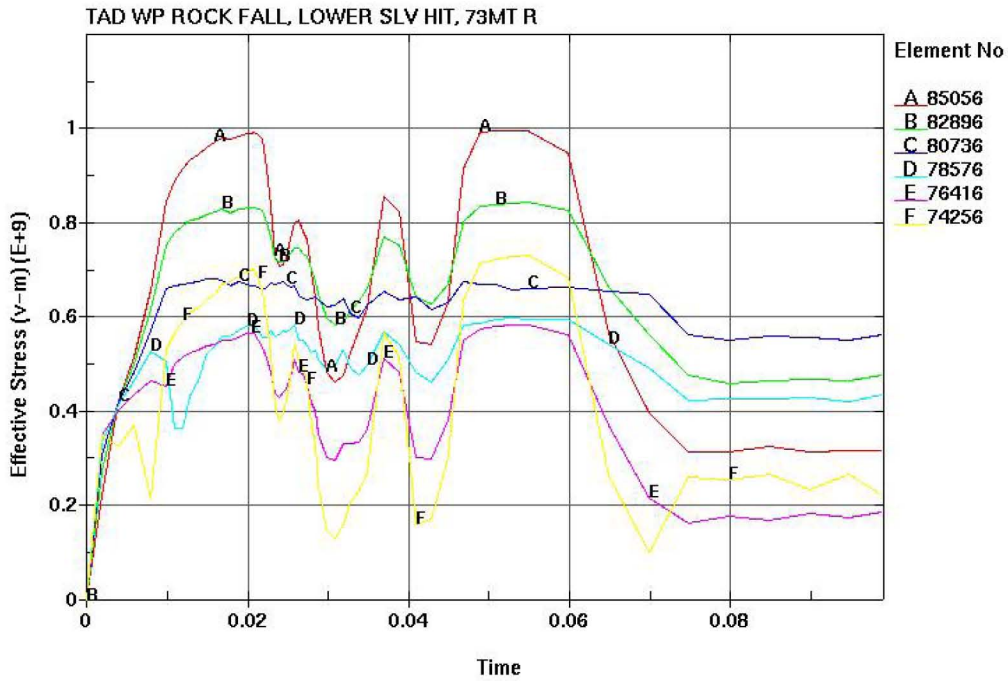
Figure 23.   TAD bearing WP, Lower Sleeve Rock Impact, Through-Wall VM Stresses (*Pa*), OCB Lower Lid, 73.5 *MT* (81 *ton*) Rock Impact at 15 *m/s* (49.2 *ft/s*) (Case #9)
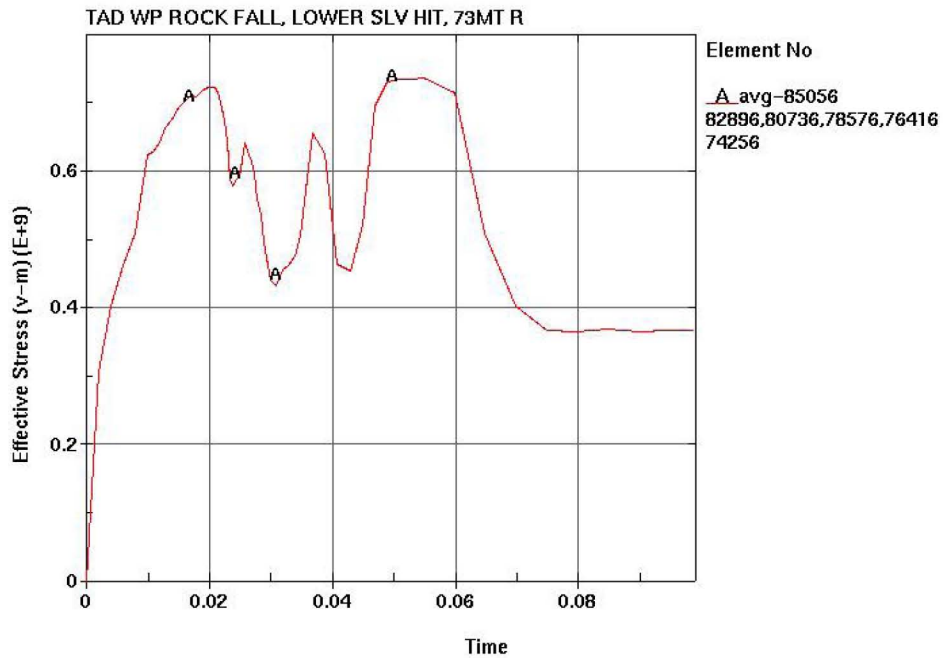
Figure 24.   TAD bearing WP Lower Sleeve Rock Impact, EWA VM Stress (*Pa*), OCB Lower Lid, 73.5 *MT* (81 *ton*) Rock Impact at 15 *m/s* (49.2 *ft/s*) (Case #9)
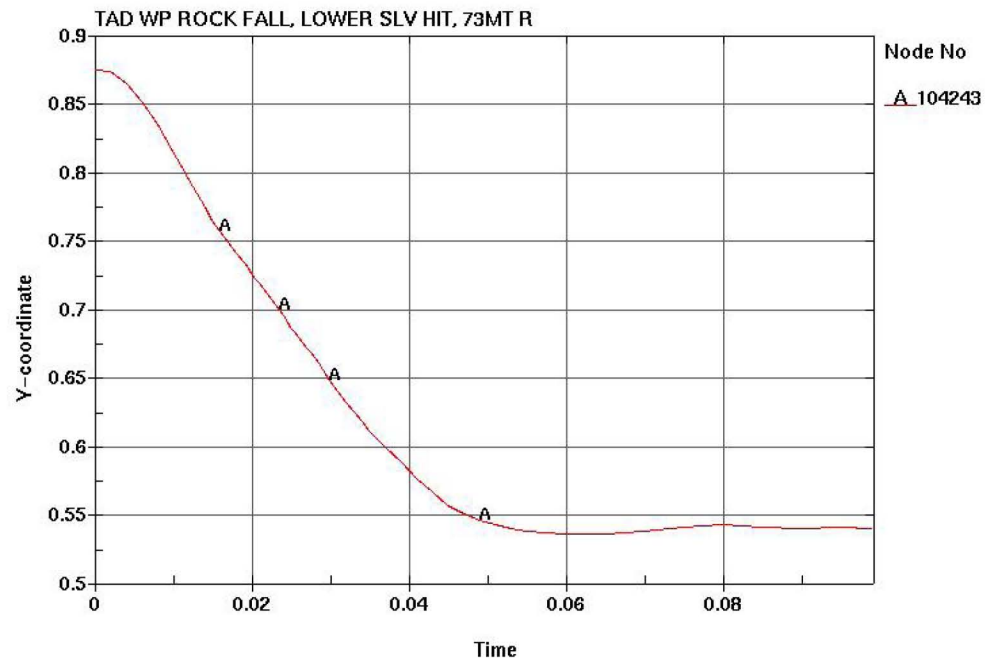
Figure 25.   TAD bearing WP Lower Sleeve Rock Impact, Y-coordinate (*m*) of Node at Element of Peak VM Stress in OCB Lower Lid, 73.5 *MT* (81 *ton*) Rock Impact at 15 *m/s* (49.2 *ft/s*) (Case #9)
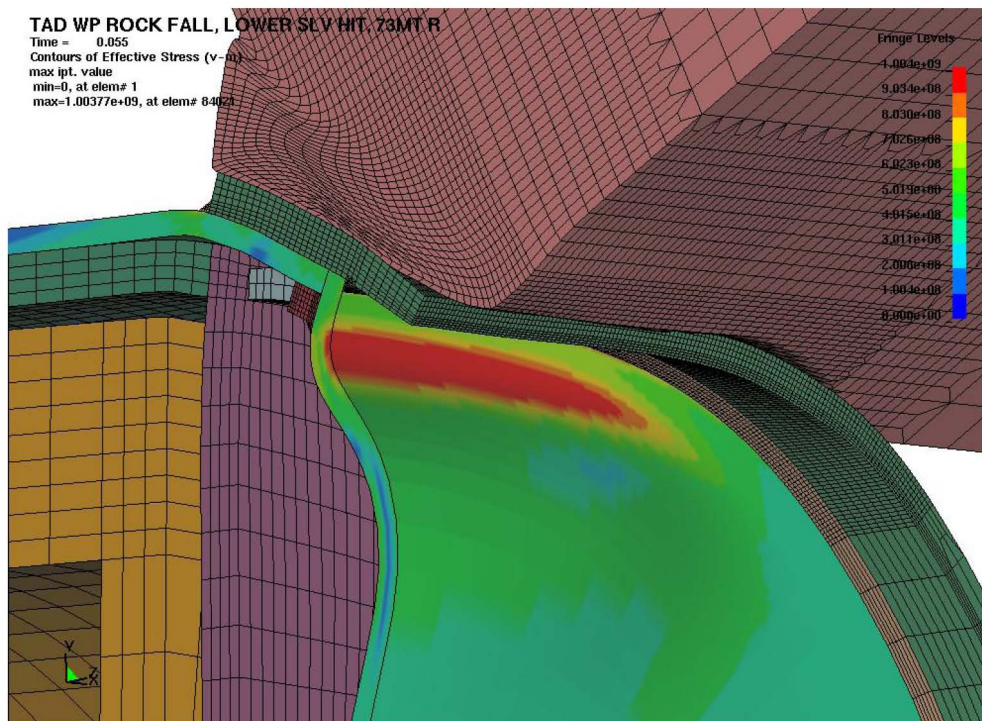
Figure 26.   TAD bearing WP Lower Sleeve Rock Impact, Contour of VM Stress in OCB Lower Lid at Peak Time, 73.5 *MT* (81 *ton*) Rock Impact at 15 *m/s* (49.2 *ft/s*) (Case #9)

ATTACHMENT II.
PLOTS OF CAPABILITY VARIABILITY INCLUDING ROCK COMPRESSIVE STRENGTH VARIABILITY
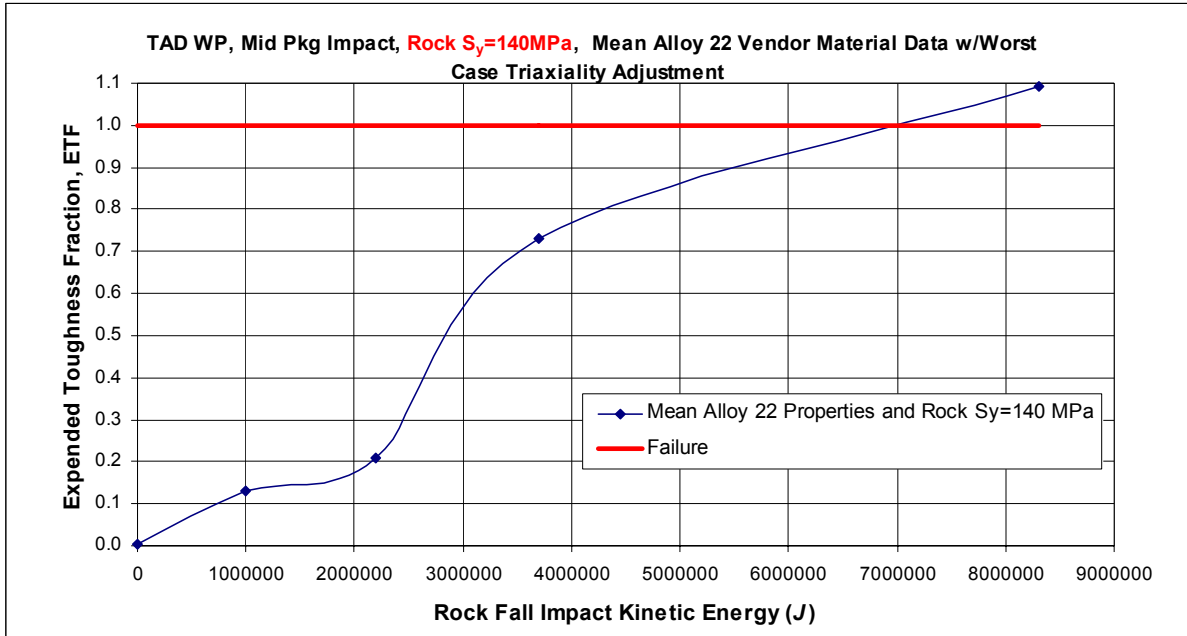
Figure 27.   Rock Compressive Strength = 140*MPa*, ETF versus *J* for all Mid WP Rock Impact Cases on TAD Bearing WP
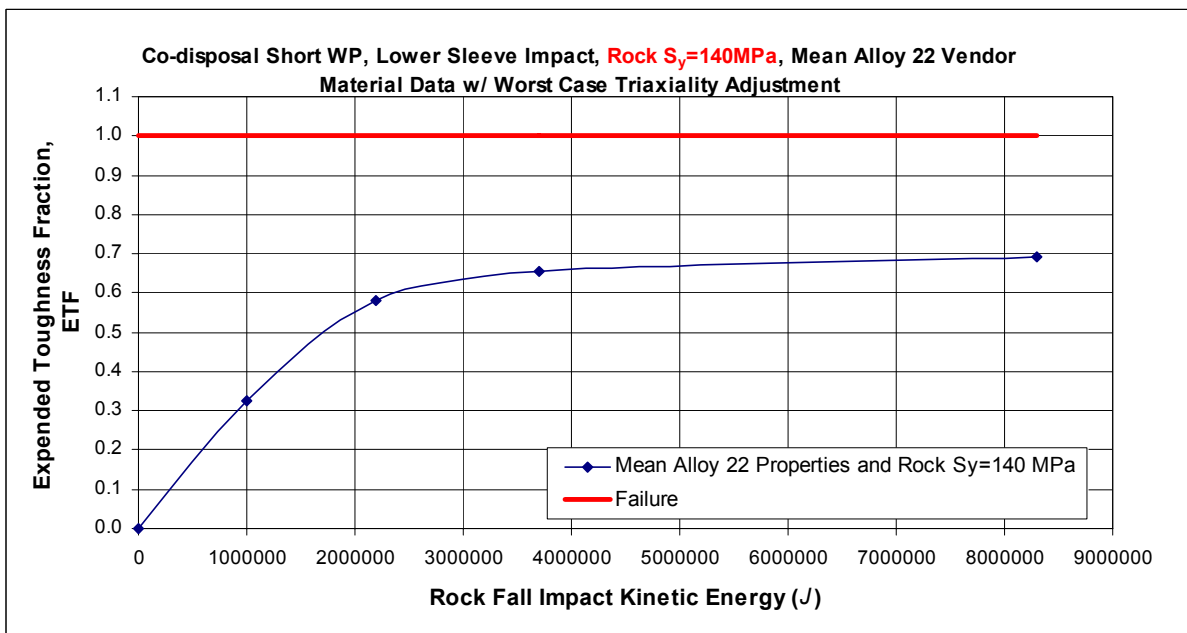
Figure 28.   Rock Compressive Strength = 140*MPa*, ETF versus *J* for all Lower Sleeve Rock Impact Cases on Co-disposal Short WP
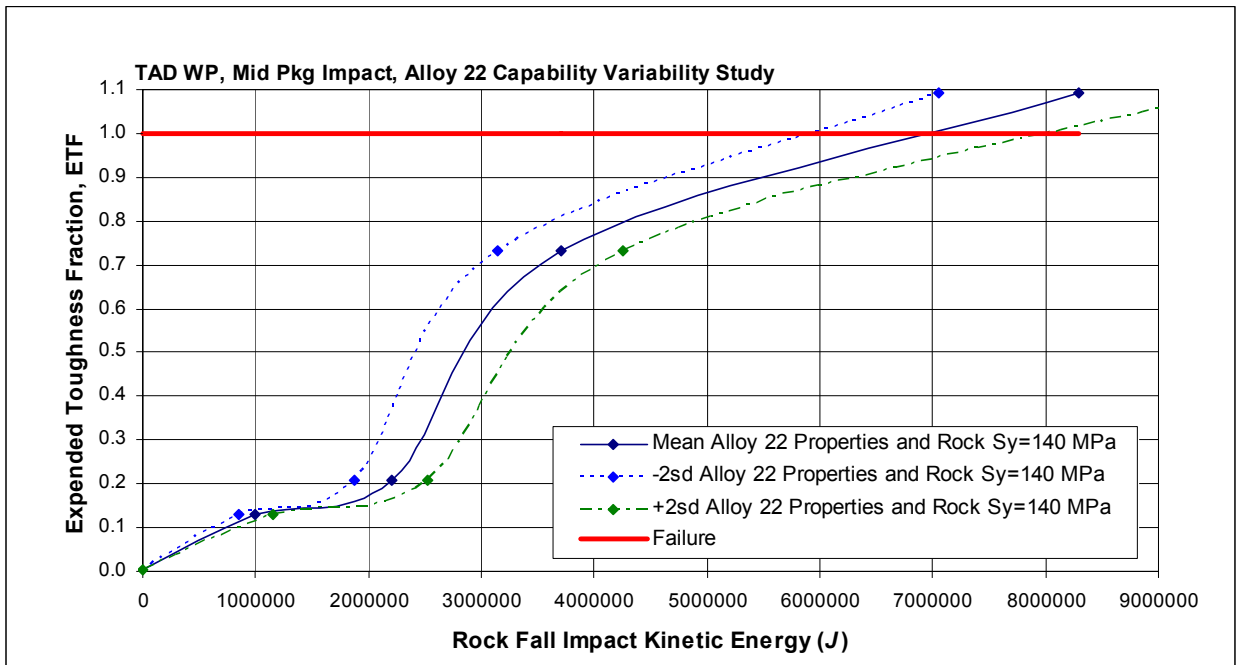
Figure 29.   Rock Compressive Strength = 140*MPa*, Mean and 2σ OCB Capability for Mid WP Rock Impacts on TAD Bearing WP
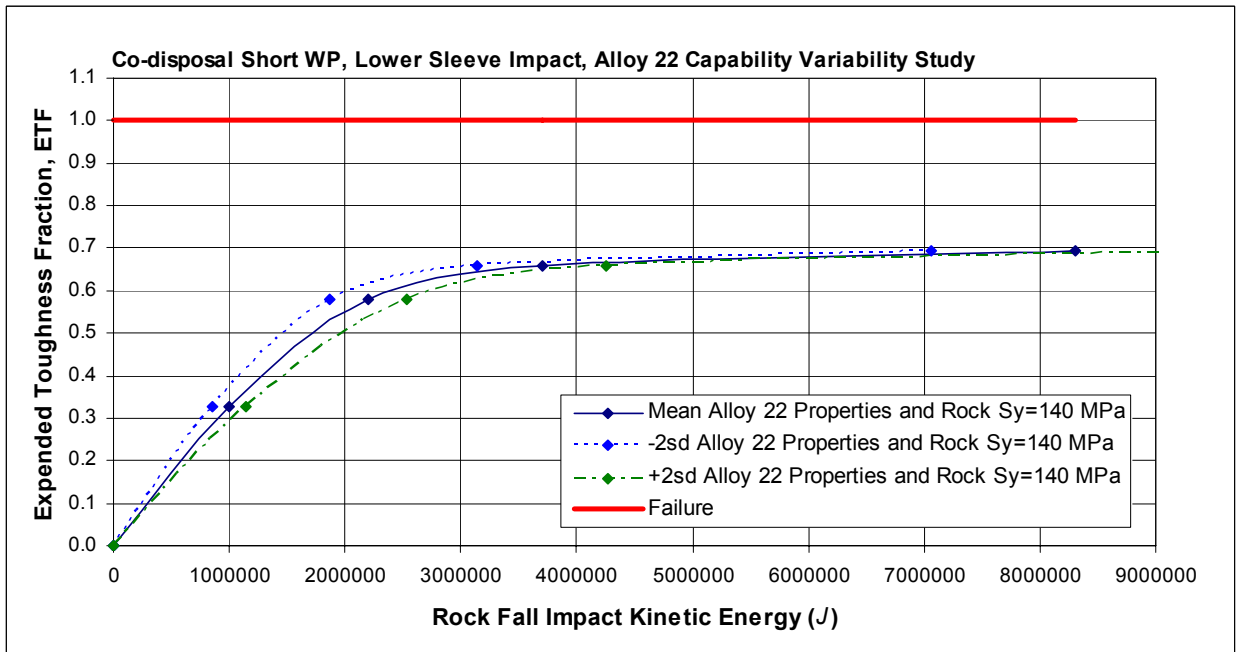
Figure 30.   Rock Compressive Strength = 140*MPa*, Mean and 2σ OCB Capability for Lower Sleeve Rock Impacts on Co-disposal Short WP
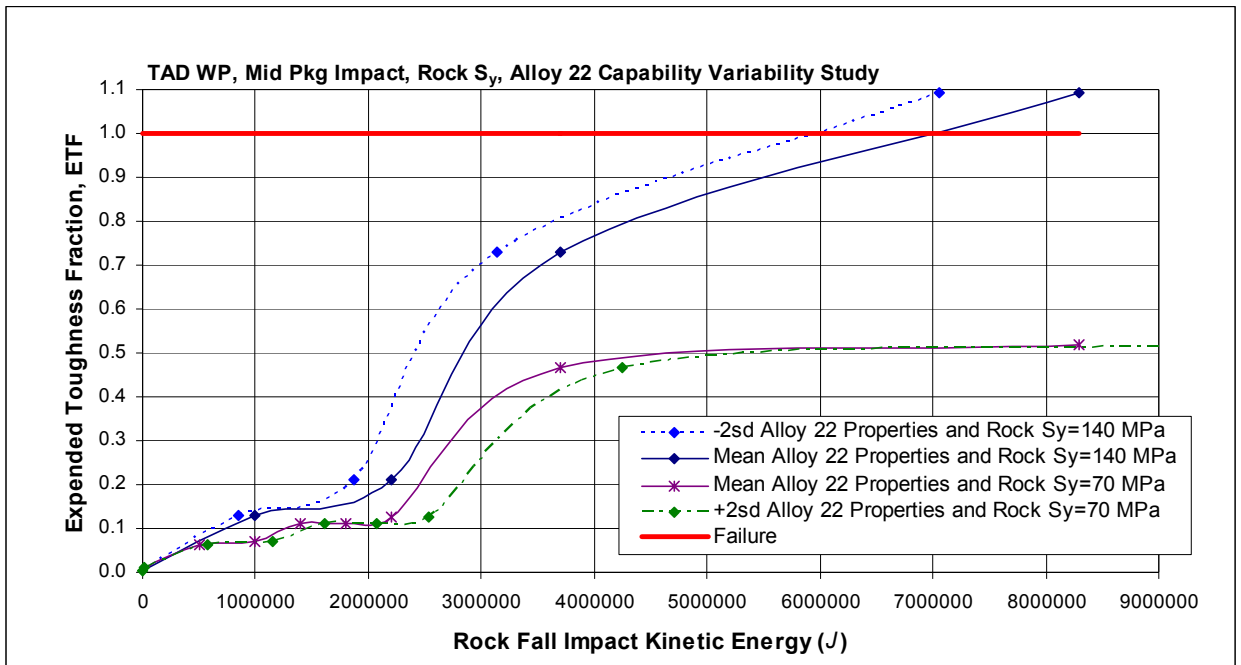
Figure 31.   Rock Compressive Strength Variability, Mean and 2σ OCB Capability for Mid WP Rock Impacts on TAD Bearing WP
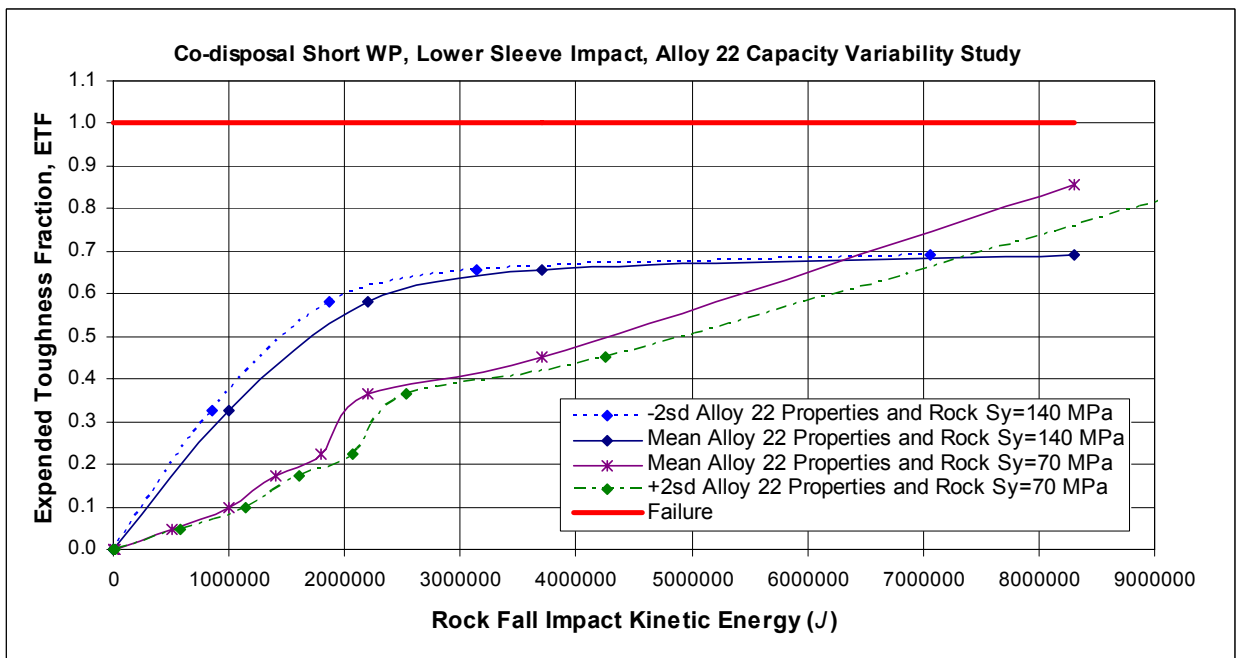
Figure 32.   Rock Compressive Strength Variability, Mean and 2σ OCB Capability for Lower Sleeve Rock Impacts on Co-disposal Short WP

Table 7.   Summary of Rock Compressive Strength Variability Study Maximum ETF Values

Case #	WP configuration	Rock Kinetic Energy	Element Number[a]	$\sigma_{vm,max}$	$\varepsilon_{vm,max}$ m/m	I_T'	ETF=I_T'/I_T
10s	TAD bearing, Mid Package Hit	3,000 J (2213 ft·lb$_f$)	100758	296 MPa (42.9 ksi)	0.0022	0.708	0.0038
13s	TAD bearing, Mid Package Hit	1.0 * 10^6 J (737,560 ft·lb$_f$)	101367	525 MPa (76.1 ksi)	0.0553	24.3	0.1299
16s	TAD bearing, Mid Package Hit	2.2 * 10^6 J (1.6 * 10^6 ft·lb$_f$)	101703	634 MPa (91.9 ksi)	0.0793	39.3	0.2097
17s	TAD bearing, Mid Package Hit	3.7 * 10^6 J (2.7 * 10^6 ft·lb$_f$)	101196	950 MPa (138 ksi)	0.2097	136.9	0.7311
18s	TAD bearing, Mid Package Hit	8.3 * 10^6 J (6.1 * 10^6 ft·lb$_f$)	101199	959 MPa (139 ksi)	0.2930	204.6	1.092
19s	Co-disposal Short, Lower Sleeve Hit	3,000 J (2213 ft·lb$_f$)	131582	112 MPa (16.24 ksi)	0.0005	0.109	0.0006
22s	Co-disposal Short, Lower Sleeve Hit	1.0 * 10^6 J (737,560 ft·lb$_f$)	131583	624 MPa (90.5 ksi)	0.1245	61.0	0.3258
25s	Co-disposal Short, Lower Sleeve Hit	2.2 * 10^6 J (1.6 * 10^6 ft·lb$_f$)	131582	814 MPa (118 ksi)	0.1861	108.9	0.5813
26s	Co-disposal Short, Lower Sleeve Hit	3.7 * 10^6 J (2.7 * 10^6 ft·lb$_f$)	131583	836 MPa (121 ksi)	0.2064	123.0	0.6567
27s	Co-disposal Short, Lower Sleeve Hit	8.3 * 10^6 J (6.1 * 10^6 ft·lb$_f$)	130697	878 MPa (127 ksi)	0.2105	129.8	0.6931

[a] Element number of solid element on outer surface of OCB for selected through-wall section.

ATTACHMENT III.
DIRECTORY LISTING (DATA DVD) OF ELECTRONIC FILES

Table 8.   File Directories, Names, Dates, Times, and Sizes of Attachment IV

Note: File sizes may vary with operating system

```
Directory of D:\Case01_TAD_A
10/09/2007  06:11 PM       10,147,888 d3hsp.gz
10/07/2007  02:28 PM        7,161,443 tada4m1_pra05.inc.gz
10/07/2007  02:28 PM           72,954 tada4m1_pra05.tg
10/07/2007  02:28 PM            8,269 tada4m1_pra05_3000J.k
10/07/2007  02:29 PM           16,990 test.stdout
          5 File(s)     17,407,544 bytes

 Directory of D:\Case02_TAD_A
10/09/2007  06:11 PM       10,522,084 d3hsp.gz
10/07/2007  02:30 PM            8,251 tada5m1s_pra05.k
10/07/2007  02:30 PM        7,052,253 tada5m1_pra05.inc.gz
10/07/2007  02:30 PM           72,851 tada5m1_pra05.tg
10/07/2007  02:30 PM           16,799 test.stdout
          5 File(s)     17,672,238 bytes

 Directory of D:\Case03_TAD_A
10/09/2007  06:05 PM       10,610,461 d3hsp.gz
10/07/2007  02:22 PM        7,332,128 tada2m3c_pra05.inc.gz
10/07/2007  02:22 PM           72,678 tada2m3c_pra05.tg
10/07/2007  02:22 PM            8,198 tada2m3c_pra05_500000J.k
10/07/2007  02:22 PM           19,081 test.stdout
          5 File(s)     18,042,546 bytes

 Directory of D:\Case04_TAD_A
10/09/2007  06:13 PM       11,016,442 d3hsp.gz
10/07/2007  02:32 PM        7,351,396 tada2m2c_pra05.inc.gz
10/07/2007  02:32 PM            8,192 tada2m2c_pra05.k
10/07/2007  02:32 PM           72,637 tada2m2c_pra05.tg
10/07/2007  02:32 PM           18,304 test.stdout
          5 File(s)     18,466,971 bytes

 Directory of D:\Case05_TAD_A
10/09/2007  06:06 PM       11,183,627 d3hsp.gz
10/07/2007  02:24 PM        7,456,813 tada2m3c_pra05.inc.gz
10/07/2007  02:24 PM           72,689 tada2m3c_pra05.tg
10/07/2007  02:24 PM            8,538 tada2m3c_pra05_1400000J.k
10/07/2007  02:24 PM           18,942 test.stdout
          5 File(s)     18,740,609 bytes

 Directory of D:\Case06_TAD_A
10/09/2007  06:07 PM       10,612,141 d3hsp.gz
10/07/2007  02:25 PM        7,332,588 tada3m1a_pra05.inc.gz
10/07/2007  02:25 PM           72,692 tada3m1a_pra05.tg
10/07/2007  02:25 PM            8,229 tada3m1a_pra05_18J.k
10/07/2007  02:25 PM           19,847 test.stdout
          5 File(s)     18,045,497 bytes

 Directory of D:\Case07_TAD_A
10/09/2007  06:08 PM       10,612,021 d3hsp.gz
```

```
10/07/2007  02:26 PM          7,332,588 tada3m1a_pra05.inc.gz
10/07/2007  02:26 PM             72,692 tada3m1a_pra05.tg
10/07/2007  02:26 PM              8,229 tada3m1a_pra05_2200000J.k
10/07/2007  02:26 PM             19,238 test.stdout
               5 File(s)     18,044,768 bytes

 Directory of D:\Case08_TAD_A
10/09/2007  06:09 PM         10,611,094 d3hsp.gz
10/07/2007  02:27 PM          7,531,977 tada4m1a_pra05b.inc.gz
10/07/2007  02:27 PM             73,393 tada4m1a_pra05b.tg
10/07/2007  02:27 PM              8,566 tada4m2a_pra05.k
10/07/2007  02:27 PM             25,549 test.stdout
               5 File(s)     18,250,579 bytes

 Directory of D:\Case09_TAD_A
10/09/2007  06:16 PM         10,739,665 d3hsp.gz
10/08/2007  10:09 AM          7,531,977 tada4m1a_pra05b.inc.gz
10/08/2007  10:09 AM             73,393 tada4m1a_pra05b.tg
10/08/2007  10:09 AM              8,675 tada4m2a_pra05_8MJ.k
10/08/2007  10:09 AM             25,628 test.stdout
               5 File(s)     18,379,338 bytes

 Directory of D:\Case10_TAD_C
10/09/2007  06:11 PM         10,596,480 d3hsp.gz
10/07/2007  02:29 PM          6,436,382 tada3m2s_pra05_mid.inc.gz
10/07/2007  02:29 PM              8,897 tada3m2s_pra05_mid.k
10/07/2007  02:29 PM             76,811 tada3m2s_pra05_mid.tg
10/07/2007  02:29 PM             17,543 test.stdout
               5 File(s)     17,136,113 bytes

 Directory of D:\Case11_TAD_C
10/09/2007  06:05 PM         10,230,534 d3hsp.gz
10/07/2007  02:21 PM          6,436,394 tada5m1s_pra05_mid.inc.gz
10/07/2007  02:20 PM              8,898 tada5m1s_pra05_mid.k
10/07/2007  02:20 PM             76,794 tada5m1s_pra05_mid.tg
10/07/2007  02:21 PM             17,899 test.stdout
               5 File(s)     16,770,519 bytes

 Directory of D:\Case12_TAD_C
10/09/2007  06:12 PM         11,989,636 d3hsp.gz
10/07/2007  02:31 PM          7,091,248 tada2m8_pra05_mid.inc.gz
10/07/2007  02:31 PM             76,600 tada2m8_pra05_mid.tg
10/07/2007  02:31 PM              8,715 tada2m8_pra05_mid_0.5MJ.k
10/07/2007  02:31 PM             18,920 test.stdout
               5 File(s)     19,185,119 bytes

 Directory of D:\Case13_TAD_C
10/09/2007  06:13 PM         11,537,589 d3hsp.gz
10/07/2007  02:31 PM          7,091,248 tada2m8_pra05_mid.inc.gz
10/07/2007  02:31 PM              8,715 tada2m8_pra05_mid.k
10/07/2007  02:31 PM             76,600 tada2m8_pra05_mid.tg
10/07/2007  02:32 PM             19,023 test.stdout
               5 File(s)     18,733,175 bytes

 Directory of D:\Case14_TAD_C
10/09/2007  06:07 PM         11,537,470 d3hsp.gz
10/07/2007  02:24 PM          7,091,248 tada2m8_pra05_mid.inc.gz
10/07/2007  02:24 PM             76,600 tada2m8_pra05_mid.tg
10/07/2007  02:24 PM              8,716 tada2m8_pra05_mid_1.4MJ.k
10/07/2007  02:24 PM             18,368 test.stdout
               5 File(s)     18,732,402 bytes
```

```
 Directory of D:\Case15_TAD_C
10/09/2007  06:08 PM       11,988,731 d3hsp.gz
10/07/2007  02:26 PM        7,091,223 tada3m2_pra05_mid.inc.gz
10/07/2007  02:26 PM           76,603 tada3m2_pra05_mid.tg
10/07/2007  02:26 PM            8,743 tada3m2_pra05_mid_1.8MJ.k
10/07/2007  02:26 PM           15,198 test.stdout
              5 File(s)     19,180,498 bytes

 Directory of D:\Case16_TAD_C
10/09/2007  06:15 PM       11,990,005 d3hsp.gz
10/08/2007  10:11 AM        7,091,223 tada3m2_pra05_mid.inc.gz
10/08/2007  10:11 AM           76,603 tada3m2_pra05_mid.tg
10/08/2007  10:11 AM            8,710 tada3m2_pra05_mid_2.2MJ.k
10/08/2007  10:11 AM           19,339 test.stdout
              5 File(s)     19,185,880 bytes

 Directory of D:\Case17_TAD_C
10/09/2007  06:09 PM       10,662,012 d3hsp.gz
10/07/2007  02:28 PM        6,748,174 tada3m2_pra05_midb.inc.gz
10/07/2007  02:28 PM           76,608 tada3m2_pra05_midb.tg
10/07/2007  02:28 PM            8,900 tada3m2_pra05_mid_3.7MJ.k
10/07/2007  02:28 PM           22,026 test.stdout
              5 File(s)     17,517,720 bytes

 Directory of D:\Case18_TAD_C
10/09/2007  06:17 PM       10,662,063 d3hsp.gz
10/08/2007  10:10 AM        6,748,174 tada3m2_pra05_midb.inc.gz
10/08/2007  10:10 AM           76,608 tada3m2_pra05_midb.tg
10/08/2007  10:10 AM            8,899 tada3m2_pra05_mid_8.3MJ.k
10/08/2007  10:10 AM           22,078 test.stdout
              5 File(s)     17,517,822 bytes

 Directory of D:\Case19_5DHLW_A
10/08/2007  11:08 AM            9,691 5dhlwa1m1_newSlv_3000J.k
10/08/2007  11:08 AM       11,078,716 5dhlwa1m1_newSlv_430kg.inc.gz
10/08/2007  10:29 AM           82,501 5dhlwa1m1_newSlv_430kg.tg
10/09/2007  05:54 PM       12,995,333 d3hsp.gz
10/08/2007  11:08 AM           18,634 test.stdout
              5 File(s)     24,184,875 bytes

 Directory of D:\Case20_5DHLW_A
10/08/2007  10:22 AM            9,934 5dhlwa2m1s_newSlv_15000J.k
10/08/2007  10:22 AM       11,043,431 5dhlwa2m1_newSlv_2MT.inc.gz
10/08/2007  10:22 AM           82,430 5dhlwa2m1_newSlv_2MT.tg
10/09/2007  06:03 PM       15,357,556 d3hsp.gz
10/08/2007  10:22 AM           18,499 test.stdout
              5 File(s)     26,511,850 bytes

 Directory of D:\Case21_5DHLW_A
10/08/2007  11:07 AM            9,887 5dhlwa2m1s_newSlv_0.5MJ.k
10/08/2007  11:07 AM       11,797,707 5dhlwa2m1_newSleeve.inc.gz
10/08/2007  11:07 AM           82,054 5dhlwa2m1_newSleeve.tg
10/09/2007  05:56 PM       14,007,602 d3thdt.gz
10/08/2007  11:07 AM           21,753 test.stdout
              5 File(s)     25,919,003 bytes

 Directory of D:\Case22_5DHLW_A
10/08/2007  10:49 AM            9,884 5dhlwa2m1s_newSlv.k
10/08/2007  10:49 AM       11,797,707 5dhlwa2m1_newSleeve.inc.gz
10/08/2007  10:49 AM           82,054 5dhlwa2m1_newSleeve.tg
10/09/2007  05:49 PM       14,106,764 d3hsp.gz
10/08/2007  10:49 AM           26,805 test.stdout
```

             5 File(s)   26,023,214 bytes

 Directory of D:\Case23_5DHLW_A
10/08/2007 10:50 AM   9,888 5dhlwa2m1s_newSlv_1.4MJ.k
10/08/2007 10:50 AM   11,797,707 5dhlwa2m1_newSleeve.inc.gz
10/08/2007 10:50 AM   82,054 5dhlwa2m1_newSleeve.tg
10/09/2007 05:53 PM   14,106,833 d3hsp.gz
10/08/2007 10:50 AM   26,825 test.stdout
             5 File(s)   26,023,307 bytes

 Directory of D:\Case24_5DHLW_A
10/08/2007 10:57 AM   9,933 5dhlwa2m1s_newSlv_1.8MJ.k
10/08/2007 10:57 AM   11,918,493 5dhlwa2m1_newSlv_28MT.inc.gz
10/08/2007 10:57 AM   82,057 5dhlwa2m1_newSlv_28MT.tg
10/09/2007 05:57 PM   14,107,049 d3hsp.gz
10/08/2007 10:58 AM   27,174 test.stdout
             5 File(s)   26,144,706 bytes

 Directory of D:\Case25_5DHLW_A
10/08/2007 10:56 AM   9,933 5dhlwa2m1s_newSlv_2.2MJ.k
10/08/2007 10:56 AM   11,918,493 5dhlwa2m1_newSlv_28MT.inc.gz
10/08/2007 10:56 AM   82,057 5dhlwa2m1_newSlv_28MT.tg
10/09/2007 05:58 PM   14,107,053 d3hsp.gz
10/08/2007 10:56 AM   27,166 test.stdout
             5 File(s)   26,144,702 bytes

 Directory of D:\Case26_5DHLW_A
10/08/2007 10:55 AM   10,239 5dhlwa5m1_newSlv_3.7MJ.k
10/08/2007 10:55 AM   11,941,708 5dhlwa5m1_newSlv_41MT.inc.gz
10/08/2007 10:55 AM   82,769 5dhlwa5m1_newSlv_41MT.tg
10/09/2007 06:00 PM   14,143,415 d3hsp.gz
10/08/2007 10:55 AM   24,194 test.stdout
             5 File(s)   26,202,325 bytes

 Directory of D:\Case27_5DHLW_A
10/08/2007 10:26 AM   11,941,708 5dhlwa5m1_newSlv_41MT.inc.gz
10/08/2007 10:26 AM   82,769 5dhlwa5m1_newSlv_41MT.tg
10/08/2007 10:26 AM   10,239 5dhlwa5m1_newSlv_8.3MJ.k
10/09/2007 06:00 PM   14,145,963 d3hsp.gz
10/08/2007 10:26 AM   33,787 test.stdout
             5 File(s)   26,214,466 bytes

 Directory of D:\Case28_5DHLW_C
10/08/2007 11:09 AM   10,086 5dhlwa1m1_newSlv_mid_3000J.k
10/08/2007 11:09 AM   6,219,650 5dhlwa1m1_newSlv_mid_430kg.inc.gz
10/08/2007 11:09 AM   91,049 5dhlwa1m1_newSlv_mid_430kg.tg
10/09/2007 05:55 PM   8,413,750 d3hsp.gz
10/08/2007 11:09 AM   19,468 test.stdout
             5 File(s)   14,754,003 bytes

 Directory of D:\Case29_5DHLW_C
10/08/2007 10:24 AM   9,759 5dhlwa2m1_newSlv_midHit_15000J.k
10/08/2007 10:24 AM   6,214,114 5dhlwa2m1_newSlv_midHit_2MT.inc.gz
10/08/2007 10:24 AM   91,328 5dhlwa2m1_newSlv_midHit_2MT.tg
10/09/2007 06:04 PM   10,983,158 d3hsp.gz
10/08/2007 10:24 AM   15,739 test.stdout
             5 File(s)   17,314,098 bytes

 Directory of D:\Case30_5DHLW_C
10/08/2007 11:07 AM   7,085,701 5dhlwa2m1_newSlv_midHit.inc.gz
10/08/2007 11:07 AM   90,944 5dhlwa2m1_newSlv_midHit.tg
10/08/2007 11:07 AM   9,669 5dhlwa2m1_newSlv_midHit_0.5MJ.k

```
10/09/2007  05:56 PM          9,575,391 d3hsp.gz
10/08/2007  11:07 AM             22,128 test.stdout
              5 File(s)     16,783,833 bytes

 Directory of D:\Case31_5DHLW_C
10/08/2007  10:50 AM          7,085,701 5dhlwa2m1_newSlv_midHit.inc.gz
10/08/2007  10:50 AM              9,666 5dhlwa2m1_newSlv_midHit.k
10/08/2007  10:50 AM             90,944 5dhlwa2m1_newSlv_midHit.tg
10/09/2007  05:52 PM          9,575,282 d3hsp.gz
10/08/2007  10:50 AM             21,632 test.stdout
              5 File(s)     16,783,225 bytes

 Directory of D:\Case32_5DHLW_C
10/08/2007  10:51 AM          7,085,701 5dhlwa2m1_newSlv_midHit.inc.gz
10/08/2007  10:51 AM             90,944 5dhlwa2m1_newSlv_midHit.tg
10/08/2007  10:51 AM             10,002 5dhlwa2m1_newSlv_midHit_1.4MJ.k
10/09/2007  05:53 PM          9,575,921 d3hsp.gz
10/08/2007  10:51 AM             21,089 test.stdout
              5 File(s)     16,783,657 bytes

 Directory of D:\Case33_5DHLW_C
10/08/2007  10:58 AM          7,085,467 5dhlwa2m1_newSlv_mid28MT.inc.gz
10/08/2007  10:58 AM             90,947 5dhlwa2m1_newSlv_mid28MT.tg
10/08/2007  10:58 AM             10,088 5dhlwa2m1_newSlv_midHit_1.8MJ.k
10/09/2007  05:58 PM          9,576,376 d3hsp.gz
10/08/2007  10:59 AM             22,547 test.stdout
              5 File(s)     16,785,425 bytes

 Directory of D:\Case34_5DHLW_C
10/08/2007  10:57 AM          7,085,467 5dhlwa2m1_newSlv_mid28MT.inc.gz
10/08/2007  10:57 AM             90,947 5dhlwa2m1_newSlv_mid28MT.tg
10/08/2007  10:57 AM             10,069 5dhlwa2m1_newSlv_midHit_2.2MJ.k
10/09/2007  05:59 PM          9,576,304 d3hsp.gz
10/08/2007  10:57 AM             21,932 test.stdout
              5 File(s)     16,784,719 bytes

 Directory of D:\Case35_5DHLW_C
10/08/2007  10:21 AM             10,076 5dhlwa5m1_newSlv_mid3.7MJ.k
10/08/2007  10:21 AM          7,044,662 5dhlwa5m1_newSlv_mid41MT.inc.gz
10/08/2007  10:21 AM             90,816 5dhlwa5m1_newSlv_mid41MT.tg
10/09/2007  06:02 PM         10,348,868 d3hsp.gz
10/08/2007  10:21 AM             22,887 test.stdout
              5 File(s)     17,517,309 bytes

 Directory of D:\Case36_5DHLW_C
10/08/2007  10:20 AM          7,044,662 5dhlwa5m1_newSlv_mid41MT.inc.gz
10/08/2007  10:20 AM             90,816 5dhlwa5m1_newSlv_mid41MT.tg
10/08/2007  10:20 AM             10,279 5dhlwa5m1_newSlv_mid8.3MJ.k
10/09/2007  06:03 PM         10,075,176 d3hsp.gz
10/08/2007  10:20 AM             22,706 test.stdout
              5 File(s)     17,243,639 bytes

 Directory of D:\GridVerification
10/09/2007  05:49 PM    <DIR>          CoarseMesh
10/09/2007  09:34 AM    <DIR>          FineMesh_Case22_5DHLW_A
10/09/2007  09:20 AM             81,408 GridVerification.xls
10/09/2007  05:48 PM    <DIR>          StandardMesh
10/09/2007  05:48 PM    <DIR>          VeryFineMesh
              1 File(s)         81,408 bytes

 Directory of D:\GridVerification\CoarseMesh
10/08/2007  02:19 PM              9,920 5dhlwa2m1s_newSlv_Crs.k
```

```
10/08/2007  02:19 PM         6,287,193 5dhlwa2m1_newSlv_Crs.inc.gz
10/08/2007  02:19 PM            82,372 5dhlwa2m1_newSlv_Crs.tg
10/08/2007  02:19 PM             3,474 CoDisp_pra05_lwr20MT_1MJ_CrsMesh_e55407MidEffStrnavg.txt
10/08/2007  02:19 PM             3,477 CoDisp_pra05_lwr20MT_1MJ_CrsMesh_e55407MSSavg.txt
10/08/2007  02:19 PM             3,479 CoDisp_pra05_lwr20MT_1MJ_CrsMesh_e55407VMavg.txt
10/08/2007  02:19 PM             3,557 CoDisp_pra05_lwr20MT_1MJ_CrsMesh_e55407Volume.txt
10/09/2007  05:49 PM         7,513,101 d3hsp.gz
10/08/2007  02:19 PM            27,349 test.stdout
               9 File(s)    13,933,922 bytes

 Directory of D:\GridVerification\FineMesh_Case22_5DHLW_A
10/09/2007  09:34 AM             3,154 CoDisp_pra05_lwr20MT_1MJ_e131583EffPlaStrnavg.txt
10/08/2007  02:21 PM             3,147 CoDisp_pra05_lwr20MT_1MJ_e131583MidEffStrnavg.txt
10/08/2007  02:22 PM             3,150 CoDisp_pra05_lwr20MT_1MJ_e131583MSSavg.txt
10/08/2007  02:21 PM             3,152 CoDisp_pra05_lwr20MT_1MJ_e131583VMavg.txt
10/08/2007  02:22 PM             3,045 CoDisp_pra05_lwr20MT_1MJ_e131583Volume.txt
               5 File(s)        15,648 bytes

 Directory of D:\GridVerification\StandardMesh
10/08/2007  02:20 PM             9,916 5dhlwa2m1s_newSlv_Std.k
10/08/2007  02:20 PM        10,090,076 5dhlwa2m1_newSlv_Std.inc.gz
10/08/2007  02:20 PM            82,090 5dhlwa2m1_newSlv_Std.tg
10/08/2007  02:20 PM             3,474 CoDisp_pra05_lwr20MT_1MJ_StdMesh_e99723MidEffStrnavg.txt
10/08/2007  02:20 PM             3,477 CoDisp_pra05_lwr20MT_1MJ_StdMesh_e99723MSSavg.txt
10/08/2007  02:20 PM             3,479 CoDisp_pra05_lwr20MT_1MJ_StdMesh_e99723VMavg.txt
10/08/2007  02:20 PM             3,557 CoDisp_pra05_lwr20MT_1MJ_StdMesh_e99723Volume.txt
10/09/2007  05:49 PM        11,738,380 d3hsp.gz
10/08/2007  02:20 PM            29,762 test.stdout
               9 File(s)    21,964,211 bytes

 Directory of D:\GridVerification\VeryFineMesh
10/08/2007  02:41 PM             9,922 5dhlwa2m1s_newSlv_vFine.k
10/08/2007  02:41 PM        12,579,836 5dhlwa2m1_newSlv_vFine.inc.gz
10/08/2007  02:41 PM            81,849 5dhlwa2m1_newSlv_vFine.tg
10/09/2007  09:07 AM             2,655 CoDisp_pra05_lwr20MT_1MJ_vFine_e138873MidEffStrnavg.txt
10/09/2007  09:07 AM             2,658 CoDisp_pra05_lwr20MT_1MJ_vFine_e138873MSSavg.txt
10/09/2007  09:07 AM             2,660 CoDisp_pra05_lwr20MT_1MJ_vFine_e138873VMavg.txt
10/09/2007  09:07 AM             2,553 CoDisp_pra05_lwr20MT_1MJ_vFine_e138873Volume.txt
10/09/2007  05:48 PM        14,816,749 d3hsp.gz
10/09/2007  09:07 AM            26,127 test.stdout
               9 File(s)    27,525,009 bytes

 Directory of D:\results
11/05/2007  12:55 PM    <DIR>          CoDisp_LwrSlvHit
11/05/2007  12:55 PM    <DIR>          CoDisp_MidPkgHit
11/05/2007  12:55 PM    <DIR>          TAD_LwrSlvHit
11/05/2007  12:55 PM    <DIR>          TAD_MidPkgHit
               0 File(s)             0 bytes

 Directory of D:\results\CoDisp_LwrSlvHit
11/05/2007  12:55 PM           388,608 CalcPRA05_rockfallOnCDSPWP_lwr_2.xls
10/02/2007  02:20 PM             3,147 CoDisp_pra05_lwr20MT_1400000J_e140114MidEffstrnavg.txt
10/02/2007  02:20 PM             3,150 CoDisp_pra05_lwr20MT_1400000J_e140114MSSavg.txt
10/02/2007  02:20 PM             3,152 CoDisp_pra05_lwr20MT_1400000J_e140114VMavg.txt
10/09/2007  09:34 AM             3,154 CoDisp_pra05_lwr20MT_1MJ_e131583EffPlaStrnavg.txt
10/02/2007  06:46 PM             3,147 CoDisp_pra05_lwr20MT_1MJ_e131583MidEffStrnavg.txt
10/02/2007  06:46 PM             3,150 CoDisp_pra05_lwr20MT_1MJ_e131583MSSavg.txt
10/02/2007  06:46 PM             3,152 CoDisp_pra05_lwr20MT_1MJ_e131583VMavg.txt
10/02/2007  02:20 PM             2,942 CoDisp_pra05_lwr20MT_500kJ_e131583MideffStrnavg.txt
10/02/2007  02:20 PM             2,945 CoDisp_pra05_lwr20MT_500kJ_e131583MSSavg.txt
10/02/2007  02:20 PM             2,947 CoDisp_pra05_lwr20MT_500kJ_e131583VMavg.txt
10/02/2007  02:20 PM             2,942 CoDisp_pra05_lwr28MT_1800000J_e131583MidEffStrnavg.txt
```

```
10/02/2007  02:20 PM          2,945 CoDisp_pra05_lwr28MT_1800000J_e131583MSSavg.txt
10/02/2007  02:20 PM          2,947 CoDisp_pra05_lwr28MT_1800000J_e131583VMavg.txt
10/02/2007  02:20 PM          2,942 CoDisp_pra05_lwr28MT_2.2MJ_e131582MidEffStrnavg.txt
10/02/2007  02:20 PM          2,945 CoDisp_pra05_lwr28MT_2.2MJ_e131582MSSavg.txt
10/02/2007  02:20 PM          2,947 CoDisp_pra05_lwr28MT_2.2MJ_e131582VMavg.txt
10/02/2007  02:20 PM          1,424 CoDisp_pra05_lwr2MT_15kJ_e107103j-MidEffStrnavg.txt
10/02/2007  02:20 PM          1,427 CoDisp_pra05_lwr2MT_15kJ_e107103j-MSSavg.txt
10/02/2007  02:20 PM          1,429 CoDisp_pra05_lwr2MT_15kJ_e107103j-VMavg.txt
10/02/2007  02:20 PM          1,424 CoDisp_pra05_lwr2MT_15kJ_e131583MidEffStrnavg.txt
10/02/2007  02:20 PM          1,427 CoDisp_pra05_lwr2MT_15kJ_e131583MSSavg.txt
10/02/2007  02:20 PM          1,429 CoDisp_pra05_lwr2MT_15kJ_e131583VMavg.txt
10/02/2007  02:20 PM          1,424 CoDisp_pra05_lwr2MT_15kJ_e140113MidEffStrnavg.txt
10/02/2007  02:20 PM          1,427 CoDisp_pra05_lwr2MT_15kJ_e140113MSSavg.txt
10/02/2007  02:20 PM          1,429 CoDisp_pra05_lwr2MT_15kJ_e140113VMavg.txt
10/02/2007  02:20 PM          1,424 CoDisp_pra05_lwr2MT_15kJ_e140115MidEffStrnavg.txt
10/02/2007  02:20 PM          1,427 CoDisp_pra05_lwr2MT_15kJ_e140115MSSavg.txt
10/02/2007  02:20 PM          1,429 CoDisp_pra05_lwr2MT_15kJ_e140115VMavg.txt
10/02/2007  02:20 PM          1,589 CoDisp_pra05_lwr2MT_500kJ_e140113MidEffStrnavg.txt
10/02/2007  02:20 PM          1,592 CoDisp_pra05_lwr2MT_500kJ_e140113MSSavg.txt
10/02/2007  02:20 PM          1,594 CoDisp_pra05_lwr2MT_500kJ_e140113VMavg.txt
10/02/2007  02:20 PM          2,737 CoDisp_pra05_lwr41MT_3.7MJ_e131583MidEffStrnavg.txt
10/02/2007  02:20 PM          2,740 CoDisp_pra05_lwr41MT_3.7MJ_e131583MSSavg.txt
10/02/2007  02:20 PM          2,742 CoDisp_pra05_lwr41MT_3.7MJ_e131583VMavg.txt
10/03/2007  08:21 AM          1,917 CoDisp_pra05_lwr430kg_3000J_e131582MidEffStrnavg.txt
10/03/2007  08:21 AM          1,920 CoDisp_pra05_lwr430kg_3000J_e131582MSSavg.txt
10/03/2007  08:21 AM          1,922 CoDisp_pra05_lwr430kg_3000J_e131582VMavg.txt
10/03/2007  08:21 AM          2,327 CoDisp_pra_lwr41MT_8MJ_e130697MidEffStrnavg.txt
10/03/2007  08:21 AM          2,330 CoDisp_pra_lwr41MT_8MJ_e130697MSSavg.txt
10/03/2007  08:21 AM         13,350 CoDisp_pra_lwr41MT_8MJ_e130697VM6.txt
10/03/2007  08:21 AM          2,332 CoDisp_pra_lwr41MT_8MJ_e130697VMavg.txt
              42 File(s)      493,374 bytes


 Directory of D:\results\CoDisp_MidPkgHit
11/05/2007  12:55 PM        517,632 CalcPRA05_rockfallOnCDSPWP_mid_2.xls
10/05/2007  03:03 PM          3,105 CoDisp_pra05_mid20MT_1.4MJ_e101787MidEffStrnavg.txt
10/05/2007  03:03 PM          3,108 CoDisp_pra05_mid20MT_1.4MJ_e101787MSSavg.txt
10/05/2007  03:03 PM          3,110 CoDisp_pra05_mid20MT_1.4MJ_e101787VMavg.txt
10/02/2007  02:20 PM          2,736 CoDisp_pra05_mid20MT_1MJ_e100908MidEffStrnavg.txt
10/02/2007  02:20 PM          2,739 CoDisp_pra05_mid20MT_1MJ_e100908MSSavg.txt
10/02/2007  02:20 PM          2,741 CoDisp_pra05_mid20MT_1MJ_e100908VMavg.txt
10/02/2007  02:20 PM          2,736 CoDisp_pra05_mid20MT_1MJ_e101802MidEffStrnavg.txt
10/02/2007  02:20 PM          2,739 CoDisp_pra05_mid20MT_1MJ_e101802MSSavg.txt
10/02/2007  02:20 PM          2,741 CoDisp_pra05_mid20MT_1MJ_e101802VMavg.txt
10/02/2007  02:20 PM          2,736 CoDisp_pra05_mid20MT_1MJ_e102054MidEffStrnavg.txt
10/02/2007  02:20 PM          2,739 CoDisp_pra05_mid20MT_1MJ_e102054MSSavg.txt
10/02/2007  02:20 PM          2,741 CoDisp_pra05_mid20MT_1MJ_e102054VMavg.txt
10/02/2007  02:20 PM          2,941 CoDisp_pra05_mid20MT_500kJ_e102054MidEffStrnavg.txt
10/02/2007  02:20 PM          2,944 CoDisp_pra05_mid20MT_500kJ_e102054MSSavg.txt
10/02/2007  02:20 PM          2,946 CoDisp_pra05_mid20MT_500kJ_e102054VMavg.txt
10/03/2007  01:45 PM          3,761 CoDisp_pra05_mid28MT_1.8MJ_e100881MidEffStrnavg.txt
10/03/2007  01:45 PM          3,764 CoDisp_pra05_mid28MT_1.8MJ_e100881MSSavg.txt
10/03/2007  01:45 PM          3,766 CoDisp_pra05_mid28MT_1.8MJ_e100881VMavg.txt
10/02/2007  02:20 PM          3,761 CoDisp_pra05_mid28MT_1800000J_e101190MidEffStrnavg.txt
10/02/2007  02:20 PM          3,764 CoDisp_pra05_mid28MT_1800000J_e101190MSSavg.txt
10/02/2007  02:20 PM          3,766 CoDisp_pra05_mid28MT_1800000J_e101190VMavg.txt
10/02/2007  02:20 PM          3,761 CoDisp_pra05_mid28MT_1800000J_e101748MidEffStrnavg.txt
10/02/2007  02:20 PM          3,764 CoDisp_pra05_mid28MT_1800000J_e101748MSSavg.txt
10/02/2007  02:20 PM          3,766 CoDisp_pra05_mid28MT_1800000J_e101748VMavg.txt
10/03/2007  01:55 PM          3,761 CoDisp_pra05_mid28MT_2.2MJ_e100881MidEffStrnavg.txt
10/03/2007  01:55 PM          3,764 CoDisp_pra05_mid28MT_2.2MJ_e100881MSSavg.txt
10/03/2007  01:55 PM          3,766 CoDisp_pra05_mid28MT_2.2MJ_e100881VMavg.txt
10/02/2007  02:20 PM          3,761 CoDisp_pra05_mid28MT_2200000J_e101190MidEffStrnavg.txt
```

```
10/02/2007  02:20 PM          3,764 CoDisp_pra05_mid28MT_2200000J_e101190MSSavg.txt
10/02/2007  02:20 PM          3,766 CoDisp_pra05_mid28MT_2200000J_e101190VMavg.txt
10/02/2007  02:20 PM          3,761 CoDisp_pra05_mid28MT_2200000J_e101748MidEffStrnavg.txt
10/02/2007  02:20 PM          3,764 CoDisp_pra05_mid28MT_2200000J_e101748MSSavg.txt
10/02/2007  02:20 PM          3,766 CoDisp_pra05_mid28MT_2200000J_e101748VMavg.txt
10/02/2007  02:20 PM          1,342 CoDisp_pra05_mid2MT_15kJ_e102054MideffStrnavg.txt
10/02/2007  02:20 PM          1,345 CoDisp_pra05_mid2MT_15kJ_e102054MSSavg.txt
10/02/2007  02:20 PM          1,347 CoDisp_pra05_mid2MT_15kJ_e102054VMavg.txt
10/02/2007  02:20 PM          1,589 CoDisp_pra05_mid2MT_500kJ_e102054MidEffStrnavg.txt
10/02/2007  02:20 PM          1,592 CoDisp_pra05_mid2MT_500kJ_e102054MSSavg.txt
10/02/2007  02:20 PM          1,594 CoDisp_pra05_mid2MT_500kJ_e102054VMavg.txt
10/03/2007  01:08 PM          3,679 CoDisp_pra05_mid41MT_3.7MJ_e100848MidEffStrnavg.txt
10/03/2007  01:08 PM          3,682 CoDisp_pra05_mid41MT_3.7MJ_e100848MSSavg.txt
10/03/2007  01:08 PM          3,684 CoDisp_pra05_mid41MT_3.7MJ_e100848VMavg.txt
10/02/2007  02:20 PM          3,679 CoDisp_pra05_mid41MT_3700000J_e101718MidEffStrnavg.txt
10/02/2007  02:20 PM          3,682 CoDisp_pra05_mid41MT_3700000J_e101718MSSavg.txt
10/02/2007  02:20 PM          3,684 CoDisp_pra05_mid41MT_3700000J_e101718VMavg.txt
10/03/2007  08:21 AM            809 CoDisp_pra05_mid41MT_8MJ_e100881MidEffStrnavg.txt
10/03/2007  08:21 AM            812 CoDisp_pra05_mid41MT_8MJ_e100881MSSavg.txt
10/03/2007  08:21 AM            814 CoDisp_pra05_mid41MT_8MJ_e100881VMavg.txt
10/06/2007  03:01 PM            768 CoDisp_pra05_mid41MT_8MJ_e101205MidEffStrnavg.txt
10/06/2007  03:01 PM            771 CoDisp_pra05_mid41MT_8MJ_e101205MSSavg.txt
10/06/2007  03:01 PM            773 CoDisp_pra05_mid41MT_8MJ_e101205VMavg.txt
10/02/2007  02:20 PM          2,286 CoDisp_pra05_mid430kg_3kJ_e101190MidEffStrnavg.txt
10/02/2007  02:20 PM          2,289 CoDisp_pra05_mid430kg_3kJ_e101190MSSavg.txt
10/02/2007  02:20 PM          2,291 CoDisp_pra05_mid430kg_3kJ_e101190VMavg.txt
10/02/2007  02:20 PM          2,286 CoDisp_pra05_mid430kg_3kJ_e102918MidEffStrnavg.txt
10/02/2007  02:20 PM          2,289 CoDisp_pra05_mid430kg_3kJ_e102918MSSavg.txt
10/02/2007  02:20 PM          2,291 CoDisp_pra05_mid430kg_3kJ_e102918VMavg.txt
10/02/2007  02:20 PM          2,285 CoDisp_pra05_mid430kg_3kJ_e99894MidEffStrnavg.txt
10/02/2007  02:20 PM          2,288 CoDisp_pra05_mid430kg_3kJ_e99894MSSavg.txt
10/02/2007  02:20 PM          2,290 CoDisp_pra05_mid430kg_3kJ_e99894VMavg.txt
              61 File(s)      684,421 bytes


 Directory of D:\results\TAD_LwrSlvHit
11/05/2007  12:55 PM        355,328 CalcPRA05_rockfallOnWP_lwr_2.xls
09/27/2007  04:52 PM          1,989 TAD_pra05_lwr20MT_1400000J_e91750MidEffStrnAvg.txt
09/27/2007  04:52 PM          1,992 TAD_pra05_lwr20MT_1400000J_e91750MSSavg.txt
09/27/2007  04:52 PM          1,994 TAD_pra05_lwr20MT_1400000J_e91750VMstressAvg.txt
09/27/2007  04:53 PM          1,866 TAD_pra05_lwr20MT_1MJ_e85056MidEffStrnavg.txt
09/27/2007  04:53 PM          1,869 TAD_pra05_lwr20MT_1MJ_e85056MSSavg.txt
09/27/2007  04:53 PM          1,871 TAD_pra05_lwr20MT_1MJ_e85056VMavg.txt
09/27/2007  04:53 PM          1,866 TAD_pra05_lwr20MT_1MJ_e91750MidEffStrnavg.txt
09/27/2007  04:53 PM          1,869 TAD_pra05_lwr20MT_1MJ_e91750MSSavg.txt
09/27/2007  04:53 PM          1,871 TAD_pra05_lwr20MT_1MJ_e91750VMavg.txt
09/27/2007  04:52 PM          1,948 TAD_pra05_lwr20MT_500000J_e85056MidEffStrnAvg.txt
09/27/2007  04:52 PM          1,951 TAD_pra05_lwr20MT_500000J_e85056MSSavg.txt
09/27/2007  04:52 PM          1,953 TAD_pra05_lwr20MT_500000J_e85056VMstressAvg.txt
09/27/2007  04:52 PM          2,366 TAD_pra05_lwr28MT_1800000J_e91742MidEffStrnavg.txt
09/27/2007  04:52 PM          2,369 TAD_pra05_lwr28MT_1800000J_e91742MSSavg.txt
09/27/2007  04:52 PM          2,371 TAD_pra05_lwr28MT_1800000J_e91742VMavg.txt
09/27/2007  04:52 PM          2,366 TAD_pra05_lwr28MT_1800000J_e91750MidEffStrnavg.txt
09/27/2007  04:52 PM          2,369 TAD_pra05_lwr28MT_1800000J_e91750MSSavg.txt
09/27/2007  04:52 PM          2,371 TAD_pra05_lwr28MT_1800000J_e91750VMavg.txt
09/27/2007  04:52 PM          1,915 TAD_pra05_lwr28MT_2200000J_e91750MidEffStrnavg.txt
09/27/2007  04:52 PM          1,918 TAD_pra05_lwr28MT_2200000J_e91750MSSavg.txt
09/27/2007  04:52 PM          1,920 TAD_pra05_lwr28MT_2200000J_e91750VMavg.txt
09/27/2007  04:53 PM          1,423 TAD_pra05_lwr2MT_15000J_e85055MidEffStrnAvg.txt
09/27/2007  04:53 PM          1,426 TAD_pra05_lwr2MT_15000J_e85055MSSavg.txt
09/27/2007  04:53 PM          1,428 TAD_pra05_lwr2MT_15000J_e85055VMavg.txt
09/27/2007  04:53 PM          1,300 TAD_pra05_lwr2MT_500000J_e91750MidEffStrnavg.txt
09/27/2007  04:53 PM          1,303 TAD_pra05_lwr2MT_500000J_e91750MSSavg.txt
```

```
09/27/2007  04:53 PM            1,305 TAD_pra05_lwr2MT_500000J_e91750VMavg.txt
09/27/2007  04:53 PM            1,300 TAD_pra05_lwr2MT_500000J_e91752MidEffStrnavg.txt
09/27/2007  04:53 PM            1,303 TAD_pra05_lwr2MT_500000J_e91752MSSavg.txt
09/27/2007  04:53 PM            1,305 TAD_pra05_lwr2MT_500000J_e91752VMavg.txt
09/27/2007  04:53 PM            1,382 TAD_pra05_lwr430kg_3000J_e85145MidEffStrnAvg.txt
09/27/2007  04:53 PM            1,385 TAD_pra05_lwr430kg_3000J_e85145MSSavg.txt
09/27/2007  04:53 PM            1,387 TAD_pra05_lwr430kg_3000J_e85145VMavg.txt
09/27/2007  04:52 PM            2,571 TAD_pra05_lwr73MT_3700000J_e84555MidEffStrnAvg.txt
09/27/2007  04:52 PM            2,574 TAD_pra05_lwr73MT_3700000J_e84555MSSavg.txt
09/27/2007  04:52 PM            2,576 TAD_pra05_lwr73MT_3700000J_e84555VMstressAvg.txt
10/01/2007  05:55 PM            2,571 TAD_pra05_lwr73MT_3700000J_e85056MidEffStrnAvg.txt
10/01/2007  05:55 PM            2,574 TAD_pra05_lwr73MT_3700000J_e85056MSSavg.txt
10/01/2007  05:55 PM            2,576 TAD_pra05_lwr73MT_3700000J_e85056VMstressAvg.txt
09/27/2007  04:52 PM            2,571 TAD_pra05_lwr73MT_3700000J_e91750MidEffStrnAvg.txt
09/27/2007  04:52 PM            2,574 TAD_pra05_lwr73MT_3700000J_e91750MSSavg.txt
09/27/2007  04:52 PM            2,576 TAD_pra05_lwr73MT_3700000J_e91750VMstressAvg.txt
10/01/2007  02:04 PM            2,571 TAD_pra05_lwr73MT_8MJ_e85054MidEffStrnavg.txt
10/01/2007  02:04 PM            2,574 TAD_pra05_lwr73MT_8MJ_e85054MSSavg.txt
10/01/2007  02:04 PM            2,576 TAD_pra05_lwr73MT_8MJ_e85054VMavg.txt
10/01/2007  02:04 PM            2,407 TAD_pra05_lwr73MT_8MJ_e85056MidEffStrnavg.txt
10/01/2007  02:04 PM            2,410 TAD_pra05_lwr73MT_8MJ_e85056MSSavg.txt
10/01/2007  02:04 PM            2,412 TAD_pra05_lwr73MT_8MJ_e85056VMavg.txt
09/27/2007  04:52 PM            2,571 TAD_pra05_lwr73MT_920000J_e85037_MidEffStrainAvg.txt
09/27/2007  04:52 PM            2,574 TAD_pra05_lwr73MT_920000J_e85037_MSSavg.txt
09/27/2007  04:52 PM            2,576 TAD_pra05_lwr73MT_920000J_e85037_VMstressAvg.txt
              52 File(s)       460,413 bytes

 Directory of D:\results\TAD_MidPkgHit
11/05/2007  12:55 PM          633,344 CalcPRA05_rockfallOnWP_mid_2.xls
09/25/2007  04:27 PM            2,848 TAD_pra05_mid20MT_1000000J_e101802MidEffStrnAvg.txt
09/25/2007  04:27 PM            2,851 TAD_pra05_mid20MT_1000000J_e101802MSSavg.txt
09/25/2007  04:27 PM            2,853 TAD_pra05_mid20MT_1000000J_e101802VMstressAvg.txt
09/24/2007  04:38 PM            2,520 TAD_pra05_mid20MT_1400000J_e101190MidEffStrnAvg.txt
09/24/2007  04:38 PM            2,523 TAD_pra05_mid20MT_1400000J_e101190MSSavg.txt
09/24/2007  04:38 PM            2,525 TAD_pra05_mid20MT_1400000J_e101190VMstressAvg.txt
09/24/2007  04:38 PM            2,520 TAD_pra05_mid20MT_1400000J_e101748MidEffStrnAvg.txt
09/24/2007  04:38 PM            2,523 TAD_pra05_mid20MT_1400000J_e101748MSSavg.txt
09/24/2007  04:38 PM            2,525 TAD_pra05_mid20MT_1400000J_e101748VMstressAvg.txt
09/25/2007  09:36 AM            2,520 TAD_pra05_mid20MT_1400000J_e102054MidEffStrnAvg.txt
09/25/2007  09:36 AM            2,523 TAD_pra05_mid20MT_1400000J_e102054MSSavg.txt
09/25/2007  09:36 AM            2,525 TAD_pra05_mid20MT_1400000J_e102054VMstressAvg.txt
10/01/2007  02:02 PM            2,848 TAD_pra05_mid20MT_1MJ_e101190MidEffStrnAvg.txt
10/01/2007  02:02 PM            2,851 TAD_pra05_mid20MT_1MJ_e101190MSSavg.txt
10/01/2007  02:02 PM            2,853 TAD_pra05_mid20MT_1MJ_e101190VMavg.txt
10/01/2007  02:30 PM            2,848 TAD_pra05_mid20MT_1MJ_e101802MidEffStrnavg.txt
10/01/2007  02:30 PM            2,851 TAD_pra05_mid20MT_1MJ_e101802MSSavg.txt
10/01/2007  02:30 PM            2,853 TAD_pra05_mid20MT_1MJ_e101802VMavg.txt
10/01/2007  02:02 PM            2,848 TAD_pra05_mid20MT_1MJ_e102054MidEffStrnAvg.txt
10/01/2007  02:02 PM            2,851 TAD_pra05_mid20MT_1MJ_e102054MSSavg.txt
10/01/2007  02:02 PM            2,853 TAD_pra05_mid20MT_1MJ_e102054VMavg.txt
09/26/2007  01:14 PM            2,971 TAD_pra05_mid20MT_500000J_e102054MidEffStrnAvg.txt
09/26/2007  01:14 PM            2,974 TAD_pra05_mid20MT_500000J_e102054MSSavg.txt
09/26/2007  01:14 PM            2,976 TAD_pra05_mid20MT_500000J_e102054VMavg.txt
09/24/2007  04:38 PM            3,299 TAD_pra05_mid28MT_1800000J_e101190MidEffStrnAvg.txt
09/24/2007  04:38 PM            3,302 TAD_pra05_mid28MT_1800000J_e101190MSSavg.txt
09/24/2007  04:38 PM            3,304 TAD_pra05_mid28MT_1800000J_e101190VMstressAvg.txt
09/24/2007  04:38 PM            3,299 TAD_pra05_mid28MT_1800000J_e101748MidEffStrnAvg.txt
09/24/2007  04:38 PM            3,302 TAD_pra05_mid28MT_1800000J_e101748MSSavg.txt
09/24/2007  04:38 PM            3,304 TAD_pra05_mid28MT_1800000J_e101748VMstressAvg.txt
09/24/2007  04:38 PM            3,012 TAD_pra05_mid28MT_2200000J_e100839MidEffStrnAvg.txt
09/24/2007  04:38 PM            3,015 TAD_pra05_mid28MT_2200000J_e100839MSSavg.txt
09/24/2007  04:38 PM            3,017 TAD_pra05_mid28MT_2200000J_e100839VMstressAvg.txt
```

```
09/24/2007  04:38 PM          3,012 TAD_pra05_mid28MT_2200000J_e101190MidEffStrnAvg.txt
09/24/2007  04:38 PM          3,015 TAD_pra05_mid28MT_2200000J_e101190MSSavg.txt
09/24/2007  04:38 PM          3,017 TAD_pra05_mid28MT_2200000J_e101190VMstressAvg.txt
09/24/2007  04:38 PM          3,012 TAD_pra05_mid28MT_2200000J_e101199MidEffStrnAvg.txt
09/24/2007  04:38 PM          3,015 TAD_pra05_mid28MT_2200000J_e101199MSSavg.txt
09/24/2007  04:38 PM          3,017 TAD_pra05_mid28MT_2200000J_e101199VMstressAvg.txt
09/24/2007  04:38 PM          2,121 TAD_pra05_mid2MT_15000J_e101190MidEffStrainAvg.txt
09/24/2007  04:38 PM          2,124 TAD_pra05_mid2MT_15000J_e101190MSSavg.txt
09/24/2007  04:38 PM          2,126 TAD_pra05_mid2MT_15000J_e101190VMstressAvg.txt
09/24/2007  04:38 PM          1,670 TAD_pra05_mid2MT_500000J_e101190MidEffStrnAvg.txt
09/24/2007  04:38 PM          1,673 TAD_pra05_mid2MT_500000J_e101190MSSavg.txt
09/24/2007  04:38 PM          1,675 TAD_pra05_mid2MT_500000J_e101190VMstressAvg.txt
09/24/2007  04:38 PM          1,670 TAD_pra05_mid2MT_500000J_e102054MidEffStrnAvg.txt
09/25/2007  03:54 PM          1,673 TAD_pra05_mid2MT_500000J_e102054MSSavg.txt
09/24/2007  04:38 PM          1,675 TAD_pra05_mid2MT_500000J_e102054VMstressAvg.txt
09/25/2007  03:33 PM          1,670 TAD_pra05_mid2MT_500000J_e102486MideffStrnAvg.txt
09/24/2007  04:38 PM          1,673 TAD_pra05_mid2MT_500000J_e102486MSSavg.txt
09/25/2007  03:33 PM          1,675 TAD_pra05_mid2MT_500000J_e102486VMstressAvg.txt
09/24/2007  04:38 PM          2,203 TAD_pra05_mid430kg_3000J_e101190MidEffStrnAvg.txt
09/24/2007  04:38 PM          2,206 TAD_pra05_mid430kg_3000J_e101190MSSavg.txt
09/24/2007  04:38 PM          2,208 TAD_pra05_mid430kg_3000J_e101190VMstressAvg.txt
09/24/2007  04:38 PM          2,202 TAD_pra05_mid430kg_3000J_e99894MidEffStrainAvg.txt
09/24/2007  04:38 PM          2,205 TAD_pra05_mid430kg_3000J_e99894MSSavg.txt
09/24/2007  04:38 PM          2,207 TAD_pra05_mid430kg_3000J_e99894VMstressAvg.txt
09/24/2007  04:38 PM          3,759 TAD_pra05_mid73MT_3700000J_e101190MidEffStrnAvg.txt
09/24/2007  04:38 PM          3,762 TAD_pra05_mid73MT_3700000J_e101190MSSavg.txt
09/24/2007  04:38 PM          3,764 TAD_pra05_mid73MT_3700000J_e101190VMstressAvg.txt
09/24/2007  04:38 PM          3,759 TAD_pra05_mid73MT_3700000J_e101199MidEffStrnAvg.txt
09/24/2007  04:38 PM          3,762 TAD_pra05_mid73MT_3700000J_e101199MSSavg.txt
09/24/2007  04:38 PM          3,764 TAD_pra05_mid73MT_3700000J_e101199VMstressAvg.txt
10/10/2007  07:06 PM          3,759 TAD_pra05_mid73MT_8MJ_e100764MidEffStrnavg.txt
10/10/2007  07:06 PM          3,762 TAD_pra05_mid73MT_8MJ_e100764MSSavg.txt
10/10/2007  07:06 PM          3,764 TAD_pra05_mid73MT_8MJ_e100764VMavg.txt
10/10/2007  07:15 PM          3,759 TAD_pra05_mid73MT_8MJ_e100770MidEffStrnavg.txt
10/10/2007  07:15 PM          3,762 TAD_pra05_mid73MT_8MJ_e100770MSSavg.txt
10/10/2007  07:15 PM          3,764 TAD_pra05_mid73MT_8MJ_e100770VMavg.txt
10/01/2007  02:53 PM          3,759 TAD_pra05_mid73MT_8MJ_e101199MidEffStrnavg.txt
10/01/2007  02:53 PM          3,762 TAD_pra05_mid73MT_8MJ_e101199MSSavg.txt
10/01/2007  02:53 PM          3,764 TAD_pra05_mid73MT_8MJ_e101199VMavg.txt
09/24/2007  04:38 PM          4,169 TAD_pra05_mid73MT_920000J_e101190MidEffStrnAvg.txt
09/24/2007  04:38 PM          4,172 TAD_pra05_mid73MT_920000J_e101190MSSavg.txt
09/24/2007  04:38 PM          4,174 TAD_pra05_mid73MT_920000J_e101190VMstressAvg.txt
09/24/2007  04:38 PM          4,169 TAD_pra05_mid73MT_920000J_e102054MidEffStrnAvg.txt
09/24/2007  04:38 PM          4,172 TAD_pra05_mid73MT_920000J_e102054MSSavg.txt
09/24/2007  04:38 PM          4,174 TAD_pra05_mid73MT_920000J_e102054VMstressAvg.txt
10/10/2007  07:22 PM          3,012 TAD_pra_mid28MT_2.2MJ_e103422MidEffStrnavg.txt
10/10/2007  07:22 PM          3,015 TAD_pra_mid28MT_2.2MJ_e103422MSSavg.txt
10/10/2007  07:22 PM          3,017 TAD_pra_mid28MT_2.2MJ_e103422VMavg.txt
10/01/2007  02:02 PM          3,759 TAD_pra_mid73MT_8MJ_e102066MidEffStrnavg.txt
10/01/2007  02:02 PM          3,762 TAD_pra_mid73MT_8MJ_e102066MSSavg.txt
10/01/2007  02:02 PM          3,764 TAD_pra_mid73MT_8MJ_e102066VMavg.txt
              85 File(s)      882,559 bytes

 Directory of D:\Sens_RockSy
10/25/2007  07:39 AM          2,491 5DHLW_pra_lwr20MT_1MJ_Sy140_e131583MidEffStrnavg.txt
10/25/2007  07:39 AM          2,496 5DHLW_pra_lwr20MT_1MJ_Sy140_e131583VMavg.txt
10/25/2007  07:39 AM          2,942 5DHLW_pra_lwr28MT_2MJ_Sy140_e131583MideffStrnavg.txt
10/25/2007  07:39 AM          2,947 5DHLW_pra_lwr28MT_2MJ_Sy140_e131583VMavg.txt
10/25/2007  07:39 AM          2,983 5DHLW_pra_lwr41MT_3.7MJ_e131583MidEffStrnavg.txt
10/25/2007  07:38 AM          2,988 5DHLW_pra_lwr41MT_3.7MJ_e131583VMavg.txt
10/25/2007  07:38 AM          2,286 5DHLW_pra_lwr41MT_8MJ_Sy140_e131028MidEffStrnavg.txt
10/25/2007  07:38 AM          2,291 5DHLW_pra_lwr41MT_8MJ_Sy140_e131028VMavg.txt
```

```
10/25/2007  07:38 AM           1,753 5DHLW_pra_lwr430kg_3kJ_Sy140_e131582MidEffStrnavg.txt
10/25/2007  07:38 AM           1,758 5DHLW_pra_lwr430kg_3kJ_Sy140_e131582VMavg.txt
11/05/2007  01:04 PM         448,000 CalcPRA05_rockfallOnCDSPWP_lwr_Sy140.xls
11/05/2007  01:04 PM         719,360 CalcPRA05_rockfallOnWP_mid_Sy140.xls
10/23/2007  03:38 PM    <DIR>        Case10_TAD_C_RockSy140
10/23/2007  03:36 PM    <DIR>        Case13_TAD_C_RockSy140
10/23/2007  03:33 PM    <DIR>        Case16_TAD_C_RockSy140
10/23/2007  03:28 PM    <DIR>        Case17_TAD_C_RockSy140
10/23/2007  03:22 PM    <DIR>        Case18_TAD_C_RockSy140
10/25/2007  01:58 PM    <DIR>        Case19_5DHLW_A_RockSy140
10/25/2007  01:58 PM    <DIR>        Case22_5DHLW_A_RockSy140
10/25/2007  01:59 PM    <DIR>        Case25_5DHLW_A_RockSy140
10/25/2007  01:59 PM    <DIR>        Case26_5DHLW_A_RockSy140
10/25/2007  01:59 PM    <DIR>        Case27_5DHLW_A_RockSy140
10/23/2007  03:21 PM           2,849 TAD_pra_mid20MT_1MJ_Sy140_e101367MidEffStrnavg.txt
10/23/2007  03:21 PM           2,854 TAD_pra_mid20MT_1MJ_Sy140_e101367VMavg.txt
10/23/2007  03:20 PM           2,849 TAD_pra_mid20MT_1MJ_Sy140_e101802MidEffStrnavg.txt
10/23/2007  03:20 PM           2,854 TAD_pra_mid20MT_1MJ_Sy140_e101802VMavg.txt
10/23/2007  03:20 PM           3,792 TAD_pra_mid28MT_2MJ_Sy140_e100839MidEffStrnavg.txt
10/23/2007  03:20 PM           3,797 TAD_pra_mid28MT_2MJ_Sy140_e100839VMavg.txt
10/23/2007  03:20 PM           3,792 TAD_pra_mid28MT_2MJ_Sy140_e101703MideffStrnavg.txt
10/23/2007  03:20 PM           3,797 TAD_pra_mid28MT_2MJ_Sy140_e101703VMavg.txt
10/23/2007  03:20 PM           1,958 TAD_pra_mid430kg_3kJ_Sy140_e100758MidEffStrnavg.txt
10/23/2007  03:20 PM           1,963 TAD_pra_mid430kg_3kJ_Sy140_e100758VMavg.txt
10/23/2007  03:20 PM           3,964 TAD_pra_mid73MT_3.7MJ_Sy140_e101196MidEffStrnavg.txt
10/23/2007  03:20 PM           3,969 TAD_pra_mid73MT_3.7MJ_Sy140_e101196VMavg.txt
10/23/2007  03:20 PM           3,965 TAD_pra_mid73MT_3MJ_Sy140_e101199MidEffStrnavg.txt
10/23/2007  03:20 PM           3,970 TAD_pra_mid73MT_3MJ_Sy140_e101199VMavg.txt
10/23/2007  03:20 PM          21,960 TAD_pra_mid73MT_8MJ_Sy140_e101199MidEffStrnall6.txt
10/23/2007  03:20 PM           3,760 TAD_pra_mid73MT_8MJ_Sy140_e101199MidEffStrnavg.txt
10/23/2007  03:20 PM          21,960 TAD_pra_mid73MT_8MJ_Sy140_e101199VMall6.txt
10/23/2007  03:20 PM           3,765 TAD_pra_mid73MT_8MJ_Sy140_e101199VMavg.txt
              30 File(s)      1,290,113 bytes

 Directory of D:\Sens_RockSy\Case10_TAD_C_RockSy140
10/23/2007  03:38 PM       9,651,981 d3hsp.gz
10/23/2007  03:38 PM           8,929 tada3m2s_pra05_mid140.k
10/23/2007  03:38 PM          17,167 test.stdout
               3 File(s)      9,678,077 bytes

 Directory of D:\Sens_RockSy\Case13_TAD_C_RockSy140
10/23/2007  03:35 PM      10,966,431 d3hsp.gz
10/23/2007  03:36 PM           8,733 tada2m8_pra05_mid140.k
10/23/2007  03:35 PM          19,692 test.stdout
               3 File(s)     10,994,856 bytes

 Directory of D:\Sens_RockSy\Case16_TAD_C_RockSy140
10/23/2007  03:33 PM       9,656,885 d3hsp.gz
10/23/2007  03:33 PM           8,794 tada3m2_pra05_mid_2.2MJ140.k
10/23/2007  03:32 PM          22,607 test.stdout
               3 File(s)      9,688,286 bytes

 Directory of D:\Sens_RockSy\Case17_TAD_C_RockSy140
10/23/2007  03:28 PM      10,126,191 d3hsp.gz
10/23/2007  03:28 PM           8,931 tada3m2_pra05_mid_3.7MJ140.k
10/23/2007  03:28 PM          22,953 test.stdout
               3 File(s)     10,158,075 bytes

 Directory of D:\Sens_RockSy\Case18_TAD_C_RockSy140
10/23/2007  03:21 PM       9,051,125 d3hsp.gz
10/23/2007  03:21 PM           8,923 tada3m2_pra05_mid_8.3MJ140.k
10/23/2007  03:21 PM          23,723 test.stdout
```

        3 File(s)   9,083,771 bytes

 Directory of D:\Sens_RockSy\Case19_5DHLW_A_RockSy140
10/25/2007 07:39 AM   9,723 5dhlwa1m1_newSlv_3000J140.k
10/25/2007 07:39 AM   12,996,302 d3hsp.gz
10/25/2007 07:39 AM   19,362 test.stdout
        3 File(s)   13,025,387 bytes

 Directory of D:\Sens_RockSy\Case22_5DHLW_A_RockSy140
10/25/2007 07:39 AM   9,912 5dhlwa2m1s_newSlv140.k
10/25/2007 07:40 AM   14,106,698 d3hsp.gz
10/25/2007 07:40 AM   26,030 test.stdout
        3 File(s)   14,142,640 bytes

 Directory of D:\Sens_RockSy\Case25_5DHLW_A_RockSy140
10/25/2007 07:40 AM   9,964 5dhlwa2m1s_newSlv_2.2MJ140.k
10/25/2007 07:40 AM   14,107,082 d3hsp.gz
10/25/2007 07:40 AM   26,562 test.stdout
        3 File(s)   14,143,608 bytes

 Directory of D:\Sens_RockSy\Case26_5DHLW_A_RockSy140
10/25/2007 07:41 AM   10,268 5dhlwa5m1_newSlv_3.7MJ140.k
10/25/2007 07:41 AM   14,145,600 d3hsp.gz
10/25/2007 07:41 AM   31,209 test.stdout
        3 File(s)   14,187,077 bytes

 Directory of D:\Sens_RockSy\Case27_5DHLW_A_RockSy140
10/25/2007 07:41 AM   10,542 5dhlwa5m1_newSlv_8.3MJ140.k
10/25/2007 07:42 AM   14,144,378 d3hsp.gz
10/25/2007 07:42 AM   27,220 test.stdout
        3 File(s)   14,182,140 bytes